

UC Irvine

UC Irvine Electronic Theses and Dissertations

Title

Advancing Process-Based Nonstationary Analysis of Climate Extremes: Modeling, Uncertainty Assessment and Multivariate Attribution

Permalink

<https://escholarship.org/uc/item/7q467744>

Author

Ragno, Elisa

Publication Date

2019

Peer reviewed|Thesis/dissertation

UNIVERSITY OF CALIFORNIA,
IRVINE

Advancing Process-Based Nonstationary Analysis of Climate Extremes:
Modeling, Uncertainty Assessment and Multivariate Attribution

DISSERTATION

submitted in partial satisfaction of the requirements
for the degree of

DOCTOR OF PHILOSOPHY

in Civil Engineering

by

Elisa Ragno

Dissertation Committee:
Professor Amir AghaKouchak, Chair
Professor Steven J. Davis
Professor Kuo-lin Hsu

2018

An edited version of Chapter 4 was published by AGU © 2018 American Geophysical
Union
All other materials © 2018 Elisa Ragno

DEDICATION

To Alessandro,
To mamma Caterina and papà Antonio,
To Alice, Anna, e Maurizio.

TABLE OF CONTENTS

	Page
LIST OF FIGURES	vi
LIST OF TABLES	x
ACKNOWLEDGMENTS	xi
CURRICULUM VITAE	xii
ABSTRACT OF THE DISSERTATION	xiv
1 Introduction	1
1.1 Climate Extremes	2
1.1.1 Defining Extreme Events	2
1.1.2 Evidence of a Changing Climate	3
1.2 Climate Extremes and Society	8
1.3 Modeling a Changing Climate	9
1.3.1 Stationary versus Nonstationary	11
1.4 Nonstationary Models	15
1.4.1 Detection and Attribution Studies	16
1.5 Improving our Understanding and Ability to Model Extremes in a Changing Climate	17
 2 A Generalized Framework for Process-based Nonstationary Extreme Value Analysis	 20
2.1 Method	22
2.1.1 Process-Based Nonstationarity Extreme Value Analysis	22
2.1.2 Generalized Extreme Value (GEV)	27
2.1.3 Generalized Pareto (GP)	28
2.1.4 Log-Pearson Type III (LP3)	29
2.2 Parameter Estimation: Bayesian Analysis and Markov Chain Monte Carlo Sampling	31
2.3 Model Diagnostics and Selection	32
2.3.1 Standard Transformation	33
2.3.2 Probability and Quantile Plots	34

2.3.3	Kolmogorov-Smirnov Test	34
2.3.4	Model Selection based on Model Complexity	35
2.3.5	Model Selection based on Minimum Residual	36
2.4	Predictive Distribution	36
2.5	Return Level Curves under Nonstationarity	37
2.5.1	Effective Return Level	38
2.5.2	Expected Waiting Time	39
2.6	Explanatory Analysis: Mann-Kendall and White Tests	40
2.6.1	Mann-Kendall	40
2.6.2	White Test	41
2.7	Results	42
2.7.1	Application 1: Modeling discharge with urbanization as the physical driver	43
2.7.2	Application 2: Modeling temperature with CO ₂ as the physical covariate	45
2.7.3	Application 3: Modeling sea level rise with time as the covariate	48
2.7.4	Application 4: Modeling precipitation under a stationary assumption	51
2.8	Conclusion	52
2.9	Supporting Information: ProNEVA User Manual	54
2.9.1	ProNEVA Folder Content	55
2.9.2	RUN ProNEVA	56
2.9.3	ProNEVA Results	69
3	On the Probability of Rare Events	71
4	Quantifying Changes in Future Intensity-Duration-Frequency Curves Using Multi-Model Ensemble Simulations	77
4.1	Introduction	78
4.2	Data	80
4.3	Methodology	82
4.3.1	Distance Components Test	82
4.3.2	Extreme Value Analysis for IDF curves	84
4.3.3	Incorporating Multi-Model Simulations for IDF curve Analysis	87
4.4	Results	91
4.5	Conclusion and Discussion	98
4.6	Supporting Information	100
5	Multivariate Attribution of Extremes Using Copulas	115
5.1	Methodology	118
5.1.1	Copula and Conditional Copula	118
5.1.2	Detection of Changes	120
5.2	Data	123
5.3	Result	124
5.4	Discussion and Conclusion	127

6 Conclusion	130
Bibliography	134

LIST OF FIGURES

	Page
2.1 Flowchart representing the core structure of the Matlab Toolbox ProNEVA .	26
2.2 ProNEVA results for Application 1: Modeling discharge in Ferson Creek with urbanization as the physical driver of change. a) Discharge data and percent of urbanization in the basin; b) Discharge data as a function of urbanization.	43
2.3 ProNEVA results for Application 1: Modeling discharge in Ferson Creek with urbanization as the physical driver of change. a) Return Level curves based on a stationary model; b) Return Level base on a nonstationary model considering an urbanization area equal to 37% of the catchment area; c) Expected return level curves, i.e. ensemble medians, under stationary and nonstationary assumption; d) Effective return period, i.e. return period as a function of the percent of urbanized area.	44
2.4 ProNEVA results for Application 2: Modeling temperature maxima with CO ₂ emissions as the physical covariate. a) Temperature and CO ₂ time series; b) Annual temperature maxima as a function of CO ₂ emissions in the atmosphere	46
2.5 ProNEVA results for Application 2: Modeling temperature maxima with CO ₂ emissions as the physical covariate. a) Return Level curves based on a stationary model; b) Return Level base on a nonstationary model considering CO ₂ emissions equal to 4.9 GtCO ₂	47
2.6 ProNEVA results for Application 2: Modeling temperature maxima with CO ₂ emissions as the physical covariate. Effective return period, i.e. return period as a function of CO ₂ emissions.	47
2.7 ProNEVA results for Application 3: Modeling sea level rise with time as the covariate. Sea Level in the city of Trieste (IT).	48
2.8 ProNEVA results for Application 3: Modeling sea level rise with time as the covariate. a) Return Level curves based on a stationary model; b) Return Level base on a nonstationary model considering equal to 45 years from the first observation; c) Expected return level curves, i.e. ensemble medians, under stationary and nonstationary assumption; d) Effective return period, i.e. return period as a function of the covariate, here time.	49
2.9 ProNEVA results for Application 3: Modeling sea level rise with time as the covariate. Waiting time.	50
2.10 ProNEVA results for Application 4: Modeling precipitation under a stationary assumption. Precipitation excesses.	51

2.11	ProNEVA results for Application 4: Modeling precipitation under a stationary assumption. a) Return Level curves under the stationary assumption; b) Return Level curves under the temporal nonstationary assumption for a value of the covariate within the period of observation.	52
2.12	Content of the folder ProNEVA.	56
2.13	ProNEVA GUI - Data&Model for selecting data, distribution, and model type.	57
2.14	ProNEVA GUI. Select priors and trends for the GEV parameters.	59
2.15	ProNEVA GUI. Select threshold type along with priors and trends for the GP parameters.	60
2.16	ProNEVA GUI. Select priors and trends for the LP3 parameters.	61
2.17	ProNEVA GUI for selecting the parameters for MCMC along with complementary options such as tests, plots, and save.	61
3.1	Probability of observing a T-year event at least once in N-years ($P(x_T \in X)$): Comparing $P(x_T \in X)$ for different lengths of records (Equation 3.3; solid lines) relative to the case of $N \rightarrow \infty$ (Equation 3.4; dashed lines).	73
3.2	The universal chart indicating the likelihood of observing an extreme events	74
3.3	The likelihood of observing a rare event (e.g., T=50-yr, 100-yr, 500-yr) for 50 years (left) and 100 (right) years of observations.	75
3.4	The likelihood of observing a 50-yr (left) and 100-yr (right) events for different lengths of records (N=15 to N=200 years).	76
4.1	Comparison between 1-day extreme historical records (grey dotted line) and future climate (RPC4.5 orange and RCP8.5 red dotted line) ECDFs. The shaded dotted lines represent the uncertainty on the future climate. The inner boxes show the right tail behavior of the distributions. A) San Diego - CA, E) Chicago - IL, M) Atlanta - GA.	89
4.2	Conceptual explanation of the methodology adopted to quantify changes in the occurrences of historical events under future climate.	91
4.3	RCP 8.5 - Comparison between current (grey lines) and future climate scenario (red lines) IDF curves, along with 90 % confidence intervals, given an average return interval of 25 years.	93
4.4	RCP 8.5 - Comparison between current (grey lines) and future climate scenario (red lines) IDF curves, along with 90 % confidence intervals, given an average return interval of 50 years.	94
4.5	RCP 8.5 - Comparison between current (grey lines) and future climate scenario (red lines) IDF curves, along with 90 % confidence intervals, given an average return interval of 100 years.	95
4.6	a) Return periods under future climate of events currently associated with return periods of 50-, and 100-year in urban locations across the U.S.: expected projected return periods (dots) along with inter-quartile range (IQR - grey lines). b) Safety factors (i.e., ratio of medians of the future relative to the past IDF curves). c) Total annual mean precipitation of historical records.	97

4.7	Return periods under future climate of events historically associated with return periods of 50-, and 100-year in California. Expected projected return periods (dots) and 90 % confidence interval (gray lines).	98
4.8	RCP 4.5 - Comparison between current (grey lines) and future climate scenario (orange lines) IDF curves, along with 90 % confidence intervals, given an average return interval of 25 years.	103
4.9	RCP 4.5 - Comparison between current (grey lines) and future climate scenario (orange lines) IDF curves, along with 90 % confidence intervals, given an average return interval of 50 years.	104
4.10	RCP 4.5 - Comparison between current (grey lines) and future climate scenario (orange lines) IDF curves, along with 90 % confidence intervals, given an average return interval of 100 years.	105
4.11	So-called safety factor (i.e., the ratio of medians of the future relative to the past IDF curves) for 25- and 100-year events.	106
4.12	Percent of GCMs showing a statistical significant trend in the time series of extreme maxima precipitation intensities based on Mann - Kendall trend test. Significance level 5%.	106
4.13	Percent of GCMs showing a statistical significant trend in the time series of extreme maxima precipitation intensities based on Mann - Kendall trend test. Significance level 1%.	107
4.14	Percent of GCMs showing a statistical significant trend in the time series of extreme maxima precipitation intensities based on Mann - Kendall trend test. Significance level 10%.	107
4.15	Percent of GCMs showing a statistical significant trend in the time series of extreme maxima precipitation intensities (Mann-Kendall trend test, significance level 5%) and statistical significant variability in the residuals (White test, significance level 5%).	107
4.16	a) Example of annual time series with a significant trend and b) constant variance of the residuals - RCP8.5 Salt Lake City ; c) example of annual time series with a significant trend and d) time dependent variance of the residuals - RCP8.5 Washington D.C..	108
4.17	RCP 4.5 - California - Comparison between current (grey lines) and future climate scenario (orange lines) IDF curves, along with 90 % confidence intervals, given an average return interval of 25 years.	109
4.18	RCP 4.5 - California - Comparison between current (grey lines) and future climate scenario (orange lines) IDF curves, along with 90 % confidence intervals, given an average return interval of 50 years.	110
4.19	RCP 4.5 - California - Comparison between current (grey lines) and future climate scenario (orange lines) IDF curves, along with 90 % confidence intervals, given an average return interval of 100 years.	111
4.20	RCP 8.5 - California - Comparison between current (grey lines) and future climate scenario (red lines) IDF curves, along with 90 % confidence intervals, given an average return interval of 25 years.	112

4.21	RCP 8.5 - California - Comparison between current (grey lines) and future climate scenario (red lines) IDF curves, along with 90 % confidence intervals, given an average return interval of 50 years.	113
4.22	RCP 8.5 - California - Comparison between current (grey lines) and future climate scenario (red lines) IDF curves, along with 90 % confidence intervals, given an average return interval of 100 years.	114
5.1	Effect of the dependence structure of the copula model (τ) on the marginal distribution u for fixed value of the joint conditional probability $C_{u v}$	122
5.2	(I, D) scatter plots and Frank copulas. Model CCSM4: a) Scatter plot in \mathbb{R} and $[0, 1] \times [0, 1]$ domain and b) Fitted Frank Copulas. Model CNRM-CM5: c) Scatter plot in \mathbb{R} and $[0, 1] \times [0, 1]$ domain and d) Fitted Frank Copulas. Model MIROC-ESM: e) Scatter plot in \mathbb{R} and $[0, 1] \times [0, 1]$ domain and f) Fitted Frank Copulas.	126
5.3	Detected changes in the precipitation characteristics (I, D) . M1, M2, and M3 denote the models CCSM4, CNRM-CM5, and MIROC-ESM, respectively. Panel a, c, and e show the corresponding 25-, 50-, and 100-year events, respectively, in the alternative natural world. Panel b,d, and e represents the effect of the dependence structure on the marginal distribution $u = F_I(I)$ for a fixed value of the joint conditional probability, $C_\delta(F_I F_D(d))$, equal to 0.96, 0.98, and 0.99 respectively	128

LIST OF TABLES

	Page
2.1 GEV dependence models	28
2.2 GP dependence models	29
2.3 LP3 dependence models	31
2.4 Standard Transformations	33
2.5 List of ProNEVA outputs	70
4.1 List of Global Climate Models used	101
4.2 Observed Changes in Median and 90th quantile of 1-day precipitation event.	102
4.3 Cities in California investigated in the study.	102
4.4 List of LOCA downscaled Global Climate Models used for California	102
5.1 List of Kendall's τ and Frank copula parameter δ for the models, i.e. CCSM4, CNRM-CM5, MIROC-ESM, and runs, i.e. HNR, HR, investigated.	124

ACKNOWLEDGMENTS

Thank you Professor Amir AghaKouchak for believing in me when almost 5 years ago I knocked for the first time at your office door. I will always be grateful for the opportunity you gave me. Otherwise, my life would have been quite different, for better or worse! Thank you for being an incredibly generous mentor and for treating your group's members like family.

Thank you to the committee members, Professor Steven J. Davis and Professor Kuo-lin Hsu, for taking the time to go through my work and for providing thoughtful feedbacks.

Thank you to my buddy Omid and all my former and current officemates for the fun time in the office.

Thank you to Professor Efi Foufoula-Georgiou group who adopted me as an adjunct member. We had a great time together.

Thank you to the Italians at UCI who made me feel “home”. Many thanks to Enrico, Marco, Andrea, Michele and Paolo.

Thank you to the lovely Eftychia and the little twins, Simoni e Dimitri, who took care of me during this last year.

Thank you to my family who has been and will always be my safe island. Many thanks to mom, dad, Anna, Maurizio, Roberta, Luciano, and my beloved Sicily.

A special thanks goes to my nice Alice who, with her sweetness and joy, turned upside down the life of all of us.

Finally, thank you to my sweetheart Alessandro without whom my life would have been flavourless.

CURRICULUM VITAE

Elisa Ragno

EDUCATION

Doctor of Philosophy in Civil Engineering	2018
University of California, Irvine	<i>Irvine, CA</i>
Master of Science in Structural Civil Engineering	2012
Politecnico di Milano	<i>Milano, Italy</i>
Bachelor of Science in Civil Engineering	2006
Politecnico di Milano	<i>Milano, Italy</i>

RESEARCH EXPERIENCE

Graduate Research Assistant	2014–2018
University of California, Irvine	<i>Irvine, California</i>

TEACHING EXPERIENCE

Teaching Assistant	Winter 2017
ENGRCEE 81B: Civil Engineering Practicum II.	
University of California, Irvine	<i>Irvine, CA</i>
Teaching Assistant	Winter 2016
ENGRCEE 173/273: Watershed Modeling.	
University of California, Irvine	<i>Irvine, CA</i>

REFEREED JOURNAL PUBLICATIONS

Ragno, E., AghaKouchak, A., Love, C. A., Cheng, L., Vahedifard, F., and Lima, C. H. R. (2018). Quantifying changes in future IntensityDurationFrequency curves using multimodel ensemble simulations. *Water Resources Research*, 54, 17511764. <https://doi.org/10.1002/2017WR021975>.

Sadegh, M., Moftakhari, H., Gupta, H. V., **Ragno, E.**, Mazdiyasni, O., Sanders, B., Matthew, R., and AghaKouchak, A. (2018). Multihazard scenarios for analysis of compound extreme events. *Geophysical Research Letters*, 45. <https://doi.org/10.1029/2018GL077317>.

Sadegh, M., **E. Ragno**, and A. AghaKouchak (2017), Multivariate Copula Analysis Toolbox (MvCAT): Describing Dependence and Underlying Uncertainty using a Bayesian Framework, *Water Resources Research*, 53, 51665183, doi:10.1002/2016WR020242.

Vahedifard, F., AghaKouchak, A., **Ragno, E.**, Shahrokhbadi, S., and Mallakpour, I. (2017). Lessons from the Oroville dam. *Science*, 355(6330), 1139-1140.

Vahedifard, F., Tehrani, F. S., Galavi, V., **Ragno, E.**, and AghaKouchak, A. (2017). Resilience of MSE Walls with Marginal Backfill under a Changing Climate: Quantitative Assessment for Extreme Precipitation Events. *Journal of Geotechnical and Geoenvironmental Engineering*, 143(9), 04017056.

Mazdiyasni, O., AghaKouchak, A., Davis, S.J., Madadgar, S., Mehran, A., **Ragno, E.**, Sadegh, M., Sengupta, A., Ghosh, S., Dhanya, C.T. and Niknejad, M., 2017. Increasing probability of mortality during Indian heat waves. *Science Advances*, 3(6), p.e1700066.

Ragno, E., AghaKouchak, A., Cheng, L., and Sadegh, M., A Generalized Framework for Process-based Nonstationary Extreme Value Analysis. *Water Resources Research*. (Ready for submission).

Ragno, E., AghaKouchak, A., Multivariate Attribution of Extremes Using Copulas. (In preparation).

CONFERENCE PAPERS

Jasim, F. H., Vahedifard, F., **Ragno, E.**, AghaKouchak, A., and Ellithy, G. Effects of Climate Change on Fragility Curves of Earthen Levees Subjected to Extreme Precipitations. *Geo-Risk 2017* (pp. 498-507).

SOFTWARE

Process-Based Nonstationary Extreme Value Analysis (ProNEVA)
Matlab toolbox for extreme value analysis

ABSTRACT OF THE DISSERTATION

Advancing Process-Based Nonstationary Analysis of Climate Extremes:
Modeling, Uncertainty Assessment and Multivariate Attribution

By

Elisa Ragno

Doctor of Philosophy in Civil Engineering

University of California, Irvine, 2018

Professor Amir AghaKouchak, Chair

Extreme weather events are inherent in climate variability and they can cause ecosystem alterations, infrastructure damages, suspension of food supply chains, and loss of lives. Today's highly populated and urbanized society is more vulnerable than ever to natural hazards and their disruptive consequences. Projected population growth and changes in climate variability are expected to exacerbate the societal and economic impact of climatic extremes. The scientific community, global organizations, and other stakeholders have all recognized the urgency of improving our understanding of both natural and human-induced climate variability.

The overarching goal of this thesis is to advance the current methods for nonstationary analysis of climatic extremes and their attributions. Here we propose a methodological framework for investigating hydroclimatic extremes over time and in response to a physical driver/covariate. The Process-based Nonstationary Extreme Value Analysis (ProNEVA) framework is unique in that it allows for incorporating a physical component into traditional frequency analysis techniques to account for observed or process-based changes in the variable of interest. The model can be used for both stationary and nonstationary analyses of extremes and includes a Graphical User Interface (GUI) for easier implementation.

We then shed light on the uncertainty inherent in the estimation of climatic extremes. We propose a generalized approach for including uncertainty information in the recurrence interval of extremes. The approach offers insights on how information about extremes should be interpreted by planners and decision-makers under conditions of uncertainty.

Using the method developed in this thesis, we show how extreme precipitation is expected to change in the future. We also highlight the importance of merging information from observations and climate model simulations for risk assessment purposes.

Finally, we outline a methodological framework for attribution of changes in multiple extremes or multiple features of an extreme event. We show the potential of copula functions for attribution of changes in both the magnitude and the dependence structure between characteristics of a natural phenomenon or, more generally, between two dependent variables.

Chapter 1

Introduction

Extreme weather events are inherent in the climate variability and communities around the world must face and coexist with them. In 1953 a combination of high spring tides, storm surge, wind, and very large waves in the North Sea caused extensive flooding in the U.K. and Northern Europe. The Netherlands lost 1,800 people (MetOffice, 2013). In 2003 the heatwave in Europe caused 15,000 deaths in France, Portugal, and Italy (Fink et al., 2004); the 2003 European summer was recorded as the hottest since 1500 AD (Stott et al., 2002; Black et al., 2004; Schär et al., 2004). Similarly, deadly summer heatwaves have afflicted Indian population since 2013 (Mazdiyasni et al., 2017). From 1997 to late 2009 the Millennium Drought, or the “Big Dry” (Heberger, 2011), affected southern Australia (AghaKouchak et al., 2014b; Heberger, 2011). Rainfall below average and consequent scarcity of surface water resources impacted the country’s ecosystem and economy (Van Dijk et al., 2013). In 2005, Hurricane Katrina struck the Mississippi Deltaic Plain and caused about 1,570 deaths and \$ 40-50 billion in monetary losses in New Orleans (LA)(Day et al., 2007). During the winter of 2013-2014, the U.K. was hit by an extreme storm surge, a series of intense storms, and prolonged and persistent rainfall causing widespread flooding throughout the country, damaging properties and threatening lives (Thorne, 2014). In 2012-2016, the state

of California experienced a severe drought caused by lack of precipitation and extremely high temperatures (AghaKouchak et al., 2014a; Swain, 2015; Funk et al., 2014). Consequent low water levels in the reservoirs reduced the hydropower generation (Gleick, 2016; Tarroja et al., 2016) and caused an over-exploitation of groundwater resources (Taylor et al., 2013; Xiao et al., 2017).

The historical extreme events previously mentioned are only a few examples of natural hazards that communities across the globe have experienced. Observations of historical extremes and projections of future changes to natural hazards are critical for better preparation and management of societal impacts. Therefore, a comprehensive understanding and characterization of extremes is required to enhance societal resilience and to their impacts such as ecosystem alterations, infrastructure damages, suspension of the food supply chain, and, most importantly, loss of lives (IPCC, 2014b).

1.1 Climate Extremes

1.1.1 Defining Extreme Events

A univocal definition of extreme events does not exist. In general, *extreme events* refer to: (1) events with small probability of occurrence (rare events) based on a probability density function estimated from observations; (2) events that lead to significant socioeconomic impacts (i.e., events above a specific impact-related threshold) (Seneviratne et al., 2012). However, in practice the two definitions often (but not necessarily) match, meaning that events causing severe damages are also the ones with a small probability of occurrence (Seneviratne et al., 2012). It is worth noting that, not all the extremes cause disruptions and, analogously, not all the damages are caused by extreme events. For example, in February 2017, Oroville Dam (Northern California) suffered from structural damages and 2,000 people leaving downstream

were evacuated. Damages and the consequent state of emergency were caused by moderate rainfall along with a combination of antecedent conditions, and even the age of the dam might have played a role in the impact (Vahedifard et al., 2017a).

1.1.2 Evidence of a Changing Climate

Extremes are expected to exhibit a great deal of variability under natural forcings. However, there is evidence that human activities (including anthropogenic emissions, urbanization, deforestation) have altered the occurrence and impact of extreme events. The observed and projected changes related to climate extremes pertain to both changes in their frequency and severity (probability-based extremes) and to changes in the exposure and vulnerability of the sites affected by them (impact-based extremes).

The projected increase in population residing in urban areas is predicted to exacerbate the potential losses and damages caused by natural hazards (Gu et al., 2015). Pielke and Landsea (1998) showed that the observed increase in the damages experienced as a consequence of hurricanes along the US coasts disappears when the results are normalized considering the coastal population growth and the improved living conditions. Similarly, the 2005 flood in Mumbai would have caused 80% more losses and would have affected 20% more people if it had occurred in 2015, independently of the effect of climate change (Bouwer et al., 2007).

If on one hand the exposure and vulnerability to natural hazards have increased, on the other hand there is evidence of changes in the statistics of extreme events, e.g., heatwaves, storms, droughts, surges, mainly because of the increase in greenhouse gas (GHG) emissions, such as CO₂, deriving from anthropogenic activities.

Over the past decades, we have observed increasing surface temperatures (e.g., Alexander et al., 2006; Barnett et al., 1999; Villarini et al., 2010; Melillo et al., 2014; Diffenbaugh et al.,

2015; Fischer and Knutti, 2015; Mazdidasni and AghaKouchak, 2015), more intense rainfall events (e.g., Alexander et al., 2006; Zhang et al., 2007; Villarini et al., 2010; Min et al., 2011; Marvel and Bonfils, 2013; Westra et al., 2013; Cheng et al., 2014; Fischer and Knutti, 2016; Mallakpour and Villarini, 2017; Ragno et al., 2018), changes in river discharge (e.g., Villarini et al., 2009a,b; Hurkmans et al., 2009; Stahl et al., 2010), and sea level rise (e.g., Holgate, 2007; Haigh et al., 2010; Wahl et al., 2011; Vermeer and Rahmstorf, 2009; Cabanes et al., 2001; Rignot et al., 2011; Vandenberg-Rodes et al., 2016; Moftakhari et al., 2017a). A warming climate implies an intensification of the water cycle, i.e. an increase in the frequency and intensity of tropical storms, floods, and droughts, due to the positive feedback between temperature and water vapor (e.g. Trenberth, 2011; Manabe and Wetherald, 1975; Marengo and Espinoza, 2016; Huntington, 2006; Gloor et al., 2013; Held and Soden, 2006; Groisman et al., 2004; Wu et al., 2013). In the following, a brief review of the literature on different types of extremes is provided.

Heatwaves

European summer heatwaves, in particular multi-day heatwaves associated with warm night temperature and high humidity, are projected to become more frequent (Schär et al., 2004; Meehl and Tebaldi, 2004; Beniston, 2004; Clark et al., 2006), in accordance to observed past trends (Tank et al., 2005; Della-Marta et al., 2007), and the geographical patterns are consistent across models and health indicators (Fischer and Schär, 2010). Furthermore, Cueto et al. (2010) showed that the duration and intensity of heatwaves in the city of Mexicali (Mexico) increased during summer months, and more than doubled in number since 1970. Besides, the same pattern is found in projections (Cueto et al., 2010).

Mazdidasni and AghaKouchak (2015) found a significant increase in the co-occurrence of drought and heatwaves across the United States, which enhances their impact on environment and society. Other evidence of increase in extreme heatwaves can be found in the literature

(e.g., Coumou and Rahmstorf, 2012; Peng et al., 2011; Frich et al., 2002; Khaliq et al., 2005; Lau and Nath, 2012; Mazdiyasni et al., 2017).

Cyclones

Exceptional tropical cyclones have occurred since 2004, however, a formal detection of a change is obstructed by the short length of records, large variability in the number and intensity of storms and incomplete understanding of the driving forces (Coumou and Rahmstorf, 2012). Webster et al. (2005) observed an increase in number and proportion of hurricanes reaching categories 4 and 5, in North Pacific, Indian, and Southwest Pacific Oceans, even though the number of cyclones and cyclone days has decreased in the past decades, except in North Atlantic.

Elsner et al. (2008) reported that the Atlantic tropical cyclones are getting stronger due to the increase in the ocean temperature, while signals of changes over the rest of the tropics are too weak to be observed. However, assuming a warmer sea, more energy will be available to be converted into tropical cyclone wind (Elsner et al., 2008). Knutson et al. (2010) observed that, even though it is not possible to attribute past changes in tropical cyclone activities to the increase in GHG emission, future projections based on theory and high-resolution dynamical models consistently indicate that a warming climate will increase the intensity and frequency of tropical cyclones. However, the results show large variations across the existing climate models (Knutson et al., 2010).

Droughts

Damberg and AghaKouchak (2014) investigated the amplitude and frequency of drought in the Southern and Northern Hemisphere over the past 3 decades using satellite gauge-adjusted precipitation observations. Areas in southwest United States, Amazon, the Horn of Africa,

Northern India and the Mediterranean region showed a drying trend, while southwest Asia, Central America, northern Australia, and parts of eastern Europe exhibited a wetting trend.

While there are regional drought trends in historical data, there seem to be little evidence of a significant trend in droughts at a continental to global scale in historical observations (Sheffield et al., 2012). However, several contradictory reports have been published based on different indicators and data sets leading to different results (Trenberth et al., 2014). For example, Dai (2013) concluded that the observed aridity since 1950 over land is consistent with model predictions suggesting that in the next 30-90 years widespread droughts will be expected. Sheffield and Wood (2008) estimated, in a warming climate, an increase in long-term droughts, driven mainly by a lack of precipitation associated with increase in evaporation. Overall, the projected increase in heating of the ocean and atmosphere from anthropogenic activities is expected to intensify future droughts causing more socioeconomic damages (Trenberth et al., 2014).

Heavy Precipitation

Groisman et al. (2005) investigated changes in heavy precipitations. They found that extratropical regions, including United States, have experienced an increase in extreme precipitation due to a GHG-enriched atmosphere (Groisman et al., 2005). Similarly, Allan and Soden (2008) examined extreme precipitations in tropical regions. Using satellite observations, they found that heavy precipitation has increased during warm periods, and decreased during cold periods. Their results were also confirmed with climate model simulations (Allan and Soden, 2008).

Using fingerprint methods, Min et al. (2011) showed that the observed intensification of heavy precipitation over the northern hemisphere is attributable to increases in GHG. Comparable results can be found in Westra et al. (2013), who investigated annual maximum

daily precipitation on a global scale during the 20th and early 21st century. They estimated a rate of increase in annual maximum daily rainfall intensity between 5.9 and 7.7 % per °C of globally averaged near-surface atmospheric temperature (Westra et al., 2013). Westra et al. (2013) attributed the observed changes not only to the increase in temperatures but also to changes in atmospheric circulation. Donat et al. (2016) investigated changes in both total and extreme precipitation on a global scale in dry and wet regions. They observed an increase in extreme daily precipitation in both regions. They showed that changes in dry regions are highly dependent on temperature changes.

However, precipitation patterns are complex, and opposite trends can be observed on both a spatial and time scale. For example, Zheng et al. (2015) explored changes in seasonal and annual precipitation in the greater Sydney using gauged observations. On an annual temporal scale, he recorded an increase in precipitation extremes for storm duration less than 2 hours, while a decrease in precipitation higher than 3 hours (except 12 hr). On a seasonal scale, Zheng et al. (2015) observed an increase in summer extremes, while a decrease in autumn and winter precipitation. Based on their results, Zheng et al. (2015) argued possible opposing signals in summer and winter seasons. Wang and Zhou (2005) analyzed extreme precipitation across China during 1961-2001. They observed increases in extreme precipitation (mainly in summer) in the southwest, northwest, and east of China, while decreases (mainly in spring and autumn) in the center, north and northeast of China. Moreover, they showed that extreme precipitation over Yangtze River basin has increased by 10-20 % every 10 years during summer (Wang and Zhou, 2005). In a recent study Swain et al. (2018) showed that anthropogenic forcing is projected to increase in the frequency of wet extremes in the 21st century. They also showed that while the mean precipitation is not expected to change substantially in the future, there is a high chance of significant increases in extreme dry-to-wet precipitation events (Swain et al., 2018).

It is important to highlight the fact that the confidence in studies related to precipitation

changes depends on the density of the available gauge network (e.g., Groisman et al., 2005; Westra et al., 2013). Good quality and quantity of observations are also beneficial for global climate models. Donat et al. (2016) noted that model uncertainties are largest in regions where the quality of observations is not good. Min et al. (2011) and Allan and Soden (2008) have also noticed that climate models underestimate extreme precipitation magnitude in response to increase in CO₂.

1.2 Climate Extremes and Society

Urban and rural community development, economic prosperity, and human wealth and health rely on proper management of quality and quantity of water resources, and, more generally, on the resilience, coping, and adaptive capacity of settlements (Cardona et al., 2012). Flood protection systems, for example, allow human settlement and economic prosperity in low lying areas (Viglione et al., 2014; Di Baldassarre et al., 2013).

A comprehensive characterization of climate extremes has a fundamental societal importance (Alexander, 2016), as demonstrated by the *Weather and Climate Extremes* Grand Challenge of the the World Climate Research Programme (WCRP). WCRP organizes workshops and conferences with the aim of improving the current knowledge on analysis and prediction of Earth system variability and change. Research outputs are then implemented for practical applications that will benefit society (WCRP, 2018). The WCRP Joint Scientific Committee (JSC), together with sponsors, stakeholders, and a network of scientists, identifies a number of Grand Challenges (GC) representing research areas to be improved. *Weather and Climate Extremes* WCRP Grand Challenge focuses on enhancing our physical understanding and prediction of extreme events in a changing climate which are supporting tools for decision and policy makers, and stakeholders.

A better characterization of climate extreme in a changing climate is in line with the main objective of the United Nation 2030 Agenda for Sustainable Development, adopted by world leaders in September 2015, (UN, 2015). Indeed, Goal 11, *Make cities inclusive, safe, resilient and sustainable*, (UN, 2015), will greatly benefit from a more comprehensive knowledge of climate extremes to guarantee basic services, good quality of life, and societal and economic development, limiting the threat of natural hazard. One of the goals of this dissertation is to contribute to the existing methodological frameworks for evaluating changes in extreme events and their impacts.

1.3 Modeling a Changing Climate

The effects of human activities on freshwater systems, land use land cover change and on likelihood of extreme events threatening humans and ecosystems motivate predicting changes in extremes beyond the range of observed variability (Wagener et al., 2010). Currently, climate change and variability is investigated using physical-based models or statistical models.

Physical-based models are built on fundamental laws of nature (e.g., energy, mass and momentum conservation) solved in latitude-longitude-height grid (Flato et al., 2013). Models such as the Atmosphere–Ocean General Circulation Model (AOGCM) attempt to reproduce the dynamics between atmosphere, ocean, land, and sea ice, and are used in the Intergovernmental Panel on Climate Change (IPCC) climate assessment studies (Taylor et al., 2012). AOGCMs can be forced considering different scenarios of GHG and/or aerosol forcing (Flato et al., 2013) to reproduce the observed or simulate the future climate. Models known as Earth System Model (ESM) originate from AOGCM, but include biogeochemical processes, i.e. the carbon cycle and its connections to the terrestrial and oceanic ecosystems (Flato, 2011). They represent the most comprehensive models to simulate observed and future climate, though still the simulations are subject to high uncertainties (Flato et al.,

2013). Given their complexity, ESMs of Intermediate Complexity (IC) have been introduced for case of studies in which coarser spatial resolution and simplified processes are sufficient (Flato et al., 2013). Regional Climate Models (RCM) are AOGCMs capable of describing climate feedback mechanisms acting at the regional scale (high resolution, down to 10km or less) and do not typically include interactive ocean and sea ice components (Flato et al., 2013).

The ability of the physical-based models to reproduce historical observation is tested by comparing historical model simulations against historical observations. Several studies have shown reliability of climate models for providing valuable information about the future climate (Fischer and Knutti, 2016), but they also point out to significant limitations in their real-life applications (e.g. Brands et al., 2013; Nasrollahi et al., 2015). The main advantage of climate models is that they offer the opportunity of running different past and future conditions/scenarios (e.g., pre-industrial, anthropogenic emissions, natural forcings) to understand the response of extreme events. Climate models, however, are based on our current understanding of the dynamics of the natural system, which is partial. Consequently, their outcomes can be biased (e.g., Tebaldi and Knutti, 2007; Mehran et al., 2014). Moreover, climate models are sensitive to the initial state and hence, each run represents only one possible outcome the future climate can potentially follow (Flato et al., 2013). For this reason, an ensemble of simulations is often considered. Furthermore, climate models are computationally demanding, especially at higher spatial and temporal resolutions.

An alternative option to physical-based models is represented by statistical models, which investigate and project the effect of a changing climate on the variable of interest via covariates. The choice of the covariate is based on the observed correlation between pairs of variables or on prior knowledge of the physical processes relating them. Several methods have been proposed in the literature for studying changes in frequency and severity of ex-

tremes across space and/or time (Katz et al., 2002; Sankarasubramanian and Lall, 2003; Mailhot et al., 2007; Huard et al., 2009; Villarini et al., 2010; Vogel et al., 2011; Zhu et al., 2012; Willems et al., 2012; Katz, 2013; Obeysekera and Salas, 2013; Salas and Obeysekera, 2014; Yilmaz and Perera, 2014; Mirhosseini et al., 2014; Volpi et al., 2015; Read and Vogel, 2015; Sadegh et al., 2015; Krishnaswamy et al., 2015; Mirhosseini et al., 2015; Mondal and Mujumdar, 2015; Lima et al., 2016; Sarhadi and Soulis, 2017). For example, Lima et al. (2018) employed a Poisson regression model to investigate the influence of temperature and precipitation on the risk of fire in Brazilian Amazon, revealing that the effect of temperature can be stronger than the effect of rainfall. Another example is the work by Rosner et al. (2014), who introduced a methodology for flood risk assessment integrating the concepts of under- and over-preparedness to decide whether to adopt a time dependent statistical model or not. The advantage of statistical models resides in their computational efficiency, and numerical simplicity compared to physical-based models. On the other hand, they highly depend on the length of record, and the type of statistical model used, the choice of distribution function selected as representative of the observations, and on the observed empirical relationship between the variables of interest, which may not be representative of the reality.

1.3.1 Stationary versus Nonstationary

Currently, infrastructure design and risk assessment procedures, frequency analysis of natural hazards, and water resource management heavily rely on statistical models. Statistical models rely on limited observations from natural processes and hence, it is likely that our observations are not sufficient to fully understand the behavior of extreme events (Klemeš, 1974). Most current operational design, risk assessment and frequency analysis models rely on stationary stochastic models for estimating invariant characteristics of a climate variable from historical observations (Koutsoyiannis and Montanari, 2015). In such models, inference for the future relies on historical observations.

Stationarity corresponds to an assumption defining the properties of a stochastic model (here, statistics of the distribution and extremes do not change over time). In contrast, nonstationarity refers to a process in which the characteristics of the time series and extremes change over time (Katz, 2010; Cheng et al., 2014).

After Milly et al. (2008) proclaimed the death of the stationarity assumption, asserting that anthropogenic activities have compromised the natural system fluctuation within a given envelope of variability, the debate around the validity of the stationary assumption has gained a great deal of attention (Koutsoyiannis and Montanari, 2015). It has triggered a stimulating discussion within the scientific community on whether or not new paradigms should be adopted for infrastructure design, water management and risk assessment. Specifically, the debate related to the assumption of stationarity versus nonstationarity gravitates mainly around the following questions:

- Is nonstationarity a property of the natural system or a property of a numerical model?
- How do we select between a stationary and a nonstationary model?
- Can we test for nonstationarity given the available observations?
- If a nonstationary framework is adopted, what is its predictability power?

Nonstationarity as a property of a numerical model

Change in climate records is expected given that the Earth is in a constant state of change (Montanari et al., 2013; Koutsoyiannis, 2005). Following an increased number of studies investigating nonstationarity in climate data, the World of Meteorological Organization (WMO, 2012) has released a note in which it clearly states that “all natural systems are nonstationary, unequivocally and unconditionally”. On the contrary, a numerical/statistical model can be either stationary or nonstationary, it is only a matter of mathematical

representation of the natural phenomena (Montanari and Koutsoyiannis, 2014). Given that the natural system is nonstationary per se, the stationarity versus nonstationarity discussion must shift on the choice of the numerical/statistical model for inferring the future from observations.

Selecting between a stationary and a nonstationary model

Reviewing the debate about stationarity versus nonstationarity models, three main (and opposing) perspectives can be identified in the literature about the choice of model:

1. Stationary models should be the rule. Invariant properties of the natural system can be inferred from the past (Lins and Cohn, 2011; Montanari and Koutsoyiannis, 2014). Stationary stochastic models are well understood, and they can include long term persistence (LTP) (e.g., Cohn and Lins, 2005);
2. Stationary models should be the rule, and nonstationary models should only be adopted when observed changes are caused by a well-understood physical process. The nonstationary component will be defined as a deterministic component and hence, it will reduce the overall uncertainties. Uncertainty reduction can only be accepted if the physical information included in the statistical model improve our knowledge of the natural system (e.g., Koutsoyiannis and Montanari, 2007, 2015; Matalas, 1997, 2012; Montanari and Koutsoyiannis, 2014; Lins and Cohn, 2011; Serinaldi and Kilsby, 2015; Stedinger and Griffis, 2011; Luke et al., 2017);
3. Nonstationary models should be the rule if there is evidence of change in the observations or model simulations (Cheng et al., 2014; Katz, 2010; Cooley, 2013). This perspective does not require a full understanding of all the underlying processes. In this viewpoint, regardless of the cause of change (e.g., anthropogenic activities, nat-

ural variability), risk assessment and frequency analysis methods should account for changes in statistics of extremes.

4. Nonstationary models should be the rule. Humans have altered the natural cycle and “wait-and-see” (Milly et al., 2008) approach can no longer be used. New paradigms which can help us predict beyond what we have observed are required (Milly et al., 2008; Vogel et al., 2011; Wagener et al., 2010).

Testing for nonstationarity

Thus far, selection of a nonstationary model has been conditioned on the statistical significance of change in observations based on hypothesis testing, for example, monotonic trend test and change point detection (e.g., Villarini et al., 2009a; Vogel et al., 2011). However, detecting changes given the observations can be challenging because many drivers of climate variability influence the results, e.g., long term persistence and human induced climate change (Villarini et al., 2009a). Moreover, hydrological records are usually short when compared to geological timescales (Matalas, 1997), and the null hypothesis of the test may be ill-posed. Indeed, hypothesis tests are proved by contradiction, and if there is no agreement with the natural system, the test results are not acceptable a priori (Cohn and Lins, 2005).

The predictability power of nonstationary models

In the case that a nonstationary model is selected, it is important to assess its capabilities to predict statistics of future events. The discussion concerning the predictability power of the model hinges mainly around the uncertainty of future estimates. Indeed, estimations to be informative should be within an acceptable uncertainty range (Stedinger and Griffis, 2011). In the literature, two opposite positions concerning the effect of model selection on uncertainty can be identified:

1. The assumption of a nonstationarity increases the degree of uncertainty in the future, because of lack of information on how the observed trend will propagate in the future (Beven2016, Lins2011, Matalas1997, Matalas2012, Serinaldi2014a, Stedinger2011);
2. The assumption of nonstationarity, if it is modeled as a deterministic component, will induce a reduction of the uncertainty. This reduction is not acceptable when the change observed is not well understood (Koutsoyiannis2005, Koutsoyiannis2015)

1.4 Nonstationary Models

Given the importance of correctly estimating the probability of rare events and in the light of observed changes in both occurrence of and exposure to natural hazards, several studies have considered nonstationary models for extreme value analysis to address temporal changes in statistics of extremes (e.g., Katz et al., 2002; Sankarasubramanian and Lall, 2003; Mailhot et al., 2007; Huard et al., 2009; Villarini et al., 2010; Vogel et al., 2011; Zhu et al., 2012; Willems et al., 2012; Katz, 2013; Obeysekera and Salas, 2013; Salas and Obeysekera, 2014; Yilmaz and Perera, 2014; Mirhosseini et al., 2014; Cheng et al., 2014; Cheng and AghaKouchak, 2014; Volpi et al., 2015; Read and Vogel, 2015; Sadegh et al., 2015; Krishnaswamy et al., 2015; Mirhosseini et al., 2015; Mondal and Mujumdar, 2015; Lima et al., 2016; Sarhadi and Soulis, 2017; Luke et al., 2017; Salas et al., 2018; Yan et al., 2018; Bracken et al., 2018; Ragno et al., 2018). Among those, Cooley et al. (2007) proposed a spatio-temporal Bayesian hierarchical modeling approach for defining Intensity-Duration-Frequency (IDF) maps for flood management in the Front Range of Colorado. Villarini et al. (2009a) presented a framework for dealing with annual maximum peak discharge values under nonstationary conditions. Rosner et al. (2014) introduced a methodology for flood risk assessment integrating the concepts of under- and over-preparedness in a nonstationary context. Cheng et al. (2014) developed a Bayesian-based framework for analyzing time-dependent extremes. Re-

liable nonstationary analysis, however, requires understanding the deterministic process(es) causing time-variant behavior (Cohn and Lins, 2005; Koutsoyiannis, 2005; Montanari and Koutsoyiannis, 2014; Lins and Cohn, 2011; Koutsoyiannis and Montanari, 2015; Serinaldi and Kilsby, 2015). For this reason, projecting observed historical trends may lead to unreliable estimates of frequency for future extremes (Serinaldi and Kilsby, 2015; Luke et al., 2017). One limitation of the existing methodologies lies in the use of mainly observed historical data for nonstationary extreme value analysis, with some assumption on future trends. In this dissertation, this research gap is addressed and methodologies have been proposed for integrating (a) physically-based covariates; and (b) climate model projections for describing change in extremes.

1.4.1 Detection and Attribution Studies

Within the discussion about human footprint on the natural system, one of the primary uses of climate models is to investigate how the natural system would respond in the case of different forcings. Detection and attribution studies aim to identify and quantify to what extent human activities have resulted in significant changes in climate variables.

Different methodologies are adopted in attribution studies. In regression-based fingerprint methods, (Hasselmann, 1993; Hegerl et al., 1996; Zhang et al., 2007; Santer et al., 2013, e.g.,) observations are regressed onto a pattern derived from a numerical simulation with known external forcing(s). Non-fingerprint methods (e.g., Kolmogorov-Smirnov test, Cramer Von Mises test), similarly, rely on running a global climate model with known forcing(s) to reproduce a hypothetical alternative world, and then detect changes by analyzing whether observations are consistent with simulations (Knutson, 2017). Attribution studies can also rely on causality tests, such as Granger causality test (Granger, 1960), where the aim is to infer the causal relationship between external forcings, e.g., CO₂ concentration, and the

observed pattern of the climatic variable of interest, e.g. temperature (Stern and Kaufmann, 2014). Observed changes can also be attributed to changes in environmental conditions, which can be themselves attributed to the external/anthropogenic forcing, i.e. multistep attribution, (Knutson, 2017). An example could be the intensification of the water cycle, which is mainly attributed to the increase in atmosphere temperature, which in turn is caused by higher CO₂ concentration in the atmosphere as a result of human activities (Trenberth, 2011).

1.5 Improving our Understanding and Ability to Model Extremes in a Changing Climate

The threat of natural hazards on human safety and economic development is well recognized. Population growth and consequent urban expansion have increased the exposure of lives and goods to climate-related extremes. Moreover, human activities have been identified as the major driver of the observed changes in the natural variability of the climate, causing extreme events to become more frequent and more intense. The overarching goal of this dissertation is to improving our understanding and our ability to model extreme events in a changing climate.

In Chapter 2, we present a generalized, process-based and flexible statistical methodological framework for extreme value analysis considering the observed changes in the characteristics of extremes (nonstationary assumption) and their physically-based covariates/drivers (i.e., underlying processes). The latter is particularly important because changes in extremes are often linked to physical processes, which purely statistical models cannot handle. Therefore, our framework, namely Process-based Nonstationary Extreme Value Analysis (ProNEVA) model, is designed to incorporate process-based nonstationarity assumptions into extreme

value analysis. The proposed framework is flexible enough to handle models based on a user-defined covariate (process-based or temporal), so that any type of nonstationarity can be represented. ProNEVA builds upon a newly-developed hybrid evolution Markov Chain Monte Carlo (MCMC) approach for numerical parameters estimation and uncertainty assessment. This leads to more robust uncertainty estimates of return levels, return periods, and risks of climatic extremes under both stationary and nonstationary assumptions. We show the potential and versatility of ProNEVA considering four different hydroclimatic applications: peak over threshold precipitation, annual maxima discharge affected by urban expansion, annual maxima sea level, and annual maxima temperatures influenced by the CO₂ emissions in the atmosphere. The intent is to provide a modeling framework accessible to a broad audience and thus, a Graphical User Interface (GUI) of the model is also provided (see Section 2.9).

In Chapter 3, we discuss the need to communicate the uncertainty associated with extreme values estimated from statistical models used in risk assessment and infrastructure design. This uncertainty is inherent in extreme value analysis procedures because of the limited amounts of observed rare events in our records. We provide a universal chart from which decision-makers can derive the level of confidence associated with the estimated probability (or return period) of rare events. The only information required to assess the level of confidence are the length of records and the return period of the event of interest. We believe that users, including decision-makers, should be aware of the information that can be obtained from an existing record in relation to the information they are interested to infer (expected extreme events) from that same observations. Consequently, we recommend an approach that offers confidence associated with estimated rare events as a function of length of record.

In Chapter 4, we propose a framework for assessing the resilience of infrastructure and landslide hazard in a warming climate (Ragno et al., 2018). Traditionally, infrastructure design and rainfall-triggered landslide models rely on the notion of stationarity, which assume

that the statistics of extremes do not change significantly over time. However, in a warming climate, infrastructure and natural slopes will likely face more severe climatic conditions, with potential human and socio-economic consequences. Here, we outline a framework for quantifying climate change impacts based on the magnitude and frequency of extreme rainfall events using bias-corrected historical and multi-model projected precipitation extremes. The approach evaluates changes in rainfall Intensity-Duration-Frequency (IDF) curves and their uncertainty bounds using a nonstationary model based on Bayesian inference. We show that highly populated areas across the United States may experience extreme precipitation events up to 20% more intense and twice as frequent, relative to historical records, despite the expectation of unchanged annual mean precipitation.

In Chapter 5, we focus on detection and attribution of extremes. Understanding to what extent human activities have altered the occurrence of extreme events can provide insight for further studies on the physical relationship between natural variables. The methodologies available and commonly used for detection and attribution studies, however, rely on a modeling assumption of independence between climatic variables. In the real world, climatic variables or features of a natural phenomena are interdependent. To overcome this limitation, we suggest a new methodology to detect changes in a multivariate context via copula functions. The approach proposed here is applied to precipitation characteristics, i.e. intensity and duration. The method is able to account for changes in the dependence structure between pairs of variables or characteristics of the same variable, as well as changes in their absolute values. Multivariate models, such as copulas, offer an alternative tool to investigate the relationship between one variable and its covariates by directly modeling their dependence structure preserving the stochastic nature of the marginals. The capability of detecting changes in all the aspects of extreme precipitation is of great importance especially for water-related risk reduction strategies, climate change adaptation measures, and infrastructure design procedure.

Chapter 2

A Generalized Framework for Process-based Nonstationary Extreme Value Analysis

Natural hazards pose significant threats to the public safety, infrastructure integrity, natural resources, and economic development around the globe. In recent years, the frequency and impacts of extremes have increased substantially in many parts of the world (e.g., Melillo et al., 2014; Coumou and Rahmstorf, 2012; Alexander et al., 2006; Mazdiyasni et al., 2017; Mallakpour and Villarini, 2017; Hallegatte et al., 2013; Wahl et al., 2015; Vahedifard et al., 2016; Jongman et al., 2014; AghaKouchak et al., 2014b). For this reason, there is a great deal of interest in understanding how extreme events will change in the future. Historical observations are the main source of information on extremes (Klemeš, 1974; Koutsoyiannis and Montanari, 2007) and stochastic models are used to infer frequency and variability of extremes based on historical records (e.g., Katz et al., 2002).

Stochastic models used to study extremes can be broadly categorized into two groups: sta-

tionary and nonstationary (e.g., Salas and Pielke Sr, 2002; Coles and Pericchi, 2003; Griffis and Stedinger, 2007; Obeysekera and Salas, 2013; Serinaldi and Kilsby, 2015; Madsen et al., 2013; Koutsoyiannis and Montanari, 2015). In a stationary model, the observations are assumed to be drawn from a probability distribution function with constant parameters (i.e., statistics of extremes do not change over time). In a nonstationary model, however, the parameters of the underlying probability distribution function change over time or respond to a given covariate (i.e., model accounts for changes in statistics of extremes).

Water resources practices have traditionally adopted stationary models primarily for the sake of simplicity (Milly et al., 2008), though changes in the water cycle and Earth system processes are inherent (Montanari et al., 2013). Over the past decades, increasing surface temperatures (e.g., Barnett et al., 1999; Villarini et al., 2010; Melillo et al., 2014; Diffenbaugh et al., 2015; Fischer and Knutti, 2015; Mazdiyasni and AghaKouchak, 2015), more intense rainfall events (e.g., Zhang et al., 2007; Villarini et al., 2010; Min et al., 2011; Marvel and Bonfils, 2013; Westra et al., 2013; Cheng et al., 2014; Fischer and Knutti, 2016; Mallakpour and Villarini, 2017), changes in river discharge (e.g., Villarini et al., 2009a,b; Hurkmans et al., 2009; Stahl et al., 2010), and sea level rise (e.g., Holgate, 2007; Haigh et al., 2010; Wahl et al., 2011) have been observed and attributed to anthropogenic climate change. The observed hydrologic trends, which can be in response to a physical process (e.g., changes in emissions, temperatures, climatic cycles) or only perceived (statistical) (Matalas, 1997), have challenged the stationary assumption.

Several studies have promoted the idea of moving away from stationary models to ensure capturing the changing properties of extremes (Milly et al., 2008). However, some have criticized this viewpoint particularly because the assumption of nonstationarity implies adding a deterministic component in the stochastic process, which must be justified by a well-understood process (Koutsoyiannis, 2011; Matalas, 2012; Lins and Cohn, 2011; Koutsoyiannis and Montanari, 2015). Montanari and Koutsoyiannis (2014) noted that more efforts should focus on

including relevant physical processes in stochastic models, and suggested stochastic-process-based models as a way to bridge the gap between physically-based models without statistics and statistical models without physics.

Following the recommendation by Montanari and Koutsoyiannis (2014), we propose a generalized framework named *Process-based Nonstationary Extreme Value Analysis* (ProNEVA) in which the nonstationarity component is defined by a temporal or process-based dependence of the observed extremes on an explanatory variable (i.e., a physical driver). Here, process-based dependence corresponds to a process or driver that can alter the statistics of extremes. For example, ProNEVA can be used for analyzing changes in extreme temperatures using CO₂ emissions as the covariate. It is widely recognized that higher amount of CO₂ in the atmosphere results in a warmer climate (e.g., Zwiers et al., 2011; Fischer and Knutti, 2015; Barnett et al., 1999). For this reason, CO₂ emissions can be considered a process-based covariate for studying temperature extremes. Other examples include temperature or large scale climatic circulations as covariates for rainfall, and CO₂ concentration or temperature as covariates for sea level rise.

2.1 Method

2.1.1 Process-Based Nonstationarity Extreme Value Analysis

Extreme Value Theory (EVT) provides the bases for estimating the magnitude and frequency of hazardous events (including natural and non-natural extreme events) (Coles, 2001). Most applications utilize either the Generalized Extreme Value distribution (GEV) or the Generalized Pareto distribution (GP) for describing the behavior of extremes. The former is applied to the annual maxima of a variable (e.g., a time series consisting of the most extreme daily rainfall from each year of the record), while the latter is used to describe extremes

above a predefined threshold (e.g., all independent river flow values above the flood stage). Both GEV and GP allow incorporating nonstationarity through varying parameters. Several studies have investigated methodologies for testing the assumptions of stationarity and nonstationarity in hydrology, climatology, and earth system sciences (e.g., Katz et al., 2002; Sankarasubramanian and Lall, 2003; Cooley et al., 2007; Mailhot et al., 2007; Huard et al., 2009; Villarini et al., 2009a, 2010; Vogel et al., 2011; Zhu et al., 2012; Willems et al., 2012; Katz, 2013; Obeysekera and Salas, 2013; Salas and Obeysekera, 2014; Rosner et al., 2014; Yilmaz and Perera, 2014; Mirhosseini et al., 2014; Cheng and AghaKouchak, 2014; Volpi et al., 2015; Read and Vogel, 2015; Sadegh et al., 2015; Krishnaswamy et al., 2015; Mirhosseini et al., 2015; Mondal and Mujumdar, 2015; Lima et al., 2016; Sarhadi and Soulis, 2017; Salas et al., 2018; Yan et al., 2018; Bracken et al., 2018; Ragno et al., 2018).

A number of packages and software tools are currently available including the R (Team, 2013) package *ismev* (Gilleland et al., 2013; Gilleland and Katz, 2016) where nonstationarity is modeled as linear regression function of generic covariates (Gilleland et al., 2013). The package *extRemes* - version ≥ 2.0 offers EVA capability and evaluates the underlying uncertainties with respect to parameters (Gilleland and Katz, 2016). *extRemes* also allows a tail-dependence analysis and a declustering technique for peak over threshold analysis. The package *climextRemes* (available also in Python) builds upon *extRemes* and includes an estimate of the risk ratios for event attribution analyses. R packages *vgam* and *gamlss* are available for modeling nonstationarity through generalized additive models (see for example Villarini et al. (2009a)). The package *GEVcdn* estimates the parameters of a nonstationary GEV distribution using a conditional density method (Cannon, 2010), and it is specific for hydroclimate variables.

Cheng et al. (2014) developed a Bayesian-based framework, *Nonstationary Extreme Value Analysis* (NEVA) toolbox for estimating the parameters of a GEV and GP distributions for time-dependent extremes along with uncertainty quantification (available in Matlab Matlab

(2017)). In the nonstationary case, the parameters are modeled as a linear function of time. NEVA plots return level curves based on the concept of expected waiting time (Wigley, 2009; Olsen et al., 1998; Salas and Obeysekera, 2014) and effective return level (Katz et al., 2002). The package *nonstationary Flood Frequency Analysis* estimates the parameters of the Log-Pearson Type III distribution as a linear function of time, based on Bayesian inference approach (Luke et al., 2017). The *tsEVA* toolbox implements the Transformed-Stationary (TS) methodology described in Mentaschi et al. (2016), which comprises of, first, a transformation of a nonstationary time series into a stationary one, so that the stationary EVA theory can be applied, and then a reverse-transformation of the results to include the nonstationary components in the GEV and the GP distributions.

However, the existing tools for implementing EVA under the nonstationary assumption have a number of limitations, mainly lack of a generalized framework for incorporating physically based covariates. Moreover, most existing tools are incapable of handling the estimation of parameters which depend on a generic physical covariate (e.g., when the parameters are estimated as a non-linear function of a covariate). To address the above limitations, we present ProNEVA, which builds upon NEVA package (Cheng et al., 2014) but expands to process-based nonstationary extreme value analysis. In addition to stationary EVA, ProNEVA allows nonstationary analysis using both time and a physical covariate. Using time indicates that changes in a variable over time will be used for EVA, where as in the latter, changes of a variable in response to a physical driver will be considered. Figure 2.1 depicts the core structure of ProNEVA.

ProNEVA offers parameter estimation, uncertainty quantification, and a comprehensive assessment of the goodness of fit. The key features of ProNEVA are described as follows: (a) the model includes the most common distribution functions used for extreme value analysis including the GEV, GP, and LP3 distributions; (b) for nonstationary analysis, the users can select both the covariate and the choice of function for describing change in parameters;

(c) the covariate can be any user-defined physical covariate; (d) the model also includes a default time-covariate (i.e., describing change over time without a physical covariate); (e) the function describing change in parameters with respect to the covariate can be linear, exponential, or quadratic; (f) the users can select the GP distribution threshold (peak-over-threshold) as a constant value or as a linear quantile regression function of the choice covariate; (g) ProNEVA estimates the distribution parameters based on a Bayesian inference approach; (h) the model allows using a wide range of priors for parameters including the uniform, normal, and gamma distributions; (i) ProNEVA samples from the posterior distribution function of the parameters using a newly-developed hybrid evolution Markov Chain Monte Carlo (MCMC) approach (Sadegh et al., 2017), which provides a more robust numerical parameter estimation and uncertainty quantification; (j) different model diagnostics and model selection indices (e.g., RMSE, AIC, BIC) are implemented to provide supporting information; (k) ProNEVA includes additional exploratory data analysis tools such as the Mann-Kendall test for monotonic trends and the White test for homoscedasticity in time series; (l) in addition to the source code, a Graphical User Interface (GUI) for ProNEVA is also available for easier implementation (Section 2.9); (m) finally, ProNEVA is intended for a broad audience and hence, it is structured such that the users can easily customize and modify it based on their needs.

In the reminder of the paper, a detailed description of ProNEVA is provided. Four different example application are presented with different variables (e.g., precipitation, sea levels, temperature, river discharge) and different covariates (time, CO₂ emissions in the atmosphere, urbanization). ProNEVA can be used for analyzing annual maxima (also known as block maxima) using the GEV and LP3 distributions, and peaks over threshold (POT) or partial duration series using the GP distribution. In the following, we provide a brief overview of the extreme value models and their parameters.

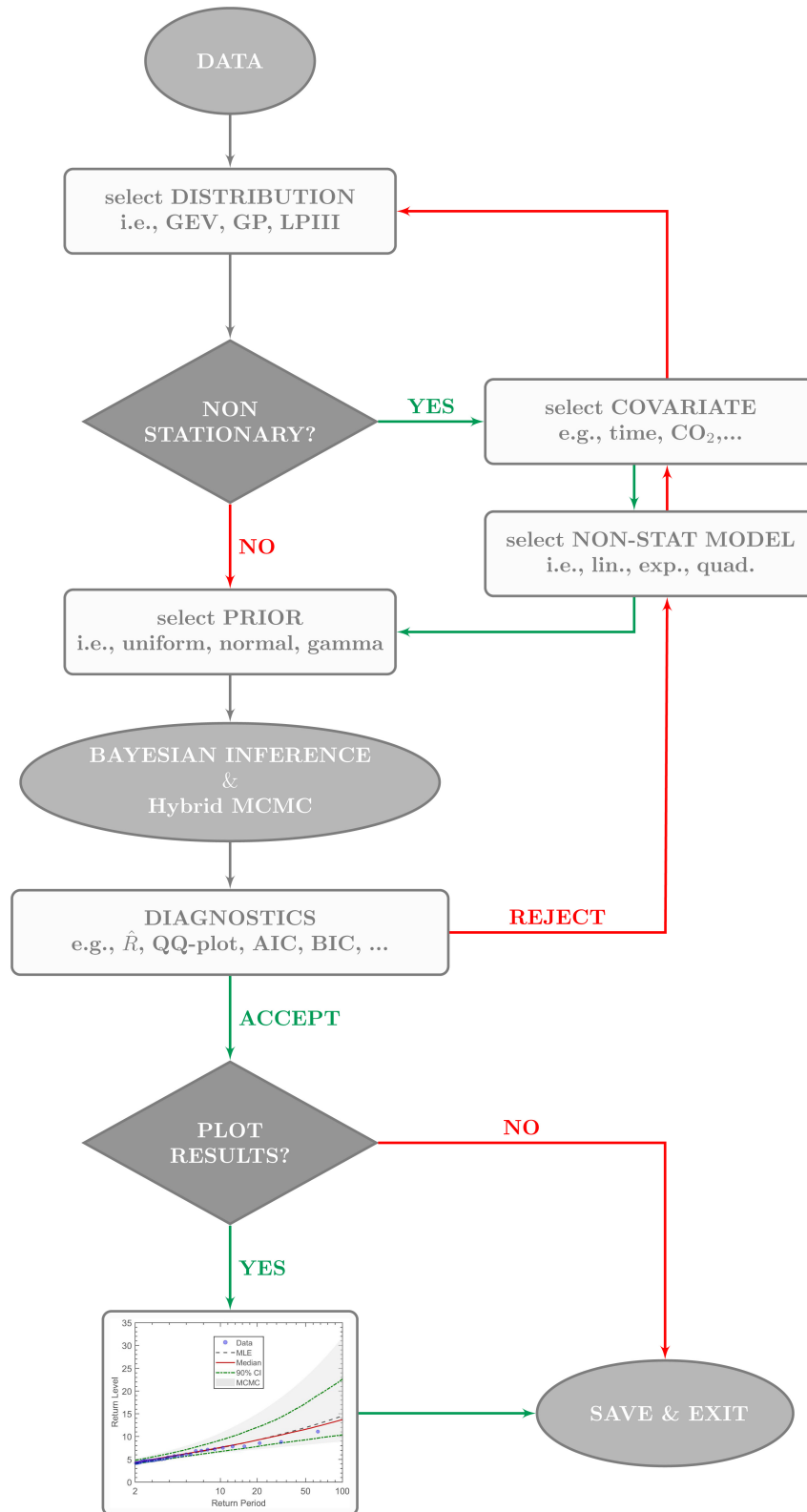


Figure 2.1: Flowchart representing the core structure of the Matlab Toolbox ProNEVA

2.1.2 Generalized Extreme Value (GEV)

The GEV function is used for block maxima time series. The National Oceanic and Atmospheric Administration (NOAA), for example, derives precipitation Intensity-Duration-Frequency (IDF) curves based on the GEV distribution. GEV is also widely used in other fields including bridge performance assessment (e.g., Ming et al., 2009), among others. The GEV cumulative distribution function is (Coles, 2001):

$$\Psi_{GEV}(X) = \exp\left\{-\left(1 + \xi \cdot \left(\frac{X - \mu}{\sigma}\right)\right)^{-\frac{1}{\xi}}\right\} \quad (2.1)$$

for $\xi \cdot \left(\frac{X - \mu}{\sigma}\right) > 0$. μ , σ , and ξ are the parameters of the distribution: μ is the location parameter and represents the center of the distribution; $\sigma > 0$ is the scale parameter and describes the distribution of the data around μ ; ξ is the shape parameter and defines the tail behavior of the distribution.

The stationary GEV model can be extended for dependent series by letting the parameters of the distribution be a function of a general covariate X_c , i.e., $\mu(X_c)$, $\sigma(X_c)$, $\xi(X_c)$, (Coles, 2001). Hence, the nonstationary form of eq. 2.1 is described as:

$$\Psi_{GEV}(X|X_c) = \exp\left\{-\left(1 + \xi(X_c) \cdot \left(\frac{X - \mu(X_c)}{\sigma(X_c)}\right)\right)^{-\frac{1}{\xi(X_c)}}\right\} \quad (2.2)$$

For each of the three parameters, the users can select a function to describe change in parameters with respect to time or a covariate (Table 2.1). The function for each parameter does not constrain the functional relationship used for the other parameters. To ensure the positivity of the scale parameter, $\sigma(X_c)$ is modeled in the log-scale, (Coles, 2001; Katz, 2013). Consequently, the exponential function is not available for $\sigma(X_c)$. Moreover, the shape parameter $\xi(X_c)$ is known to be a difficult parameter to precisely estimate even in the stationary case, (Coles, 2001), especially for short time series, (Papalexiou and Koutsoyiannis, 2013).

Table 2.1: GEV dependence models

type	model	$\mu(X_c)$	$\ln(\sigma(X_c))$	$\xi(X_c)$
Linear	$B_l \cdot X_c + A_l$	✓	✓	✓
Quadratic	$C_q \cdot X_c^2 + B_q \cdot X_c + A_q$	✓	✓	—
Exponential	$A_e \cdot \exp(B_e \cdot X_c)$	✓	—	—

For this reason, only the linear function is included for $\xi(X_c)$.

2.1.3 Generalized Pareto (GP)

The GP distribution is used for time series sampled based on the POT method. GP is widely used for studying extreme wind speeds when storms exceeding a certain wind speed are of interest (Holmes and Moriarty, 1999). The GP distribution has also been applied to precipitation (e.g., De Michele and Salvadori, 2003a) earthquake data (e.g., Pisarenko and Sornette, 2003) and economic data (e.g., Gençay and Selçuk, 2004), among others. The GP cumulative distribution function is as follows (Coles, 2001):

$$\Psi_{GP}(X) = 1 - \left(1 + \xi \cdot \left(\frac{X - u}{\sigma}\right)\right)^{-\frac{1}{\xi}} \quad (2.3)$$

for a large enough threshold, u , such that $X > u$, $\sigma > 0$ and $\left(1 + \xi \cdot \left(\frac{X - u}{\sigma}\right)\right) > 0$. In particular, if \mathbf{X} is a block maxima series following a GEV distribution, then the threshold excesses $\{X > u\}$ have a GP distribution. The parameter ξ of the GP distribution is equal to the parameter ξ of the corresponding GEV distribution (Coles, 2001).

In the nonstationary model of the GP distribution, both the threshold value and the parameters of the distribution can be modeled as a function of the user-covariate, (Coles, 2001).

$$\Psi_{GP}(X|X_c) = 1 - \left(1 + \xi(X_c) \cdot \left(\frac{X - u(X_c)}{\sigma(X_c)}\right)\right)^{-\frac{1}{\xi(X_c)}} \quad (2.4)$$

Table 2.2: GP dependence models

type	model	$u(X_c)$	$\ln(\sigma(X_c))$	$\xi(X_c)$
Linear	$B_l \cdot X_c + A_l$	$\checkmark^{(*)}$	\checkmark	\checkmark
Quadratic	$C_q \cdot X_c^2 + B_q \cdot X_c + A_q$	—	\checkmark	—

(*) Regression quantile (Koenker and Bassett, 1978)

Analogously to the GEV case, ProNEVA allows incorporating different functional forms for describing change in parameters over time or with respect to a covariate (Table 2.2). The same considerations for the GEV parameter functional forms are applied to GP distribution too. In addition, the users can specify the type of threshold u . Two quantile-based options are available: constant or linear. In the case of a linear threshold, a linear regression quantile model is adopted. The α -regression quantile function is (Koenker and Bassett, 1978; Kyselý et al., 2010)

$$\mathbf{Y} = \mathbf{X} \cdot \mathbf{U}(\alpha) + \mathbf{r}^+ - \mathbf{r}^- \quad (2.5)$$

where $0 < \alpha < 1$ is the quantile, \mathbf{Y} is the column vector of n -observations, $\mathbf{X} = [\mathbf{X}_c \quad \mathbf{I}_n]$ with \mathbf{X}_c being the column vector of covariance and \mathbf{I}_n the n -identity vector, $\mathbf{U} = [u_1 \quad u_0]'$ is the vector of the regression coefficients, and \mathbf{r}^+ and \mathbf{r}^- are respectively the positive and negative parts of the residuals. Then, $\mathbf{U}(\alpha)$ is calculated as the optimal solution to eq. 2.6 (Koenker and Bassett, 1978; Kyselý et al., 2010).

$$\alpha \cdot \mathbf{I}_n' \cdot \mathbf{r}^+ + (1 - \alpha) \cdot \mathbf{I}_n' \cdot \mathbf{r}^- := \min \quad (2.6)$$

2.1.4 Log-Pearson Type III (LP3)

The LP3 distribution has been widely used in hydrology for flood frequency analysis after the release of the USGS Bulletin 17B (U.S. Water Resources Council, 1982). However, it has been applied to other studies, such as design magnitude of earthquakes (Gupta and

Deshpande, 1994) and evaluation of apple bud burst time and frost risk (Farajzadeh et al., 2010).

The LP3 distribution characterizes the random variable $Q = \ln(X)$, given that X follows a Pearson type III (P3) distribution (Griffis et al., 2007). Hereafter, the base-e logarithm is used, however any base can be implemented, such as base-10 as in Bulletin 17B (Griffis et al., 2007). The P3 probability density function is

$$\psi_{P3}(X) = \frac{1}{|\beta| \cdot \Gamma(\alpha)} \cdot \left(\frac{X - \tau}{\beta} \right)^{\alpha-1} \cdot \exp \left(- \frac{X - \tau}{\beta} \right) \quad (2.7)$$

defined for $\alpha > 0$, $(X - \tau)/\beta > 0$, and $\Gamma(\alpha)$ being a complete gamma function (Griffis et al., 2007). The parameters α , β , and τ are functions of the first three moments, μ_X , σ_X , γ_X , (Griffis et al., 2007):

$$\alpha = 4/\gamma_X^2 \quad (2.8)$$

$$\beta = (\sigma_X \cdot \gamma_X)/2 \quad (2.9)$$

$$\tau = \mu_X - 2 \cdot (\sigma_X/\gamma_X) \quad (2.10)$$

In the case of nonstationary analysis, the first three moments are modeled as a function of the user-defined covariate \mathbf{X}_c (Table 2.3). The GEV and GP considerations mentioned above hold for the functions to describe change in parameters.

$$\psi_{P3}(X|X_c) = \frac{1}{|\beta(X_c)| \cdot \Gamma(\alpha(X_c))} \cdot \left(\frac{X - \tau(X_c)}{\beta(X_c)} \right)^{\alpha(X_c)-1} \cdot \exp \left(- \frac{X - \tau(X_c)}{\beta(X_c)} \right) \quad (2.11)$$

Table 2.3: LP3 dependence models

type	model	$\mu_X(X_c)$	$\ln(\sigma(X_c))$	$\gamma(X_c)$
Linear	$B_l \cdot X_c + A_l$	✓	✓	✓
Quadratic	$C_q \cdot X_c^2 + B_q \cdot X_c + A_q$	✓	✓	—
Exponential	$A_e \cdot \exp(B_e \cdot X_c)$	✓	—	—

2.2 Parameter Estimation: Bayesian Analysis and Markov Chain Monte Carlo Sampling

ProNEVA estimates the parameters of the selected (non)stationary EVA distribution using a probabilistic-based approach, which provides a better characterization of the underlying uncertainty derived from both input errors and model selection. Bayesian analysis has been widely implemented for parameter inference and uncertainty quantification (e.g. Thiemann et al., 2001; Gupta et al., 2008; Cheng et al., 2014; Kwon and Lall, 2016; Sarhadi et al., 2016; Sadegh et al., 2017; Luke et al., 2017)

Let θ be the parameter of a given distribution and let $\mathbf{Y} = \{y_1, \dots, y_n\}$ be the set of n observations. Following Bayes theorem, the probability of θ given \mathbf{Y} (posterior) is proportional to the product of the probability of θ (prior) and the probability of \mathbf{Y} given θ (likelihood function). Assuming independence between the observations \mathbf{Y} :

$$p(\theta|\mathbf{Y}) \propto \prod_{i=1}^n p(\theta) \cdot p(y_i|\theta) \quad (2.12)$$

The prior brings priori information, which do not depend on the observed data, into the parameter estimation process. The choice of the prior distribution, then, is somehow subjective. The available prior options in ProNEVA include the uniform, normal, and gamma distributions, providing a variety of possibilities. ProNEVA assumes independence of parameters and hence, each parameter requires its own prior.

The likelihood function coincides with the probability density function of the distribution family (i.e. GEV, GP, or LP3) as representative of the data.

In the case of a nonstationary analysis, the vector of parameters θ includes a higher number of elements than in the stationary case, depending on the functional form selected for each of the distribution's parameters.

The posterior distribution is then delineated using a hybrid-evolution MCMC approach proposed by Sadegh et al. (2017). The MCMC simulation searches for the region of interest with multiple chains running in parallel, which share information on the fly. Moreover, the hybrid-evolution MCMC benefits from an intelligent starting point selection (Duan et al., 1993) and employs Adaptive Metropolis (AM) (Roberts and Sahu, 1997; Haario et al., 1999, 2001; Roberts and Rosenthal, 2009), differential evolution (DE) (Storn and Price, 1997; Ter Braak and Vrugt, 2008; Vrugt et al., 2009), and snooker update (Gilks et al., 1994; Ter Braak and Vrugt, 2008) algorithms to search the feasible space. The Metropolis ratio is selected to accept/reject the proposed sample, and the \hat{R} informs on the convergence of the chains, which should remain below the critical threshold of 1.1 (Gelman and Shirley, 2011; Cheng et al., 2014). For a more detailed description of the algorithm, the reader is referred to Sadegh et al. (2017).

2.3 Model Diagnostics and Selection

The purpose of fitting a statistical model, whether it is stationary or nonstationary, is to characterize the population from which the data was drawn for further analysis/inference (Coles, 2001). Hence, it is necessary to check the performance of the fitted model to the data (Coles, 2001). We implemented different matrices in the ProNEVA for goodness of fit (GOF) assessment and model selection including: quantile and probability plots for a graph-

Table 2.4: Standard Transformations

Statistical Model	Transformation	Reference Distribution
$Z_t(\tilde{\mu}(t), \tilde{\sigma}(t), \tilde{\xi}(t)) \sim GEV$	$\tilde{Z}_t = \frac{1}{\tilde{\xi}(t)} \cdot \left\{ 1 + \tilde{\xi}(t) \cdot \left(\frac{Z_t - \tilde{\mu}(t)}{\tilde{\sigma}(t)} \right) \right\}$	Std. Gumbel ⁽¹⁾
$Z_t(\tilde{u}(t), \tilde{\sigma}(t), \tilde{\xi}(t)) \sim GP$	$\tilde{Z}_t = \frac{1}{\tilde{\xi}(t)} \cdot \left\{ 1 + \tilde{\xi}(t) \cdot \left(\frac{Z_t - \tilde{u}(t)}{\tilde{\sigma}(t)} \right) \right\}$	Std. Exponential ⁽¹⁾
$Z_t(\tilde{\alpha}(t), \tilde{\beta}(t), \tilde{\tau}(t)) \sim P3$	$\tilde{Z}_t = \frac{Z_t - \tau(t)}{\beta(t)}$	Std. Gamma ⁽²⁾

⁽¹⁾ Coles (2001) ⁽²⁾ Koutrouvelis and Canavos (1999)

ical assessment, two-sample Kolmogorov-Smirnov (KS) test, Aikake Information Content (AIC), Bayesian Information Critiria (BIC), Maximum Likelihood (ML), Root Mean Square Error (RMSE), and Nash-Sutcliff Efficiency (NSE) coefficient. The hybrid-evolution MCMC approach (Sadegh et al., 2017) within the Bayesian framework provides an ensemble of solutions for the (non)stationary statistical model fitted to the data. ProNEVA uses the best set of parameters, $\hat{\theta}$, which maximizes the posterior distribution. Marginal posteriors will then provide uncertainty estimates of the estimated parameters.

2.3.1 Standard Transformation

When applied to nonstationary applications, the homogeneity in the distributional assumption requires an adjustment to the traditional GOF techniques (Coles, 2001). Consequently, ProNEVA standardizes the observations based on the underlying distribution family such that the GOF tests can be performed. Table 2.4 provides information on the transformation methods in ProNEVA. However, it is worth noting that the choice of the reference distribution is arbitrary (Coles, 2001). Here, we selected those transformations that are widely accepted in the literature (Coles, 2001; Koutrouvelis and Canavos, 1999). In the case of a LP3 distribution, the transformation can only be applied when the parameter α is constant (Koutrouvelis and Canavos, 1999). Based on Equation 2.8, this implies that the transformation can be performed only in the case of constant skewness γ_X .

2.3.2 Probability and Quantile Plots

The probability plot and quantile plot are graphical techniques for evaluating the goodness-of-fit of models. Given an ordered set of n random observations $z_{(1)} < \dots < z_{(n)}$, the empirical estimate of the probability of $z_{(i)}$ is $\bar{F}_i = i/(n+1)$, where $(n+1)$ guarantees $\bar{F}_i \neq 1$ (Coles, 2001). Assuming \hat{F} as the estimated unknown distribution function of the population, the probability plot consists of the points (Coles, 2001)

$$\left\{ \left(\hat{F}(z_{(i)}); \frac{i}{n+1} \right) : i = 1, \dots, n \right\} \quad (2.13)$$

Analogously, the quantile plot contains the points (Coles, 2001)

$$\left\{ \hat{F}^{-1}\left(\frac{i}{n+1}\right); z_{(i)} \right\} : i = 1, \dots, n \quad (2.14)$$

In both the probability and quantile plots, \hat{F} is a reasonable fit if the points are close along the unit diagonal (Coles, 2001). Moreover, both plots provide the same information, however on a different scale. Indeed, it is important to investigate both scales, because what seems an acceptable fit in one scale could be a poor fit in the other (Coles, 2001).

2.3.3 Kolmogorov-Smirnov Test

The two-sample Kolmogorov-Smirnov (KS) test is a non-parametric hypothesis testing technique which compares two samples, $Z^{(1)}$ and $Z^{(2)}$, to assess whether they belong to the same population (Massey, 1951). Being $F_{Z^{(1)}}(z)$ and $F_{Z^{(2)}}(z)$ the (unknown) statistical distributions of $Z^{(1)}$ and $Z^{(2)}$ respectively, the null-hypothesis H_0 is $F_{Z^{(1)}}(z) = F_{Z^{(2)}}(z)$, against alternatives. The KS test statistics D^* is:

$$D^* = \max_x (|F_{Z^{(1)}}(z) - F_{Z^{(2)}}(z)|) \quad (2.15)$$

H_0 is rejected when the p_{value} of the test is equal to or exceeds the selected α -level of significance, e.g., 5%. We implemented the KS test in ProNEVA as one of the methods to test the goodness-of-fit of the model. Specifically, ProNEVA generates 1000 random samples from the fitted statistical distribution or, in the case of a nonstationary analysis, from the reference distribution. Then, the KS test is performed between the random samples and the input (original or transformed) data. Finally, the rejection rate (RR), eq. 2.16, is provided as a GOF index.

$$RR = \frac{\sum(H_0 \text{ rejected})}{1000} \quad (2.16)$$

2.3.4 Model Selection based on Model Complexity

Numerical models showing a desirable level of performance efficiency with a minimum number of parameters, e.i. parsimonious models (Serago and Vogel, 2018), are usually preferred and, in the case of a nonstationary analysis, have shown to perform better (Serinaldi and Kilsby, 2015; Luke et al., 2017). Consequently, ProNEVA evaluates different GOF matrices (i.e., AIC, BIC), which account for the number of parameters within the numerical model. The Akaike Information Criterion (AIC) (Akaike, 1974, 1998; Aho et al., 2014) is formulated as follows

$$AIC = 2 \cdot (D - \hat{L}) \quad (2.17)$$

where D is the number of parameters of the statistical model and \hat{L} is the log-likelihood function evaluated at $\hat{\theta}$. The model associated with a lower AIC is considered a better fit.

The Bayesian Information Content (BIC) (Schwarz, 1978) is defined as

$$BIC = D \cdot \ln(N) - 2 \cdot \hat{L} \quad (2.18)$$

where N is the length of records. Similar to AIC, the model with lower BIC results a better fit.

2.3.5 Model Selection based on Minimum Residual

Root Mean Square Error (RMSE) and Nash-Sutcliffe Efficiency (NSE) coefficient are two matrices widely used in hydrology and climatology as GOF measurements. The focus of both is to minimize the residuals. The vector of residual **RES** is

$$\mathbf{RES} = \left(\left(\hat{F}^{-1}\left(\frac{1}{n+1}\right) - z_{(1)} \right), \dots, \left(\hat{F}^{-1}\left(\frac{i}{n+1}\right) - z_{(i)} \right), \dots, \left(\hat{F}^{-1}\left(\frac{n}{n+1}\right) - z_{(n)} \right) \right); \quad (2.19)$$

following the same notation used for defining the quantile plot. Hence,

$$RMSE = \sqrt{\frac{\sum_{i=1}^n RES_i^2}{n-1}} \quad (2.20)$$

$$NSE = 1 - \frac{\sum_{i=1}^n RES_i^2}{\sum_{i=1}^n (z_{(i)} - \text{mean}(z))^2} \quad (2.21)$$

A perfect fit is considered when $RMSE = 0$, $RMSE \in [0, \infty)$, and $NSE = 1$, $NSE \in [-\infty, 1)$.

2.4 Predictive Distribution

The primary objective of a statistical inference is to predict unobserved events (Renard et al., 2013). EVA, for example, provides the basis for estimating loads for infrastructure design and risk assessment of natural hazards (e.g., floods, extreme rainfall events). Considering a

Bayesian viewpoint, the predictive distribution can be written as (Renard et al., 2013):

$$f(\mathbf{z}|\mathbf{X}) = \int f(\mathbf{z}, \boldsymbol{\theta}|\mathbf{X}) \cdot d\boldsymbol{\theta} = \int f(\mathbf{z}|\boldsymbol{\theta}) \cdot f(\boldsymbol{\theta}|\mathbf{X}) \cdot d\boldsymbol{\theta} \quad (2.22)$$

where \mathbf{X} is the observed data, \mathbf{z} is a grid at which $f(\mathbf{z}|\mathbf{X})$ will be evaluated, $\boldsymbol{\theta}$ is the vector of parameters, $f(\mathbf{z}|\boldsymbol{\theta})$ is the pdf of the selected distribution (i.e., GEV, GP, LP3), and $f(\boldsymbol{\theta}|\mathbf{X})$ is the posterior distribution function. The predictive distribution function relies on the fitted distribution function over the parameter space, and uses the posterior distribution for uncertainty estimation (Renard et al., 2013). In practice, eq. 2.22 often cannot be derived analytically. Therefore, Renard et al. (2013) suggest to numerically evaluate it using the MCMC ensemble of solutions sampled from the posterior distribution. The probability density of the k th-element of the vector \mathbf{z} is:

$$\hat{f}(z_k|\mathbf{X}) = \frac{1}{N_{sim}} \cdot \sum_{i=1}^{N_{sim}} f(z_k|\theta_i) \quad (2.23)$$

In the nonstationary case, predictive pdf is a function of the covariate, since the distribution parameters depend on the covariates. For this reason and for a matter of representation, ProNEVA provides the predictive pdf for a number of predefined values of the covariates.

2.5 Return Level Curves under Nonstationarity

Given a time series of annual maxima, the Return Level (RL) is defined as the quantile Q_i for which the probability of an annual maximum exceeding the selected quantile is q_i (Cooley, 2013). Under the stationary assumption, the characteristics of the statistical model are constant over time, meaning that the probability q does not change on a yearly basis. The concept of Return Period (RP) is defined as the inverse of the probability of exceedance, $T_i = \frac{1}{q_i}$ in years. For example, assuming $T_i=100$ year for an event indicates that the event has

0.01 probability of occurrence in each year (Cooley, 2013). Under the stationary assumption, there is a one-to-one relationship between RL and RP (Cooley, 2013). Therefore, the RL curves are defined by the following points:

$$\left((T_i; Q_i), \quad T_i > 1yr, \quad i = 1, \dots \right) \quad (2.24)$$

RL curves are traditionally used for defining extreme design loads for infrastructure design and risk assessment of natural hazards. However, in a nonstationary context both RP and RL terms become ambiguous (Cooley, 2013) and numerous studies have attempted to address the issue. For nonstationary analysis, ProNEVA integrates two different proposed concepts: the expected waiting time (Salas and Obeysekera, 2014), for default time-covariate only, and the effective RL curves Katz et al. (2002).

2.5.1 Effective Return Level

Katz et al. (2002) proposed the concept of effective design value (or effective return level), which is defined as q -quantile, Q varying as a function of the covariate (i.e, time or physical). Therefore, for a constant value of $RP = 1/q$, where q is the yearly exceedance probability, the effective RL curves is defined by the points

$$\left((x_c, Q_q(x_c)), \quad q \in [0, 1] \right) \quad (2.25)$$

where x_c is the covariate, and $Q_q(x_c)$ is the q -quantile.

2.5.2 Expected Waiting Time

Wigley (2009) firstly introduced the concept of waiting time, i.e., the expected waiting time until an event of magnitude Q_i is exceeded, in which the probability of exceedance in each year, q_i , changes over time. Olsen et al. (1998) and, later, Salas and Obeysekera (2014) provided a comprehensive mathematical description of the suggested concept.

The event Q_{q_0} is defined as the event with the exceedance probability at time $t = 0$ equal to q_0 . Under nonstationary conditions, at time $t = 1$ the probability of exceedance of Q_{q_0} will be q_1 , at time $t = 2$, it will be q_2 , and so on. Given the selected statistical model F_Q with characteristics θ_t , $q_t = 1 - F_Q(Q_{q_0}, \theta_t)$. Hence, the probability of the event to exceed Q_{q_0} at time m is given by (Salas and Obeysekera, 2014):

$$f(m) = q_m \cdot \prod_{t=1}^{m-1} (1 - q_t) \quad (2.26)$$

where $f(1) = q_1$ and $f(m) = 1$. The cumulative distribution function (cdf) of a geometrical distribution (eq. 2.26) is:

$$F_X(x) = \sum_{i=1}^x f(i) = \sum_{i=1}^x q_i \cdot \prod_{t=1}^{i-1} (1 - q_t) = 1 - \prod_{t=1}^x (1 - q_t) \quad (2.27)$$

where x is the time at which the event occurs, $x = 1, \dots, x_{max}$, $F_X(1) = q_1$, and $F_X(x_{max}) = 1$. Therefore, the expected waiting time (or RP) in which for the first time the occurring event exceeds Q_{q_0} can be derived as

$$T = E(X) = \sum_{x=1}^{x_{max}} x \cdot f(x) = \sum_{x=1}^{x_{max}} x \cdot p_x \prod_{t=1}^{x-1} (1 - p_t) \quad (2.28)$$

Cooley (2013) simplifies eq. (2.28) as:

$$T = E(X) = 1 + \sum_{x=1}^{x_{max}} \prod_{t=1}^{x-1} (1 - p_t) \quad (2.29)$$

which gives the return period under nonstationary conditions, and it is consistent with the definition of RP in the stationary case (Salas and Obeysekera, 2014).

2.6 Explanatory Analysis: Mann-Kendall and White Tests

With the intention of providing additional explanatory data analysis, ProNEVA includes two different tests including the Mann-Kendall (MK) monotonic trend test and the White Test (WT) for evaluating homoscedasticity in the record. These tests can be used to decide whether to incorporate a trend function in one or more of the model parameters or not (i.e., deciding whether to use a stationary or nonstationary model). However, these tests are optional and are not an integral part of ProNEVA.

2.6.1 Mann-Kendall

MK trend test is a widely used test for detecting temporal monotonic changes in the data (Mann, 1945; Kendall, 1955) and thus, it has been applied for detecting nonstationarity in time series (Villarini et al., 2009a; Cheng et al., 2014). MK evaluates the monotonic trend of the time series $\mathbf{X} = \{x_1, \dots, x_i, \dots, x_n\}$ based on the Kendall's S -statistics, which is the difference between the numbers of concordant and discordant pairs (Villarini et al., 2009a),

$$S = \sum_{i < j} \text{sign}(x_i - x_j) \quad (2.30)$$

In the case when \mathbf{X} is independently and randomly distributed, $S = 0$ (Villarini et al., 2009a). For large samples, S tends to normality, and so it is possible to test the Null-Hypothesis (H_0) of no monotonic trend ($S = 0$) against the alternative, at the α -level of significance. This test is most useful for temporal nonstationary analysis. When using a process-based covariate, however, ProNEVA replaces the MK test with the zero slope test for a linear regression model between the time series of the data \mathbf{X} and the covariate \mathbf{X}_c (Shumway and Stoffer, 2011). Given $\hat{\beta}_1$ the estimated slope parameter and β_1 the true value:

$$t_{n-2} = \frac{\hat{\beta}_1 - \beta_1}{s_{\beta_1}} = \frac{\hat{\beta}_1}{s_{\beta_1}} \quad (2.31)$$

where s_{β_1} is the standard error of β_1 , n is the number of observations, and t_{n-2} is a t-distribution with $n-2$ degrees of freedom. $H_0: \beta_1 = 0$ is performed at 5% level of significance.

2.6.2 White Test

Given the regression model:

$$\mathbf{y} = \beta_0 + \beta_1 \cdot \mathbf{x}_c + u \quad (2.32)$$

the homoscedasticity assumption requires that $var\{u^2|\mathbf{x}_c\} = \sigma^2$. In the case of heteroscedasticity then, the residuals of a linear regression model will vary with the dependent variable \mathbf{x}_c , (Wooldridge, 2002). White (1980) proposed a test, the WT for heteroscedasticity, based on the estimation of u as (Wooldridge, 2002):

$$\mathbf{u}^2 = \delta_0 + \delta_1 \cdot \hat{\mathbf{y}} + \delta_2 \cdot \hat{\mathbf{y}}^2 + error \quad (2.33)$$

where $\hat{\mathbf{y}}$ is the fitted value $\hat{\mathbf{y}} = \beta_0 + \beta_1 \cdot \mathbf{x}$. H_0 is then $\delta_1 = 0$, $\delta_2 = 0$. Being $R_{u^2}^2$ the *R-squared* for the regression in equation 2.33, the Lagrange Multiplier (LM) statistic is

calculated as:

$$LM = n \cdot R_{u^2}^2 \quad (2.34)$$

which follow a χ_2^2 distribution. The test is performed at a 5% level of significance.

2.7 Results

As previously discussed, the changes in extremes observed over the past years can derive from different physical processes. In order to account for the observed changes, we need statistical tools that are able to incorporate the source of variability, which can be represented as time-covariate or a physical-based covariate. In the following, we show example applications of ProNEVA under both stationay and nonstationary assumptions including modeling changes induced by different type of covariates (both temporal and process-based changes).

In the first application, we analyze discharge data from Ferson Creek (St. Charles, IL), which has experienced intense urban development over the years. Urbanization has a direct effect on the amount of water discharged at the catchment outlet, since it increases impervious surfaces. For this reason, we use a process-based nonstationary LP3 model for fitting discharge data, in which the covariate is represented by percent of urbanized catchment area. The second application involves temperature maxima data averaged over the Contiguous United States. Many studies have shown that the amount of CO₂ in the atmosphere causes temperatures to increase. For this reason, we fit temperature data to a nonstationary GEV model, in which the covariate is represented by CO₂ emissions in the atmosphere to include the known physical relationship. In the third application, we investigate sea level in the city of Trieste (Italy), which has increased over the years. In this case, we adopted a temporal nonstationary GEV model. The last application involves precipitation data for New Or-

leans, LA in which we fit a stationary GP model, given that there is no evidence of change in statistics of extremes.

2.7.1 Application 1: Modeling discharge with urbanization as the physical driver

Since 1980, Ferson Creek (St. Charles, IL) basin has experienced land use land cover changes due to urbanization. The percent of urban areas within the catchment has increased from 20% in 1980 to almost 65% in 2010. River discharge highly depends on the land use and land cover of the basin as it determines the ratio of infiltration to direct runoff (Figure 2.2). Here, urbanization can be considered as a known physical process that has altered the runoff in the basin. To incorporate the known physical process, we investigate annual maxima discharge of the Ferson Creek (station USGS 05551200) using a process-based nonstationary LP3 model, in which the covariate, X_c , is the percent of urbanized area. LP3 is widely used for

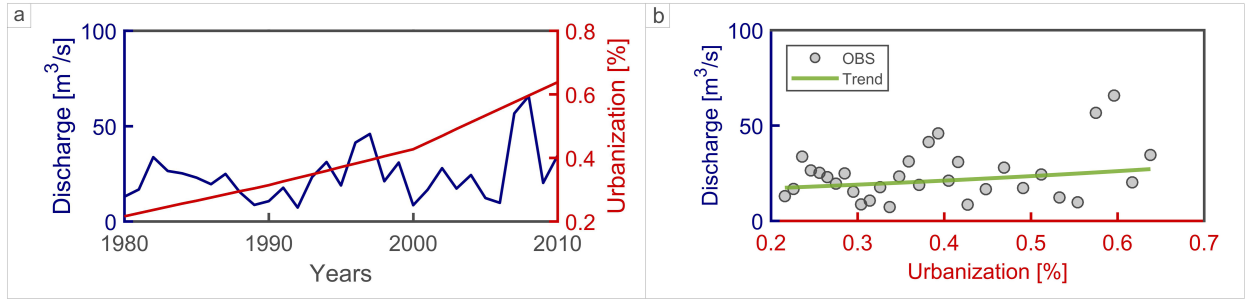


Figure 2.2: ProNEVA results for Application 1: Modeling discharge in Ferson Creek with urbanization as the physical driver of change. a) Discharge data and percent of urbanization in the basin; b) Discharge data as a function of urbanization.

modeling discharge data (Bulletin 17B, U.S. Water Resources Council (1982)). We select a nonstationary model in which the parameter μ (mean) is an exponential function of the covariate X_c . We adopt non-informative normal priors for the LP3 parameters. Figure 2.3.b shows the results of the process-based nonstationary analysis for an arbitrary value of urbanized area, here 37%. For the sake of comparison, Figure 2.3.a displays the results when

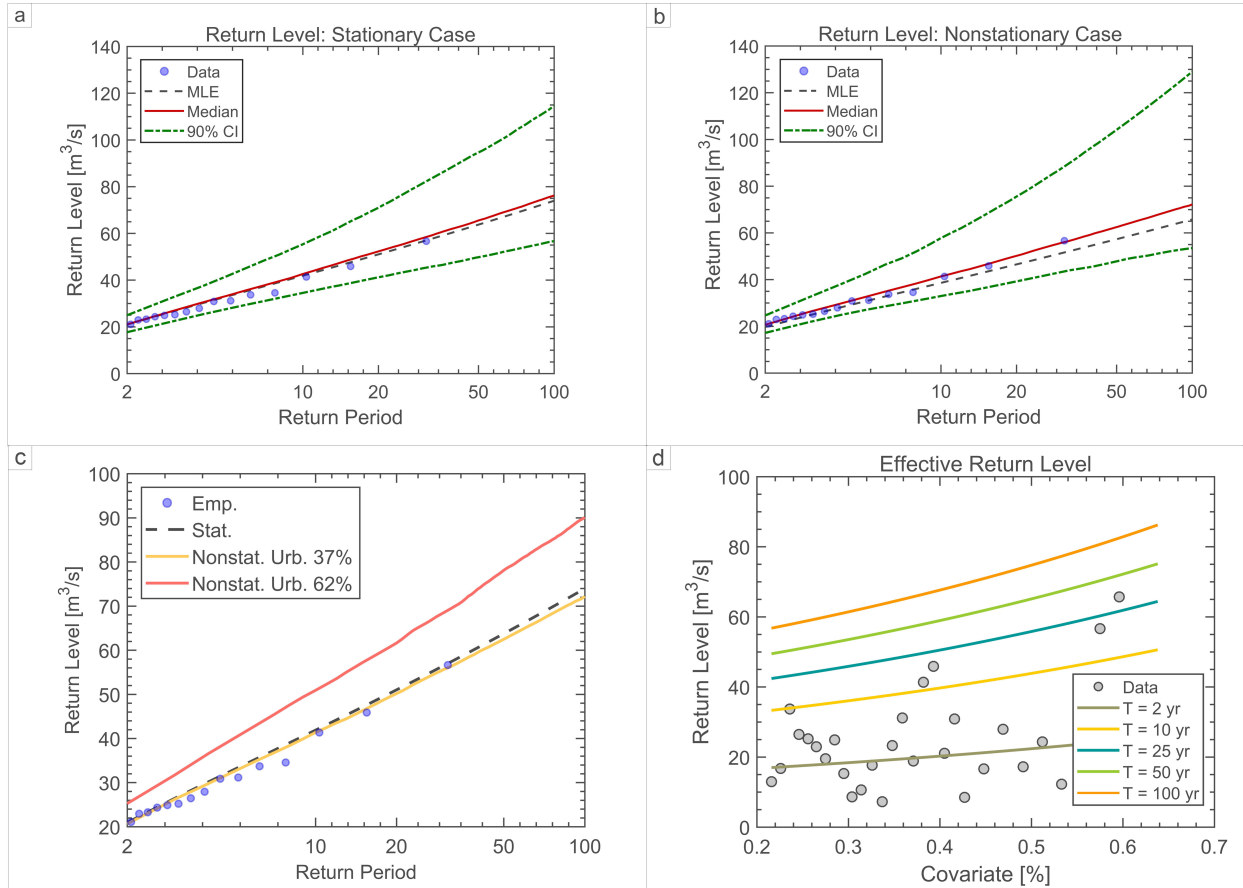


Figure 2.3: ProNEVA results for Application 1: Modeling discharge in Ferson Creek with urbanization as the physical driver of change. a) Return Level curves based on a stationary model; b) Return Level base on a nonstationary model considering an urbanization area equal to 37% of the catchment area; c) Expected return level curves, i.e. ensemble medians, under stationary and nonstationary assumption; d) Effective return period, i.e. return period as a function of the percent of urbanized area.

a stationary model is implemented. It is worth noting that the nonstationary model (Figure 2.3.b) fits extreme discharge values (high values of return period) better than the stationary model (Figure 2.3.a). While based on the AIC and BIC diagnostic tests, the stationary model and the nonstationary model perform similarly, the RMSE of the nonstationary model (25.06 m^3/s) is considerably lower than that of the stationary model (77.58 m^3/s).

Urbanization alters the runoff in the basin by reducing the amount of water that infiltrates and increasing the amount of direct runoff. Figure 2.3.c shows the ability of the statistical model to incorporate this physical process. As anticipated, the expected (ensemble median)

nonstationary return level curve associated with a 62% of urbanized area returns higher values of discharge than the one associated with a 37% of urbanized area. For example, under the nonstationary assumption, the magnitude of a 50-year event is 62.47 m³/s for 37% of urbanized area, similar to the stationary case. However, the magnitude of the 50-year event increases to 78.11 m³/s (25% more) for 62% of urbanized area. On the contrary, the stationary analysis estimates a 50-year event as an event with magnitude 63.74 m³/s, independently on the level of urbanization of the catchment. The result demonstrates that a combination between statistical concepts and physical processes is required for a correctly estimating the expected magnitude of an event. Figure 2.3.d displays the effective return level curves (Katz et al. (2002)) which summarize the impact of urbanization on discharge by describing return levels as functions of the selected covariate (x-axis), here urbanization.

2.7.2 Application 2: Modeling temperature with CO₂ as the physical covariate

Over the past decades, many studies have reported higher surface temperature (e.g.: Zhang et al., 2006; Stott et al., 2010; Melillo et al., 2014; Zwiers et al., 2011), mainly due to anthropogenic activities and consequent increase in greenhouse gasses concentration in the atmosphere. Therefore, we investigate annual maxima surface temperature for the Contiguous United States available from NOAA (NCDC archive - <https://www.ncdc.noaa.gov/cag/national/time-series>) using a process-based nonstationary GEV model in which the user-covariate is represented by CO₂ emissions over the US (Figure 2.4.a). Territorial fossil fuel CO₂ emissions data are available on Global Carbon Atlas <http://www.globalcarbonatlas.org/en/CO2-emissions> (Boden et al., 2017; BP, 2017; UNFCCC, 2017). To incorporate the observed relationship between temperature and CO₂ in the statistical model (Figure 2.4.b), we select a model in which the location and the scale parameters of the GEV distribution are linear functions of the covariate, while the shape parameter is constant. We assume

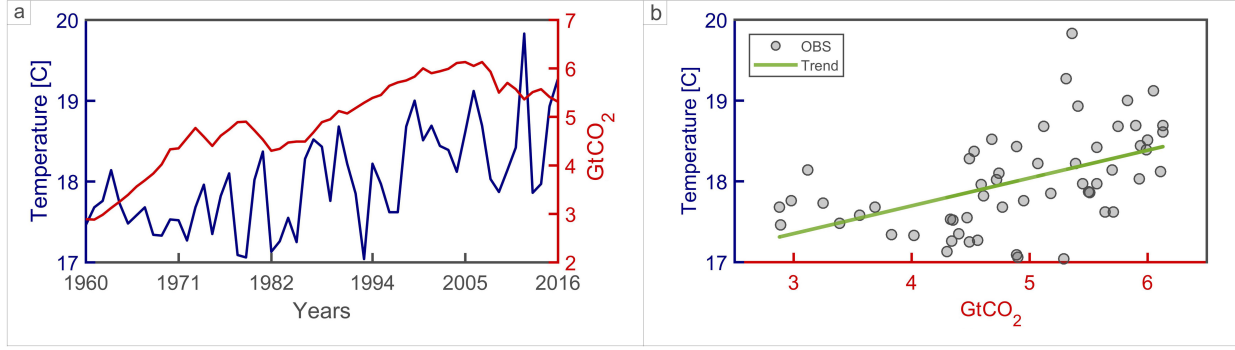


Figure 2.4: ProNEVA results for Application 2: Modeling temperature maxima with CO₂ emissions as the physical covariate. a) Temperature and CO₂ time series; b) Annual temperature maxima as a function of CO₂ emissions in the atmosphere

normal non-informative priors. Figure 2.5.b shows the results of the nonstationary model for a value of CO₂ equal to 4.9 GtCO₂. For comparison, we also plot the results when a stationary model is selected, Figure 2.5.a. One can see that the nonstationary model better captures the observed extreme events, particularly events associated with higher values of CO₂. Moreover, the diagnostics tests confirm that the nonstationary model is a better fit. For the nonstationary model, the AIC and the BIC are 93.91 and 104.13, respectively. When the stationary model is considered, both the AIC and BIC increase to 104.98 and 111.11, respectively. Lower values of AIC and BIC indicate a better model. The advantage of the AIC and BIC for model selection is their ability to account for the number of model parameters: models with higher number of parameters are penalized. Figure 2.6 shows the effective return level as a function of CO₂ emissions. The results show how temperature extremes change in response to the increasing CO₂ emissions (here, the physical co-variate). For example, looking at the expected magnitude of a 50-year event, the temperature increases of about 4%, from 18.79 °C to 19.5 °C, when the CO₂ emissions increase from 4.49 GtCO₂ to 5.51 GtCO₂. The results are consistent with the expectation that higher CO₂ leads to a warmer climate, indicating that the statistical nonstationary model is able to model the observed physical relationship between temperature and CO₂.

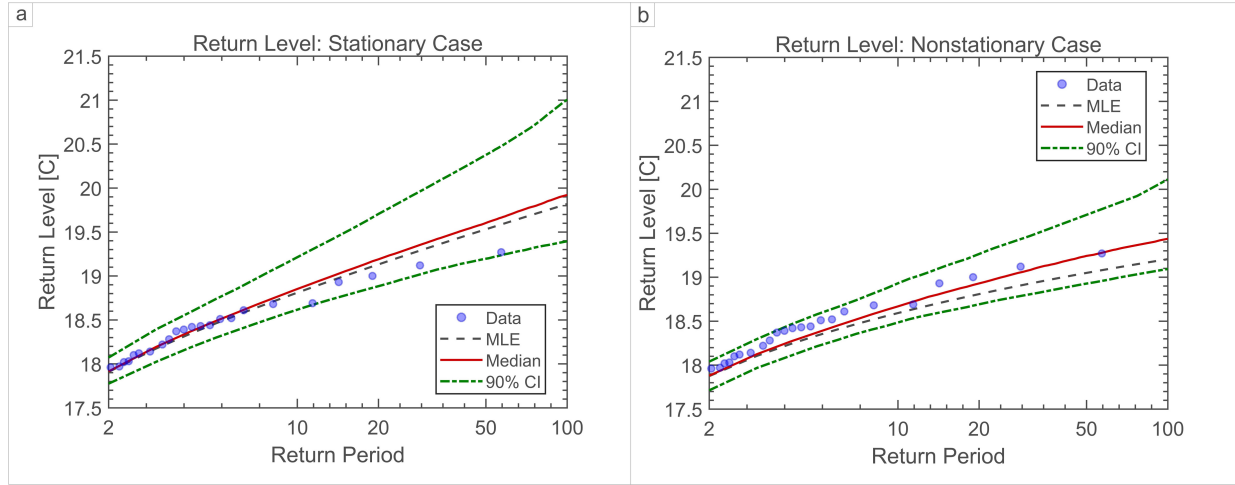


Figure 2.5: ProNEVA results for Application 2: Modeling temperature maxima with CO₂ emissions as the physical covariate. a) Return Level curves based on a stationary model; b) Return Level base on a nonstationary model considering CO₂ emissions equal to 4.9 GtCO₂.

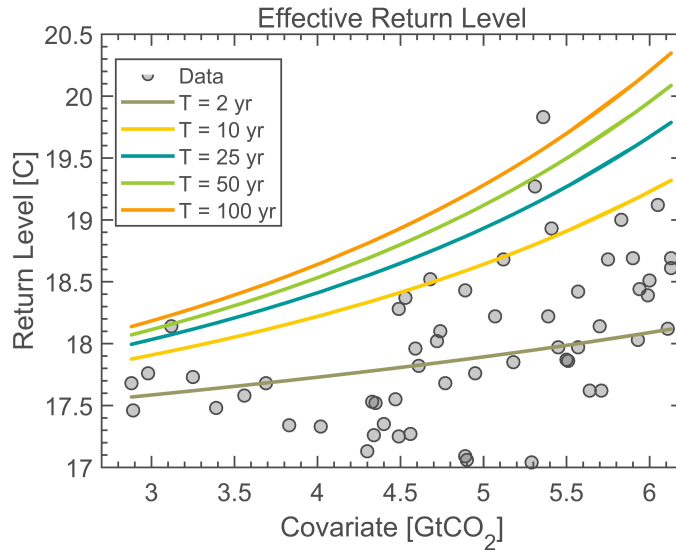


Figure 2.6: ProNEVA results for Application 2: Modeling temperature maxima with CO₂ emissions as the physical covariate. Effective return period, i.e. return period as a function of CO₂ emissions.

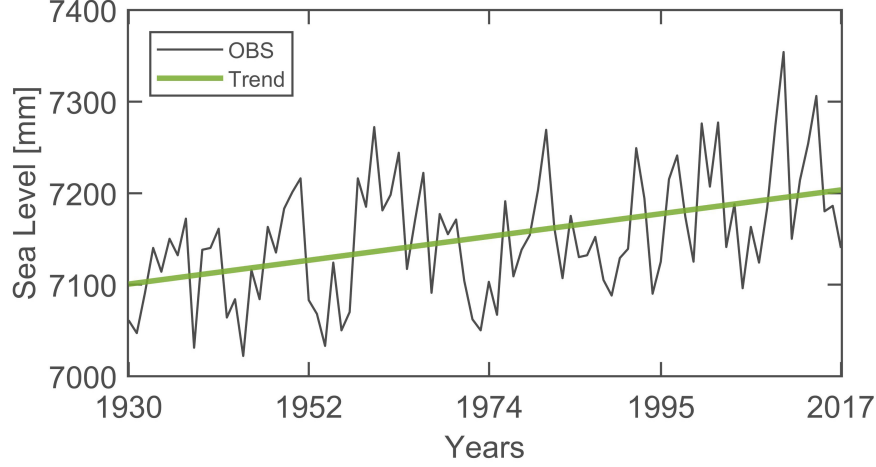


Figure 2.7: ProNEVA results for Application 3: Modeling sea level rise with time as the covariate. Sea Level in the city of Trieste (IT).

2.7.3 Application 3: Modeling sea level rise with time as the covariate

The coastal city of Trieste (Italy) has been experiencing an increase in sea level height over the years (Figure 2.7). Given the observed trend, we investigate annual maxima sea level data from the Permanent Service for Mean Sea Level (PSMSL - station ID 154) by adopting a temporal nonstationary GEV model. The location and scale parameters of the GEV distribution are modeled as linear functions of the time-covariate. The shape parameter is kept constant and we use non-informative normal priors for parameter estimation. Figure 2.8.b shows the return level curves for a fixed value of the time-covariate equal to 45 years from the first observation (i.e., 45 years into the future from the beginning of the data). The nonstationary analysis in Figure 2.8.b provides a better performance than the stationary model in Figure 2.8.a. Both the AIC and the BIC values confirm that a nonstationary model is the best choice to represent sea level observations in a changing climate. The AIC for the nonstationary model is 976.69, while it is 992.74 for the stationary model. Similarly, the BIC for the nonstationary model is 989.08, while it is 1000 for the stationary model. Lower values for AIC and BIC indicate a better model. The value of the temporal covariate

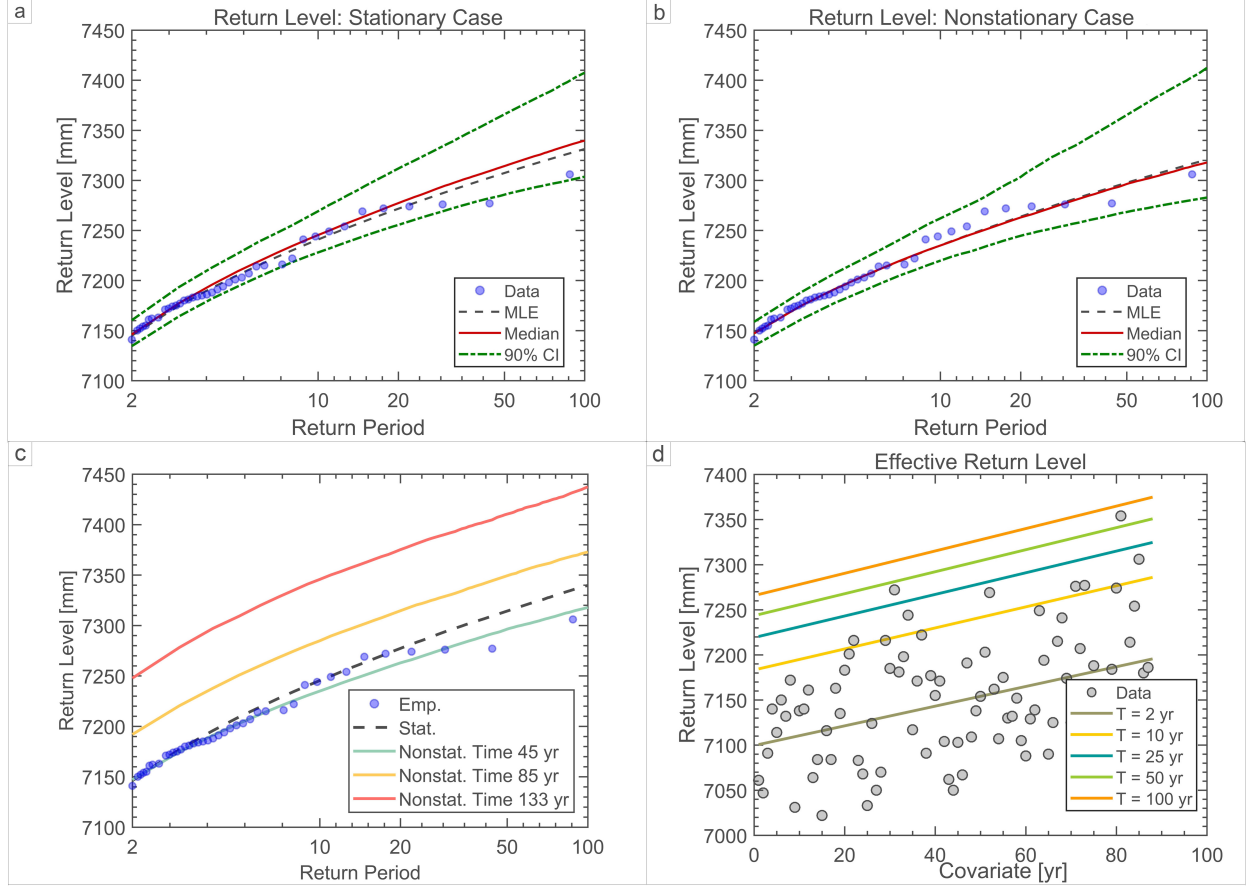


Figure 2.8: ProNEVA results for Application 3: Modeling sea level rise with time as the covariate. a) Return Level curves based on a stationary model; b) Return Level base on a nonstationary model considering equal to 45 years from the first observation; c) Expected return level curves, i.e. ensemble medians, under stationary and nonstationary assumption; d) Effective return period, i.e. return period as a function of the covariate, here time.

should be regarded as the time at which we estimate expected values of, as in this specific case, sea level. The expected (ensemble median) nonstationary return level curves in Figure 2.8.c refer to three different time at which we evaluate sea level: 45, 85, and 133 years from the first observation. Here, 133 years from the first observation is beyond the period of observations (88 years) meaning that we project into the future the observed trend and we infer from there. The observed increasing trend in the sea level records results in increasing values of sea level for higher value of the temporal covariate (Figure 2.8.c). For example, a 50 year event is equal to 7296.3 mm for time equal to 45 years from the first observation, 7349.3 mm for 85 years, and 7410.4 mm for 133 years. We register about 2% increase in

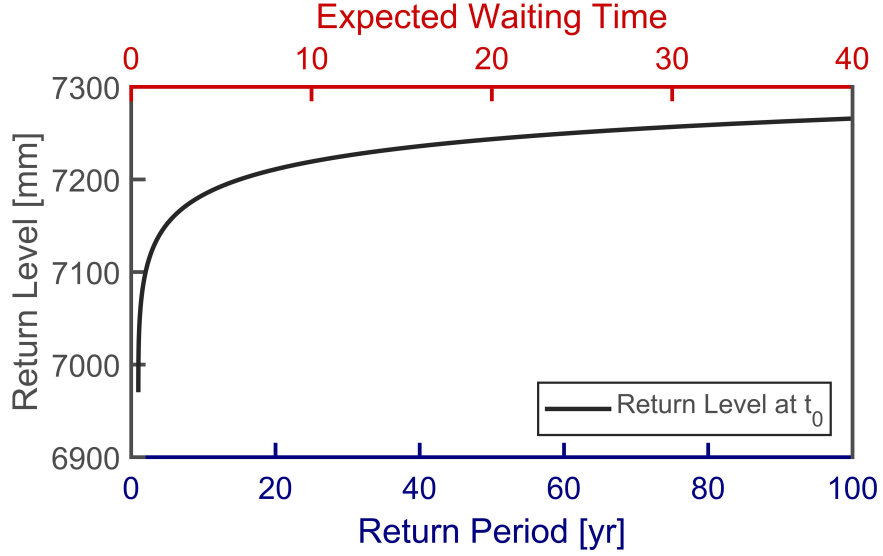


Figure 2.9: ProNEVA results for Application 3: Modeling sea level rise with time as the covariate. Waiting time.

sea level when the time of the first observation changes from 45 to 133 years, confirming the ability of the nonstationary model to reproduce the increasing trend in observations. On the contrary, the stationary analysis return a 50-year sea level equal to 7314.3 mm regardless of the first observation. Figure 2.8.d shows the effective return level (Katz et al., 2002) curves, which capture the variability over time (here, the covariate) in the observed data. In the case of a nonstationary model with a temporal covariate, it is possible to evaluate the expected waiting time (Wigley, 2009; Olsen et al., 1998; Salas and Obeysekera, 2014), which incorporates the observed changes in the sea level over time in the estimation of return periods. Figure 2.9 shows that the current return periods (lower x-axis) will change considering the observed nonstationarity (upper x-axis). For example, the 100-year sea level estimated at t_0 (beginning of the simulation) turns into a 40-year event when the observed trend over time in sea level values is taken into account.

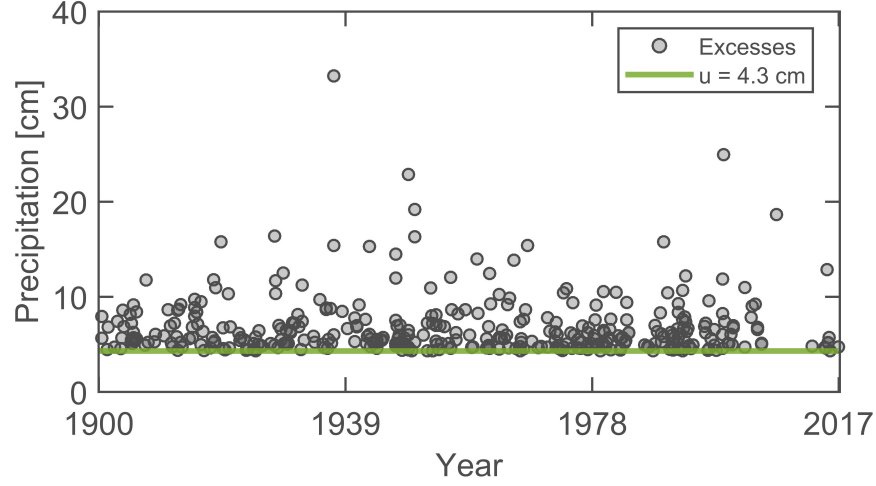


Figure 2.10: ProNEVA results for Application 4: Modeling precipitation under a stationary assumption. Precipitation excesses.

2.7.4 Application 4: Modeling precipitation under a stationary assumption

As last example application, we investigate a time series of precipitation from New Orleans, LA that does not exhibit changes in statistics of extremes. We obtain daily precipitation from the National Climatic Data Center (NCDC) archive (<https://www.ncdc.noaa.gov/cdo-web/>) for the city of New Orleans, station GHCND:USW00012930. Given that we are interested in heavy precipitation events, we use a GP distribution to focus on values above a high threshold (i.e., avoid including non-extreme values). We extract precipitation excesses considering a constant threshold of the 98th-percentile of daily precipitation values (Figure 2.10) For this application we select a stationary GP model, given that we do not have physical evidence to justify a more complex model. However, for the sake of comparison, we perform a nonstationary analysis considering the scale parameter as a linear function of time. Figure 2.11.a represents the return level curves based on a stationary model, while Figure 2.11.b depicts return level curves for a value of the covariate (here time) equal to half of the period of observation. From a comparison between the two models, the stationary model performs better. The stationary model returns values of the AIC and BIC equal to 713.3

and 721.14, respectively. For the nonstationary model the values of the AIC and BIC are higher (715.02 and 726.79, respectively). The results of this example application suggests that when no evidence of changes due to a physical process can be identified, ProNEVA favors the simplest form of model that represents the historical observations.

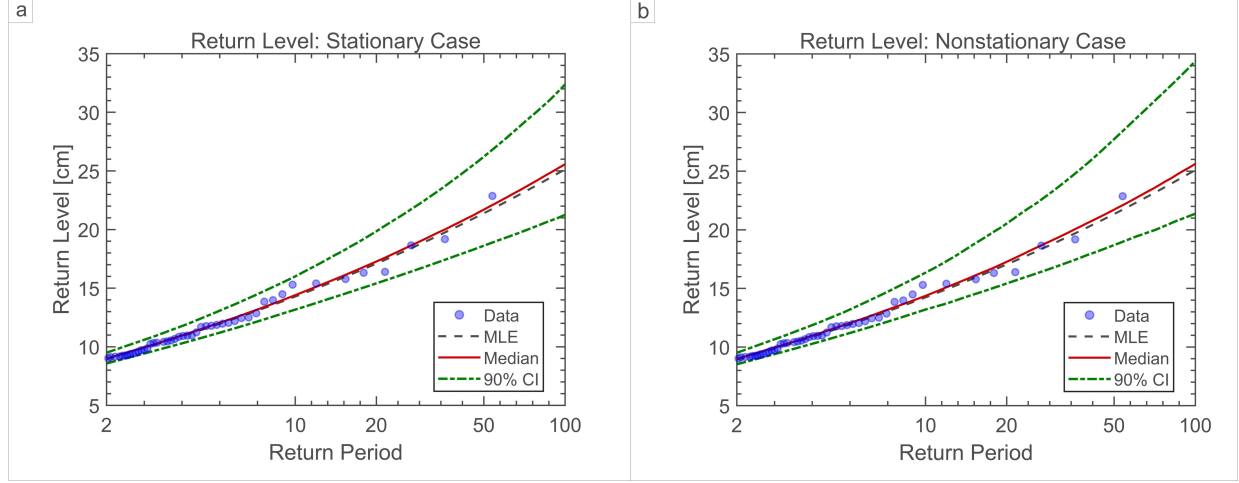


Figure 2.11: ProNEVA results for Application 4: Modeling precipitation under a stationary assumption. a) Return Level curves under the stationary assumption; b) Return Level curves under the temporal nonstationary assumption for a value of the covariate within the period of observation.

2.8 Conclusion

The ability of correctly modeling the expected magnitude and frequency of extreme events is fundamental for improving design concepts and risk assessment methods. This is particularly important for extreme events that have significant impacts on societies, infrastructure and human lives, such as extreme precipitation events causing flooding and landslides.

The observed increase in extreme events and their impacts reported from around the world has motivated moving away from the so-called stationary approach to ensure capturing the changing properties of extremes (Milly et al., 2008). However, there are opposing opinions and perspective on the need and also form of suitable nonstationary models for extreme

value analysis.

Most of the existing tools for implementing extreme value analysis under the nonstationary assumption have a number of limitations including lack of a generalized framework for: incorporating physically based covariates; and estimating parameters which depend on a generic physical covariate. To address the above limitations, we propose a generalized framework entitled *Process-based Nonstationary Extreme Value Analysis* (ProNEVA) in which the nonstationarity component is defined by a temporal or process-based dependence of the observed extremes on a physical driver (e.g., change in runoff in response to urbanization, or change in extreme temperatures in response to CO₂ emissions). ProNEVA offers temporal and process-based stationary and nonstationary extreme value analysis, parameter estimation, uncertainty quantification, and a comprehensive assessment of the goodness of fit.

The source code of ProNEVA is freely available to the scientific community. A graphical user interface (GUI) version of the model is also available to facilitate its applications (Section 2.9). We hope that ProNEVA motivates more physically-based nonstationary analysis of extreme events.

2.9 Supporting Information: ProNEVA User Manual

Process-based Nonstationary Extreme Value Analysis (ProNEVA) is a Matlab software package intended to facilitate extreme value analysis (EVA) for stationary and nonstationary models. ProNEVA estimates the parameters of the Generalized Extreme Value (GEV) distribution, the Generalized Pareto (GP) distribution, and the Log-Pearson Type III (LP3) distribution. Bayesian approach and a hybrid Markov Chain Monte Carlo (MCMC) method for sampling from the posterior distribution are implemented. ProNEVA also provides diagnostic tests and return level plots. The toolbox is released along with a Graphical User Interface (GUI) so that it can reach a broad audience. Moreover, the toolbox can be a valuable educational tool for advanced data analysis courses. By using ProNEVA software users agree to the disclaimer. ¹

¹ **Disclaimer:** The Process-based Nonstationary Extreme Value Analysis (ProNEVA) software package is provided ‘as is’ without any endorsement made and without warranty of any kind, either express or implied. While we strive to ensure that ProNEVA is accurate, no guarantees for the accuracy of the codes, output information and figures are made. ProNEVA codes and outputs can only be used at your own discretion and risk and with agreement that you will be solely responsible for any damage and that the authors and their affiliate institutions accept no responsibility for errors or omissions in ProNEVA codes, outputs, figures, and documentation. In no event shall the authors, developers or their affiliate institutions be liable to you or any third parties for any special, direct, indirect or consequential damages and financial risks of any kind, or any damages whatsoever, resulting from, arising out of or in connection with the use of ProNEVA. The user of ProNEVA agrees that the codes and algorithms are subject to change without notice.

2.9.1 ProNEVA Folder Content

The software package ProNEVA contains the following elements (Figure 2.12):

- **GUIpackage.** It is the folder that includes the source codes of the ProNEVA GUI. Do not rename or move the folder or its content.
- **ProNEVApkg.** It is the folder that contains the source codes for stationary and nonstationary extreme value analysis, diagnostic tests, and plots. Do not rename or move the folder or its contents.
- **RUN_GUI_for_ProNEVA.** It is the code to run to perform stationary and nonstationary extreme value analysis using ProNEVA. A GUI will guide users in selecting inputs and run specifics.
- **RUN_ProNEVA.** It is the code intended for users who wish to perform stationary and nonstationary extreme value analysis using ProNEVA bypassing the GUI. Such users must edit the portion of the code associated with the inputs before running it.
- **Disclaimer.** By using ProNEVA users agree to the disclaimer. Please read the document before using the software.
- **UserManual_ProNEVA.**

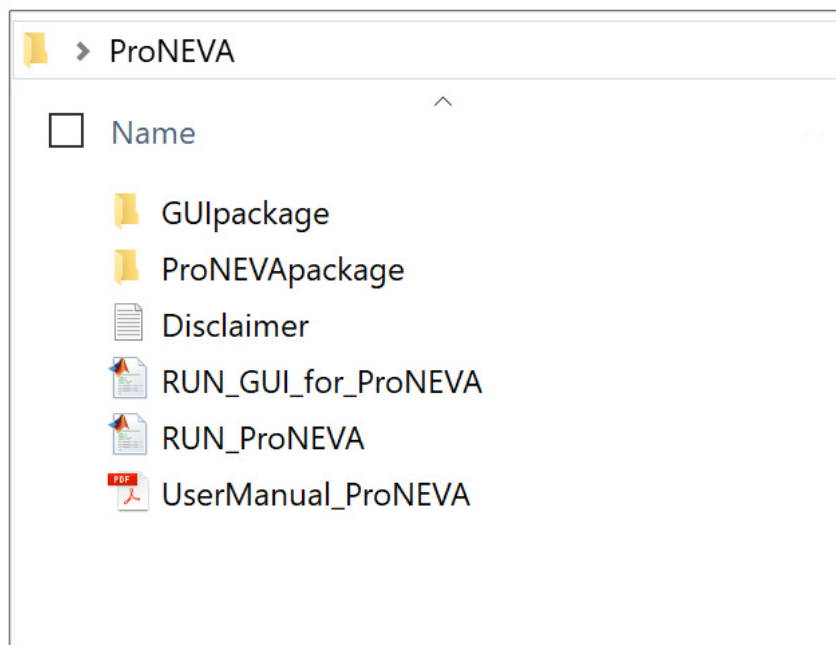


Figure 2.12: Content of the folder ProNEVA.

2.9.2 RUN ProNEVA

The ProNEVA software package can be executed via (1) the GUI or (2) the main source code based on the preference of the user. The results of the analyses do not depend on this choice.

ProNEVA via GUI

- (1) **Open** Matlab and **select** the folder “ProNEVA” as the current folder.
- (2) **Run** RUN_GUI_for_ProNEVA.m code by either (a) typing “RUN_GUI_for_ProNEVA” on the command window or (b) opening “RUN_GUI_for_ProNEVA.m” in the editor subsection and clicking the “RUN” button on the toolbar. The window in Figure 2.13 will pop up.

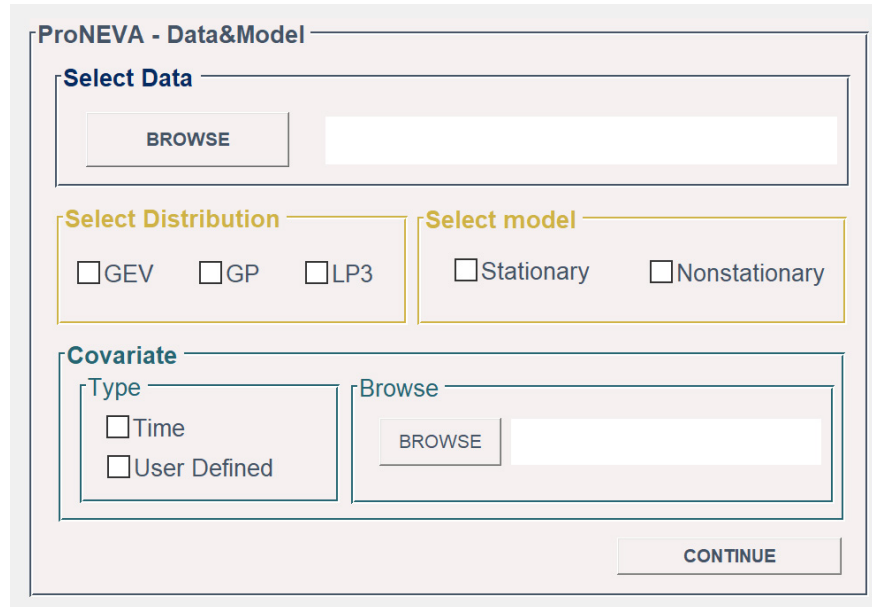


Figure 2.13: ProNEVA GUI - Data&Model for selecting data, distribution, and model type.

- (3) In the section “Select Data”, click on “**BROWSE**” and navigate to the file containing the data. The data must be formatted as **one vector** stored in a **text file** (*.txt* extension). Before uploading the file, make sure that the data are processed as follows:

GEV: Block maxima.

GP: Complete time series. The threshold will be selected in the next step.

LP3: Annual maxima in real or original space. ProNEVA will automatically transform the data in log-space.

- (4) In the section “Select Distribution”, **select** the desired distribution – GEV, GP, or LP3 – in accordance with uploaded data.
- (5) In the section “Select Model”, **select** between stationary and nonstationary analysis
- (6) In the case of a nonstationary analysis, the section “Covariate” will be active. **Select** the type of covariate between “Time” and “User Defined.” In the case of “User Defined” covariate, click on “BROWSE” and navigate to the text file containing the data. The

data must be formatted as **one vector** and the **same length** as the main variable selected in Step (3).

- (7) Click “**CONTINUE**” to continue. One of the following windows will pop up, based on the distribution type selected in Step (4):

Figure 2.14 when a **GEV** distribution is chosen. For each parameter of the GEV distribution, specify the prior distribution and associated parameters. Specifically, lower and upper bound for uniform distribution; mean and standard deviation for normal distribution; shape and scale for gamma distribution. For more details about the types of distributions refer to Matlab help. In the case of a nonstationary analysis, the trend sections will be active. Select the type of trend: “none” refers to a constant parameter. If “none” is selected for all the parameters, a stationary analysis will be performed.

Figure 2.15 when a **GP** distribution is chosen. Select the type of threshold. Select the quantile to determine the value of the threshold parameter. Insert the number of observation in one year; this variable will be used for plotting return level curves. For each parameter of the GP distribution, specify the prior distribution and associated parameters. Specifically, lower and upper bound for uniform distribution; mean and standard deviation for normal distribution; shape and scale for gamma distribution. For more details about the types of distributions, refer to the Matlab help. In the case of a nonstationary analysis, the trend sections will be active. Select the type of trend: “none” refers to a constant parameter. If “none” is selected for all the parameters, a stationary analysis will be performed.

Figure 2.16 when a **LP3** distribution is chosen. For each parameter of the LP3 distribution, specify the prior distribution and associated parameters. Specifically, lower and upper bound for uniform distribution; mean and standard deviation

ProNEVA - GEV

Location

Prior Distribution

☐ Uniform ☐ Normal ☐ Gamma

Prior Parameters

Trend

☐ none
☐ Linear
☐ Exponential
☐ Quadratic

Scale

Prior Distribution

☐ Uniform ☐ Normal ☐ Gamma

Prior Parameters

Trend

☐ none
☐ Linear
☐ Quadratic

Shape

Prior Distribution

☐ Uniform ☐ Normal ☐ Gamma

Prior Parameters

Trend

☐ none
☐ Linear

CONTINUE

Figure 2.14: ProNEVA GUI. Select priors and trends for the GEV parameters.

for normal distribution; shape and scale for gamma distribution. For more details about the types of distributions, refer to the Matlab help. In the case of a nonstationary analysis, the trend sections will be active. Select the type of trend: “none” refers to a constant parameter. If “none” is selected for all the parameters, a stationary analysis will be performed.

- (8) Click “**CONTINUE**” to continue. The last window will pop up, Figure 2.17. Specify the number of chains and iterations, and the burn-in period for MCMC. Specify the maximum return period of interest for return level curves. Select “YES” to the three questions to perform Man-Kendall trend test and White test, to plot return level curves, and to save the results.

ProNEVA - GP

Threshold

Type

☐ Constant
☐ Linear

Threshold Quantile

N. Obs. in a Year

Scale

Prior Distribution

☐ Uniform
☐ Normal
☐ Gamma

Prior Parameters

Trend

☐ none
☐ Linear
☐ Quadratic

Shape

Prior Distribution

☐ Uniform
☐ Normal
☐ Gamma

Prior Parameters

Trend

☐ none
☐ Linear

CONTINUE

Figure 2.15: ProNEVA GUI. Select threshold type along with priors and trends for the GP parameters.

- (9) Click **“RUN”** and the analysis will start. When the option to save the results is selected, the folder “Results” containing the outputs (.mat and .fig files) will be created in the folder “ProNEVA”.

ProNEVA - LP3

Mean

Prior Distribution

☐ Uniform ☐ Normal ☐ Gamma

Prior Parameters

Trend

☐ none
☐ Linear
☐ Exponential
☐ Quadratic

Standard Deviation

Prior Distribution

☐ Uniform ☐ Normal ☐ Gamma

Prior Parameters

Trend

☐ none
☐ Linear
☐ Quadratic

Skewness

Prior Distribution

☐ Uniform ☐ Normal ☐ Gamma

Prior Parameters

Trend

☐ none
☐ Linear

CONTINUE

Figure 2.16: ProNEVA GUI. Select priors and trends for the LP3 parameters.

ProNEVA - RUN

MCMC

N. Chains N. Iterations Burn-in

Return Period

Plots

Plot Return Levels? ☐ YES ☐ NO

Tests

Performe Mann-Kendall and White Tests? ☐ YES ☐ NO

Save

Save Results? ☐ YES ☐ NO

RUN

Figure 2.17: ProNEVA GUI for selecting the parameters for MCMC along with complementary options such as tests, plots, and save.

ProNEVA via Source Code

Users can perform stationary and nonstationary extreme value analysis using ProNEVA avoiding the GUI. To do so:

- (1) **Open** Matlab and **select** the folder “ProNEVA” as the current folder.
- (2) **Open** “RUN_ProNEVA.m” in Matlab Editor.
- (3) **Edit** section “Load Data”. **Replace** “DataPath\MyData.txt” with the name of the desired file. Include the file path when the file .txt is outside the folder “ProNEVA”.

```
1 %% (1) EDIT - LOAD DATA
2 fileOBS = fopen('DataPath\MyData.txt');
```

- (4) **Edit** section “Distribution Type”. Specify the distribution of interest in Line 7 based on the legend.

```
1 %% (2) EDIT - DISTRIBUTION TYPE
2 % RUNspec.DISTR.Type
3 % (i)   RUNspec.DISTR.Type = 'GEV'   Generalized Extreme Value
        Distribution
4 % (ii)  RUNspec.DISTR.Type = 'GP'    Generalized Pareto
        Distribution
5 % (iii) RUNspec.DISTR.Type = 'P3'    Pearson Typer III
6 RUNspec.DISTR.Type = 'GEV';
```

- (5) **Edit** section “Model Type”. Specify the type of model in line 5, stationary or non-stationary. In the case of nonstationary analysis, RUNspec.DISTR.Model = ‘Non-Stat’, specify the type of covariate. If RUNspec.COV.type = ‘User’, replace ‘Cov-Path\MyCovariate.txt’ with the name of the text file containing the vector of covariate. Include the file path if the file is outside the ProNEVA folder.

```

1 %% (3) EDIT - MODEL TYPE
2 % 'Stat'      : Stationary Analysis
3 % 'NonStat'   : Nonstationary Analysis
4
5 RUNspec.DISTR.Model = 'Stat';
6
7 if strcmp(RUNspec.DISTR.Model, 'NonStat');
8
9     %% EDIT - COVARIATE TYPE
10    % RUNspec.COVtype:
11    % (i)  RUNspec.COV.type = 'Time'
12    % (ii) RUNspec.COV.type = 'User'
13    RUNspec.COV.Type = 'Time';
14
15    if strcmp(RUNspec.COV.Type, 'User')
16
17        %% EDIT - SELECT FILE COVARIATE
18        fileCOV = fopen('CovPath\MyCovariate.txt');
19        % DO NOT EDIT
20        textCOV = textscan(fileCOV, '%f');
21        fclose(fileCOV);
22        RUNspec.COV.X = textCOV{1}(:);
23    end
24 end

```

- (6) **Uncomment** and **edit** the sections in Listings 2.1, 2.2, and 2.3 based on the type of distribution chosen at Step (4). For each distribution's parameter, specify the type of prior and associated parameters, following the legend at the top. In the case of a GP distribution, specify the threshold quantile and the type, along with the number of

observations in a year, used for return level plots. In the case of nonstationary analysis, define the type of trend for the different parameters.

```
1 %% (4) UNCOMMENT and EDIT if RUNspec.DISTR.Type = 'GEV'
2
3 %% Edit PRIOR
4 % (i) 'Uniform': parm1 = min | parm2 = max
5 % (ii) 'Normal' : parm1 = mean | parm2 = std
6 % (iii) 'Gamma' : parm1 = shape | parm2 = scale
7
8 % Location - MU:
9 RUNspec.PRIOR.MUdistr = 'Normal';
10 RUNspec.PRIOR.MUparm1 = 0;
11 RUNspec.PRIOR.MUparm2 = 100;
12
13 % Scale - SI:
14 RUNspec.PRIOR.SIdistr = 'Normal';
15 RUNspec.PRIOR.SIparm1 = 0;
16 RUNspec.PRIOR.SIparm2 = 10;
17
18 % Shape - XI:
19 RUNspec.PRIOR.XIdistr = 'Normal';
20 RUNspec.PRIOR.XIparm1 = 0;
21 RUNspec.PRIOR.XIparm2 = 0.2;
22
23 % DO NOT EDIT
24 if strcmp(RUNspec.DISTR.Model, 'Stat')
25
26     RUNspec.NS.MU = 'none';
27     RUNspec.NS.SI = 'none';
```

```

28     RUNspec.NS.XI = 'none';
29 else
30     %% EDIT TREND 'NonStat' case
31     % TREND LOCATION
32     % 'none' | 'Linear' | 'Quadratic' | 'Exponential'
33     RUNspec.NS.MU = 'Linear';
34     % TREND SCALE
35     % 'none' | 'Linear' | 'Quadratic'
36     RUNspec.NS.SI = 'Linear';
37     % TREND SHAPE
38     % 'none' | 'Linear'
39     RUNspec.NS.XI = 'none';
40 end

```

Listing 2.1: Section for GEV.

```

1 %% (4) UNCOMMENT AND EDIT if RUNspec.DISTR.Type = 'GP'
2
3 %% EDIT GP THRESHOLD
4 % RUNspec.THtype: (i) 'Const' | (ii) 'QR' - Quantile Regression
5 RUNspec.THtype = 'Const';
6 % RUNspec.THp: p-quantile for threshold definition [0 1]
7 RUNspec.THp = 0.98;
8 % RUNspec.NobsY: Observations in a year
9 RUNspec.NobsY = 365;
10
11 %% EDIT PRIOR
12 % (i) 'Uniform': parm1 = min | parm2 = max
13 % (ii) 'Normal' : parm1 = mean | parm2 = std
14 % (iii) 'Gamma' : parm1 = shape | parm2 = scale

```

```

15
16 % Scale
17 RUNspec.PRIOR.SIdistr = 'Normal';
18 RUNspec.PRIOR.SIparm1 = 0;
19 RUNspec.PRIOR.SIparm2 = 10;
20
21 % Shape
22 RUNspec.PRIOR.XIdistr = 'Normal';
23 RUNspec.PRIOR.XIparm1 = 0;
24 RUNspec.PRIOR.XIparm2 = 0.2;
25
26 % DO NOT EDIT
27 if strcmp(RUNspec.DISTR.Model, 'Stat')
28
29     RUNspec.NS.MU = 'none';
30     RUNspec.NS.SI = 'none';
31     RUNspec.NS.XI = 'none';
32 else
33     %% EDIT TREND 'NonStat' case
34     % TREND SCALE
35     % 'none' | 'Linear' | 'Quadratic'
36     RUNspec.NS.SI = 'Linear';
37     % TREND SHAPE
38     % 'none' | 'Linear'
39     RUNspec.NS.XI = 'none';
40 end

```

Listing 2.2: Section for GP.

```

1 %% (4) UNCOMMENT and EDIT if RUNspec.DISTR.Type = 'P3'

```

```

2
3 %% Edit PRIOR
4 % (i)   'Uniform': parm1 = min   | parm2 = max
5 % (ii)  'Normal'  : parm1 = mean  | parm2 = std
6 % (iii) 'Gamma'   : parm1 = shape | parm2 = scale
7
8 % Location - MEAN:
9 RUNspec.PRIOR.MUdistr = 'Normal';
10 RUNspec.PRIOR.MUparm1 = 0;
11 RUNspec.PRIOR.MUparm2 = 100;
12
13 % Scale - STANDARD DEVIATION:
14 RUNspec.PRIOR.SIdistr = 'Normal';
15 RUNspec.PRIOR.SIparm1 = 0;
16 RUNspec.PRIOR.SIparm2 = 10;
17
18 % Shape - SKWENESS:
19 RUNspec.PRIOR.XIdistr = 'Normal';
20 RUNspec.PRIOR.XIparm1 = 0;
21 RUNspec.PRIOR.XIparm2 = 0.2;
22
23 % DO NOT EDIT
24 if strcmp(RUNspec.DISTR.Model, 'Stat')
25
26     RUNspec.NS.MU = 'none';
27     RUNspec.NS.SI = 'none';
28     RUNspec.NS.XI = 'none';
29 else
30     %% EDIT TREND 'NonStat' case

```

```

31 % TREND LOCATION
32 % 'none' | 'Linear' | 'Quadratic' | 'Exponential'
33 RUNspec.NS.MU = 'Linear';
34 % TREND SCALE
35 % 'none' | 'Linear' | 'Quadratic'
36 RUNspec.NS.SI = 'Linear';
37 % TREND SHAPE
38 % 'none' | 'Linear'
39 RUNspec.NS.XI = 'none';
40 end

```

Listing 2.3: Section for LP3.

- (7) **Edit** MCMC information and optional results in Listing 2.4. Specify the desired number of chains and iterations, and the burn-in period for MCMC approach. Specify the maximum return period for return level curves. Finally, specify whether ProNEVA will perform the Mann-Kendall trend test and White test, plot return level curves, and save the results. When the option to save the results is selected, a folder “Results” will be created in the folder “ProNEVA” containing the analysis outputs (.mat and .fig files).

```

1 %% (5) EDIT - MCMC AND EXTRA OPTIONS
2 % MCMC
3 % Number of Chains
4 RUNspec.Nchain = 3;
5 % Number of Iterations
6 RUNspec.maxIT = 10000;
7 % Burn-in period
8 RUNspec.brn = 9000;
9 % Return Period

```

```

10 RUNspec.RP      = 100;
11
12 % Extra Options
13 % 'Y': Yes - 'N': No
14 % Save Results? 'Y' /'N'
15 EXTRAS.saveRES   = 'Y';
16 % Run Mann-Kendall and White Tests? 'Y'/'N'
17 EXTRAS.RunTests  = 'Y';
18 % Plot Return Level? 'Y'/'N'
19 EXTRAS.PlotRL    = 'Y';

```

Listing 2.4: Section for LP3.

(8) **Run** the code.

2.9.3 ProNEVA Results

When the option to save the data is selected, a folder “Results” will be created and it will contain the outputs from the run. Table 2.5 summarizes the expected outputs. However, some outputs may not be available because of the type of the input previously selected.

OUTPUT.	
CH	Parameters of the selected distribution
RhatCH	Gelman \hat{R} for convergency check
Z	Standardized Observations for GOF tests
RES	Residuals
EWT	Expected Waiting Time
Z_{q0}	Quantile associated with the EWT
RLplot.VC	Covariate values for the return level plots
PARvc	Distribution parameters for covariate equal to RLplot.VC
RLplot.RL95	Upper bound of return level curves (95-percentile)
RLplot.RL05	Lower bound of return level curves (5-percentile)
RLplot.RL50	Expected return level curves (median)
RLplot.RLm	Maximum likelihood return level curves
ERP.TT	Return period for effective return level plot
RLeff	Effective return level curves: each row corresponds to ERP.TT
PDFhat	Predictive PDF
DGN.	
KS.HH	Kolmogorov Smirnov (KS) Test Results
KS.RJrate	KS test rejection rate
AIC	Akaike Information Content
BIC	Bayesian Information Criterion
RMSE	Root Mean Square Error
NSE	NashSutcliffe model Efficiency Coefficient
TST.	
MK.H	Statistical significance of Mann-Kendall trend test
MK.p_value	p_value for the Mann-Kendall trend test
WT.H	Statistical significance of White test
WT.p_value	p_value for the White test

Table 2.5: List of ProNEVA outputs

Chapter 3

On the Probability of Rare Events

Since the beginning of time, humans have managed to cope with unavoidable, and often unpredictable, natural hazards. Today's highly populated and urbanized society is extremely vulnerable to rare events and their disruptive consequences: entire communities fight, fall, and then rise against them. Hurricane Harvey unfolded in August of 2017 along Texas coast and was one of the most recent natural hazards which caused devastating impacts due to widespread flooding (NWS, 2018). Almost 780,000 Texans evacuated their homes, and the estimated total cost in damages of the hurricane was about \$125 billion (FEMA, 2017). The news referred to the event as a 1,000-year flood (Samenow, 2017). A 1 in 1,000 year flood event is expected to be observed once in a 1,000 years on average (in statistical terms, an event with a probability of occurrence of 0.1 % ($1/1,000$) in any given year.

Determining the recurrence interval (return period) of extreme events is fundamental to infrastructure design, risk assessment, asset management and disaster relief planning and response. Generally, the return period of a rare event and its magnitude (known as return level) is inferred from limited observations - often derived by extrapolating from a distribution function fitted to the available observations (Coles, 2001). This indicates that the reliability

of return period analyses of extremes and their corresponding magnitudes are closely related to the length of record. For example, if we have only 50 years of data (typical for hydrology and climate data records), the chance that a 100-yr event has happened in this period is only 50%. This could be rephrased in a more general question such as: what is the probability of observing a T -year event given a time series of (say, precipitation) annual maxima of length N ?

Let's consider a time series $\mathbf{X} = \{X_1, \dots, X_N\}$ of N independent and identically distributed (i.i.d) observations of precipitation/temperature annual maxima. Let's assume that x_T is the T -year event of interest. Then, $P(X > x_T) = 1/T$, where x_T is the event with an exceedance probability of $1/T$ in each year. The probability that the event x_T will not be exceeded in N years is then $P(X_{(1)} < x_T, \dots, X_{(i)} < x_T, X_{(N)} < x_T)$ where $X_{(i)}$ is the event in year i . Given independence of observations, $P(X_{(1)})$ can be described as follows:

$$P(X_{(1)} < x_T, \dots, X_{(i)} < x_T, X_{(N)} < x_T) = \prod_{i=1}^N \left(1 - \frac{1}{T}\right) = \left(1 - \frac{1}{T}\right)^N \quad (3.1)$$

Hence, the complementary event, i.e. the probability that we observe x_T at least once in N years, $P(x_T \in X)$, is

$$P(x_T \in X) = 1 - P(X_{(1)} < x_T, \dots, X_{(i)} < x_T, X_{(N)} < x_T) = 1 - \left(1 - \frac{1}{T}\right)^N \quad (3.2)$$

The return period (T) can be expressed as a function of the length of record N as $T = \alpha \cdot N$, where T and N are in years and α is dimensionless. Therefore, Equation 3.2 can be rewritten as follows:

$$P(x_T \in X) = 1 - \left(1 - \frac{1}{\alpha \cdot N}\right)^N \quad (3.3)$$

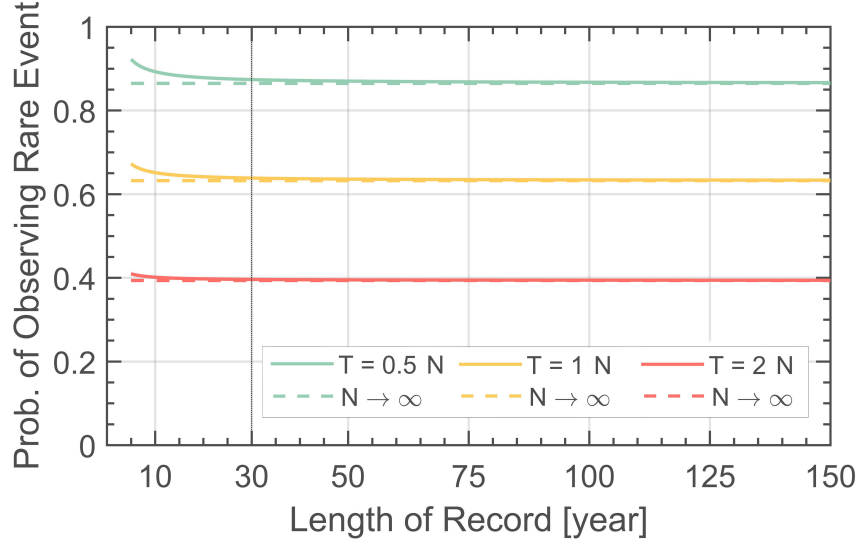


Figure 3.1: Probability of observing a T -year event at least once in N -years ($P(x_T \in X)$): Comparing $P(x_T \in X)$ for different lengths of records (Equation 3.3; solid lines) relative to the case of $N \rightarrow \infty$ (Equation 3.4; dashed lines).

For large values of N , Equation 3.3 can be approximated as

$$\lim_{N \rightarrow \infty} P(x_T \in X) = \lim_{N \rightarrow \infty} \left(1 - \left(1 - \frac{1}{\alpha \cdot N} \right)^N \right) = 1 - e^{-1/\alpha} \quad (3.4)$$

Equation 3.4 suggests that for large number of observations (N), the probability of observing an event only depends on the ratio α between the return period of interest and the length of records, and not on their absolute values. In statistical applications, a minimum of 30 elements is commonly considered necessary for significant inferences. Figure 3.1 shows that Equation 3.4 is a good approximation of the occurrence probability of a rare event when $N \geq 30$.

Figure 3.1 shows that a reliable estimation of the probability and return period of a rare event does not depend solely on the number of observations or on the rarity of the event. For example, the probability of observing a 100-year event in 100 years of data is the same as the probability of observing a 1,000 year event in 1,000 years of data. We believe that estimates of return periods of extreme events should include information on their reliability

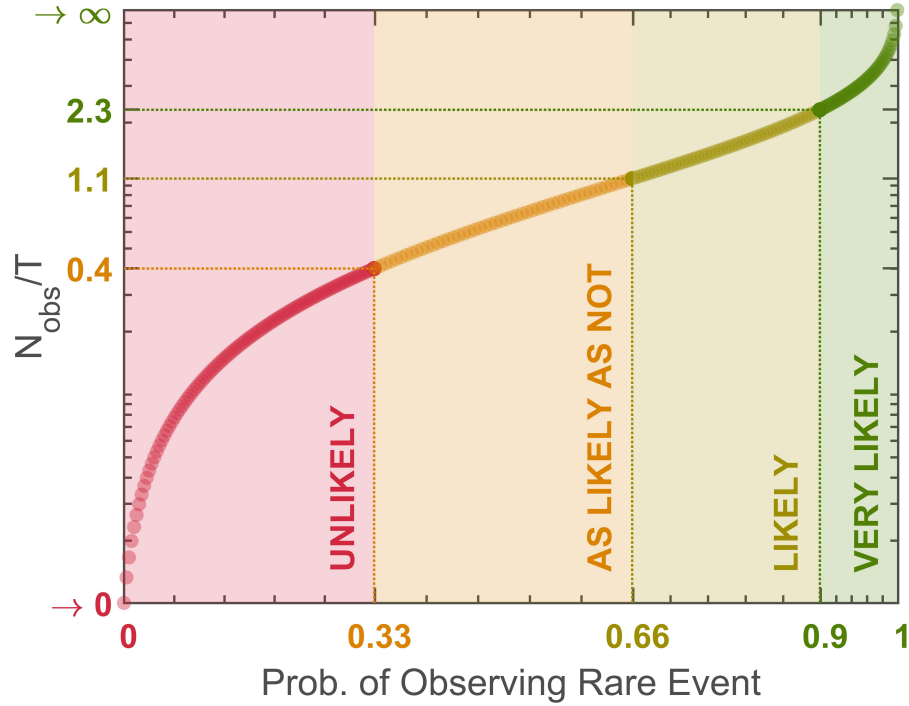


Figure 3.2: The universal chart indicating the likelihood of observing an extreme events

or our confidence in the estimates based on the available data. This is necessary to improve the way risk information is communicated to decision-makers by providing confidence in the estimated magnitude and frequency of natural hazards.

To address this gap, we implement Equation 3.4 to delineate a universal chart summarizing the likelihood of observing the rare event of interest within the available set of observation (see Figure 3.2). The goal of this figure is to communicate the confidence in the estimated return period or probability of an extreme event. To be consistent with the climate science literature, in this chart, the ratio between the length of record and the rarity of the extreme event is combined with the likelihood scale adopted by the Intergovernmental Panel on Climate Change (IPCC) Fifth Assessment Report (Mastrandrea et al., 2010).

Figure 3.2 shows that observing a T -year event is *very likely* ($P(x_T \in X) \leq 0.9$) if the number of observations are equal to or greater than $2.3T$. Observing a rare event is *likely* ($0.66 \geq P(x_T \in X) < 0.9$) when the number of observations is between T and $2.3T$, and

observing it is about *as likely as not* ($0.33 \geq P(x_T \in X) < 0.66$) when the number of observations is between $0.4T$ and T . Finally, observing a T -year event is *unlikely* ($P(x_T \in X) < 0.33$) when the number of observations is less than $0.4T$.

In the following, we show examples of the likelihood of observing specific rare events (e.g., $T = 100$ -yr event) given a fixed length of record - e.g., 50 years (Figure 3.3 left) and 100 years (Figure 3.3 right). The figure shows that a 50-year event is *as likely as not* when estimated based on 50 years of observations (Figure 3.3 left), while it only becomes *likely* when there is over 100 years of observations (Figure 3.3 right).

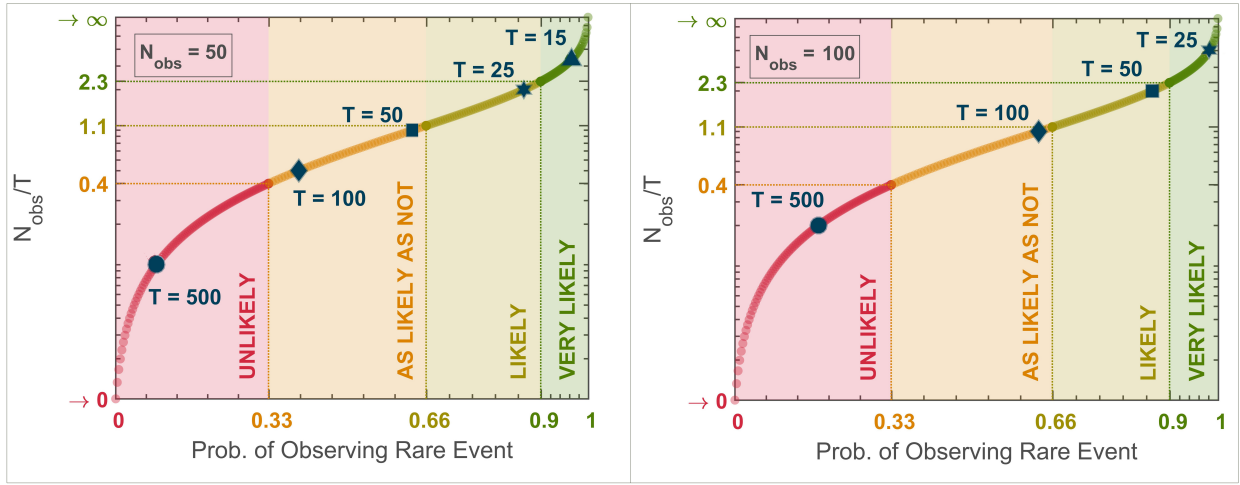


Figure 3.3: The likelihood of observing a rare event (e.g., $T=50$ -yr, 100-yr, 500-yr) for 50 years (left) and 100 (right) years of observations.

Figure 3.4 displays the likelihood of observing a 50-yr (left) and 100-yr (right) events for different lengths of records (e.g., $N=15$ to $N=200$ years). The figure highlights that an estimated 100-year event is *unlikely* to be observed when only 30 years of observation are available (Figure 3.4). In many parts of the world, the observe records barely exceed 30 years which indicates our estimates of the magnitude of extremes may be highly biased.

The results indicate that predicting future rare events requires paying special attention to the confidence in the estimates based on the available observations. Given that predicting

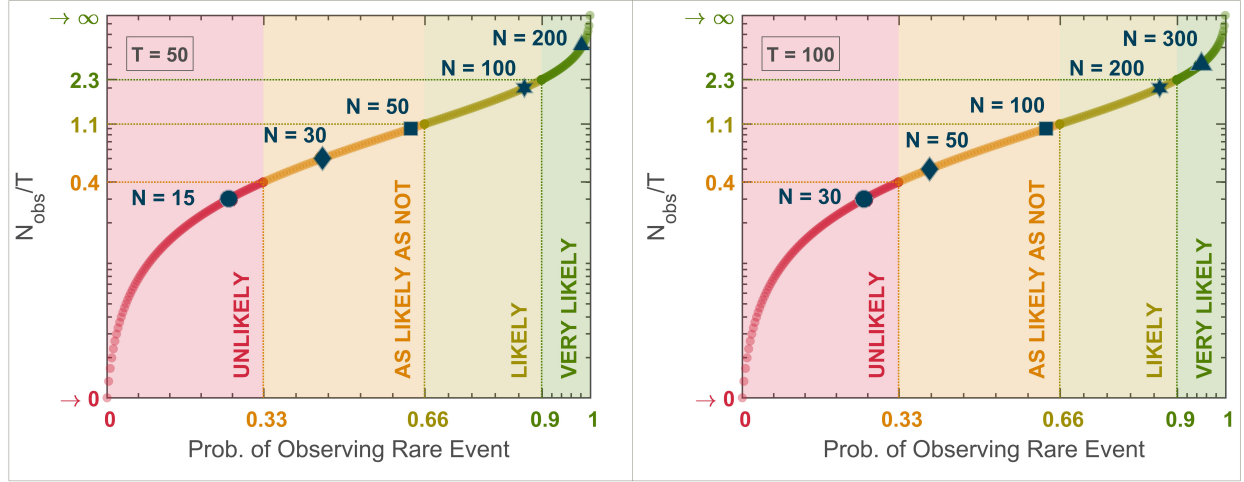


Figure 3.4: The likelihood of observing a 50-yr (left) and 100-yr (right) events for different lengths of records ($N=15$ to $N=200$ years).

rare events does not depend solely on the number of observations or on the rarity of the event of interest, we recommend adopting the proposed universal chart for communicating our confidence in estimated return periods of extreme events. This chart sheds light on uncertainties associated with the return period estimates often used for design and operational applications.

Chapter 4

Quantifying Changes in Future Intensity-Duration-Frequency Curves Using Multi-Model Ensemble Simulations

Chapter based on the following published work:

Ragno, E., AghaKouchak, A., Love, C. A., Cheng, L., Vahedifard, F., and Lima, C. H. R. (2018). Quantifying changes in future IntensityDurationFrequency curves using multimodel ensemble simulations. Water Resources Research, 54, 17511764. <https://doi.org/10.1002/2017WR021975>.

4.1 Introduction

The Fifth Assessment Report of the Intergovernmental Panel on Climate Change (IPCC - (Field et al., 2014)) states that since 1960 anthropogenic activities have likely contributed to altering the global water cycle by increasing, more than decreasing, the number of heavy precipitation events in terrestrial regions. Indeed, higher surface temperatures observed over the past decades (e.g.: Barnett et al., 1999; Melillo et al., 2014; Diffenbaugh et al., 2015; Fischer and Knutti, 2015; Mazdiyarni and AghaKouchak, 2015), mainly driven by human activities (Zhang et al., 2006; Stott et al., 2010; Melillo et al., 2014; Zwiers et al., 2011), can alter the hydrological cycle leading to more intense rainfall events (Zhang et al., 2007; Min et al., 2011; Marvel and Bonfils, 2013; Westra et al., 2013; Cheng et al., 2014; Fischer and Knutti, 2016). Reports indicate that many regions including the United States, central Africa, parts of southwest Asia (i.e., Thailand, Taiwan), Central America, Australia, and parts of eastern Europe have experienced more extreme events (DeGaetano, 2009; Melillo et al., 2014; Zheng et al., 2015; Fischer and Knutti, 2015; Wasko et al., 2016). Heavier precipitation events have increased the risk of flooding at regional scale (Field et al., 2014) and rainfall-triggered landslide activity in the U.S. over the past few decades, (Gariano and Guzzetti, 2016). Moreover, recent studies using precipitation projections from Global Climate Models (GCMs) indicate that there is a high chance of substantial impact on landslide activity in natural slopes (Robinson et al., 2017) and on the performance of man-made earthen structures (Vahedifard et al., 2017b; Jasim et al., 2017).

The observed trends and projected changes in future extreme events have called into question the preparedness of existing and future construction (Milly et al., 2008; Mailhot and Duchesne, 2010; Hallegatte et al., 2013; Moftakhari et al., 2017b; Yan et al., 2018). Current design and failure risk assessment procedures for infrastructure (e.g., dams, roads, sewer and storm water drainage systems) and earthen structures (e.g., levees, natural and engineered slopes) rely on rainfall Intensity-Duration-Frequency (IDF) curves for estimating the design

storm intensity and the corresponding flow. IDF curves represent the probable intensity of a rainfall event given a certain duration (or time of concentration - e.g., 24-hour) and an average return period (recurrence interval), estimation of which involves fitting a representative distribution function to observed precipitation (Bonnin et al., 2006). In the current procedure, the parameters of the distribution are estimated under the so-called stationary assumption (i.e., time-invariant parameters). This assumes that no significant changes are expected in magnitude or frequency, and hence in distribution parameters, of precipitation extremes over time (Milly et al., 2008).

Several studies have considered nonstationary models for extreme value analysis to address temporal changes in climate extremes (Katz et al., 2002; Sankarasubramanian and Lall, 2003; Mailhot et al., 2007; Huard et al., 2009; Villarini et al., 2010; Vogel et al., 2011; Zhu et al., 2012; Willems et al., 2012; Katz, 2013; Obeysekera and Salas, 2013; Salas and Obeysekera, 2014; Yilmaz and Perera, 2014; Mirhosseini et al., 2014; Volpi et al., 2015; Read and Vogel, 2015; Sadegh et al., 2015; Krishnaswamy et al., 2015; Mirhosseini et al., 2015; Mondal and Mujumdar, 2015; Lima et al., 2016; Sarhadi and Soulis, 2017). Among those, Cooley et al. (2007) proposed a spatio-temporal Bayesian hierarchical modeling approach for defining IDF maps for flood management in the Front Range of Colorado. Villarini et al. (2009a) presented a framework for dealing with annual maximum peak discharge under nonstationary conditions. Rosner et al. (2014) introduced a novel methodology for flood risk assessment integrating the concepts of under- and over-preparedness in a nonstationary context. Cheng et al. (2014) developed a Bayesian-based framework for analyzing time-dependent extremes. Reliable nonstationary analysis, however, requires understanding the deterministic process(es) causing time-variant behavior (Cohn and Lins, 2005; Koutsoyiannis, 2005; Montanari and Koutsoyiannis, 2014; Lins and Cohn, 2011; Koutsoyiannis and Montanari, 2015; Serinaldi and Kilsby, 2015). For this reason, projecting observed historical trends may lead to unreliable estimates of frequency for future extremes (Serinaldi and Kilsby, 2015; Luke et al., 2017).

One limitation of the methodologies proposed lies in the use of solely observed historical data for nonstationary extreme value analysis, with some assumption on future trends. However, Global Climate Models (GCM), although they exhibit high uncertainty, offer plausible scenarios of future climate and can be implemented for extreme value analysis, in particular for deriving future IDF curves. Therefore, we first outline a new methodology for deriving multi-model nonstationary IDF curves. It incorporates simulations from multiple GCMs processed using the nonstationary extreme value analysis method proposed by Cheng et al. (2014). The IDF curves derived will then include information from both climate inter-model variability and precipitation changes over time. We then introduce the concept of safety factor, i.e., ratio of medians of the future relative to the past IDF curves, for practitioners who want to account for future changes in infrastructure loads (i.e., precipitation) during the design process and risk analysis. We, finally, propose a new way of communicating the risk of hazardous climatic conditions by calculating the expected future return period (i.e., average occurrence of an event in years) of events which, based on historical observations, have a return period of 25-, 50-, and 100-year. Indeed, characterizing changes in extreme events in terms of changes in the associated return period can be more easily interpreted by both experts and non-experts. We will apply the new framework to annual precipitation maxima intensity in a number of urban areas across the United States to calculate updated future IDF curves, expected future changes in the frequency (return period) of extreme precipitation intensity, and safety factors for the locations investigated.

4.2 Data

In this study, we focus on extreme precipitation events in a number of cities across the United States (see Tables 4.2 and 4.3), where urbanization, when compounded with rare precipitation events, can lead to extreme floods and land-slide activity with potentially high

impacts on the population.

We retrieved downscaled GCM simulations of historical and projected precipitation from the Coupled Model Intercomparison Project Phase 5 (CMIP5), made available through the online archive Downscaled CMIP3 and CMIP5 Climate and Hydrology Projections (DCHP), (Brekke et al., 2013). Future projections are based on four Representative Concentration Pathways (RCPs) each of them describing a potential future GHG concentration trajectory during the 21st century (IPCC2014 - (Field et al., 2014)).

For this study, we selected the CMIP5-BCCAv2 (Bias Corrected Constructed Analogs) daily precipitation products with 1/8 degree spatial resolution, developed using the constructed analogues downscaling method, and bias-corrected based on available observations, using a quantile mapping technique, (Hidalgo et al., 2008). We selected the models in Table 4.1 that provide the following simulations: historical simulations from 1950 to 1999, and future projections between 2050 to 2099 from RCP4.5 (moderate GHG concentration trajectory) and RCP8.5 (very high GHG concentration trajectory). The interval selected for our historical simulations (1950 - 1999) coincides with the period of time in which the historical simulations were adjusted based on available observations (Hidalgo et al., 2008).

Afterwards, we processed GCM daily precipitation to obtain time series of annual maxima precipitation intensity within a water year (October through September, as defined by the United States Geological Survey - USGS) for events of 1-day to 7-day duration. The duration of precipitation events in the present study (1-day events and higher) has been constrained by the time resolution of the GCM simulations. A time series of annual maxima is retrieved as follows. Let's consider the time series of daily precipitation of the j th water year, $P^j = \{p_1^j, \dots, p_{n_j}^j\}$, where n_j is the number of days in the j th water year. The annual maximum precipitation intensity of a d -day event for the j th water year is $P_{d,max}^j = \max\{\frac{\sum_{t=1}^d p_t^j}{d}, \dots, \frac{\sum_{t=i}^{i+d-1} p_t^j}{d}, \dots, \frac{\sum_{t=n_j-d+1}^{n_j} p_t^j}{d}\}$. The time series of annual maxima is then $P_{d,max} = \{P_{d,max}^1, \dots, P_{d,max}^{ny}\}$, where ny is the total number of water years. We processed

the historical simulations and the projections independently, model by model. Each time series consists of 49 water years (number of water years contained in a 50 year period). Thus, each station has the following set of time series: $HE_{m,d}^s$, $FE45_{m,d}^s$, and $FE85_{m,d}^s$ corresponding to historical simulations, RCP4.5, and RCP8.5 projections, respectively; s indicates the urban area; m refers to the GCM; d expresses the duration of the event in days.

4.3 Methodology

4.3.1 Distance Components Test

Here, we are interested in characterizing changes in historical and future precipitation simulations. Specifically, we are interested in testing the null-hypothesis of equal distributions and equal means between extreme precipitation from historical and future simulations to assess whether the statistics of extremes are expected to change. There are specific tests for assessing equal distributions (e.g., Kolmogorov - Smirnov test (Massey, 1951), Cramér - von Mises test (Anderson, 1962), Anderson - Darling test (Anderson et al., 2011)), equal means (e.g., Analysis of Variance (ANOVA) test, Students' t-test), presence of a monotonic trend (e.g., Mann-Kendall trend test (Mann, 1945)). Here, we have adopted the Distance Components (DISCO) test proposed by Rizzo and Székely (2010) that combines equal distribution and equal mean tests. This method is a nonparametric extension of the analysis of variance (ANOVA) and the multivariate analysis of variance (MANOVA) tests as a more generalized hypothesis testing framework (Székely and Rizzo, 2013; Rizzo and Székely, 2010). Compared to the classical ANOVA and MANOVA tests, the DISCO test does not require a minimum sample size and/or homogeneity of the error variance (Rizzo and Székely, 2010), and it can be implemented under different null-hypotheses (i.e., equal means and equal distributions) eliminating the need for additional tests. Moreover, the test, available in the R package *en-*

ergy, is performed by permutation, avoiding any dependence on the choice of the distribution (Rizzo and Székely, 2010; Székely and Rizzo, 2013).

The DISCO test is derived as follows. A version of the Gini mean distance statistic between two samples $A = \{a_1, \dots, a_{n_1}\}$ and $B = \{b_1, \dots, b_{n_2}\}$ is defined as follows (Rizzo and Székely, 2010);

$$g_\alpha(A, B) = \frac{1}{n_1 \cdot n_2} \cdot \sum_{i=1}^{n_1} \sum_{j=1}^{n_2} \|a_i - b_j\|^\alpha = E[\|A - B\|^\alpha] \quad (4.1)$$

where, $\|\cdot\|$ is the Euclidean norm, and $0 < \alpha \leq 2$.

Let's consider K samples X_1, \dots, X_K of sizes n_1, \dots, n_K . Analogous to the decomposition of the variance in the ANOVA test, the total dispersion of the K samples T_α is (Rizzo and Székely, 2010; Székely and Rizzo, 2013):

$$T_\alpha = T_\alpha(X_1, \dots, X_K) = \frac{N}{2} \cdot g_\alpha(X, X) \quad (4.2)$$

where $N = \sum_{k=1}^K n_k$, and X is the pooled sample. Moreover, the within-sample dispersion, W_α , and the between-sample dispersion, S_α , are (Rizzo and Székely, 2010; Székely and Rizzo, 2013):

$$W_\alpha = W_\alpha(X_1, \dots, X_K) = \sum_{k=1}^K \frac{n_k}{2} \cdot g_\alpha(X_k, X_k) \quad (4.3)$$

$$S_\alpha = S_\alpha(X_1, \dots, X_K) = \sum_{1 \leq i < k \leq K} \left[\frac{n_j + n_k}{2N} \right] \cdot \left[\frac{n_j \cdot n_k}{n_j + n_k} \cdot \varepsilon_\alpha(X_j, X_k) \right] \quad (4.4)$$

where $\varepsilon_\alpha = (2g_\alpha(X_j, X_k) - g_\alpha(X_j, X_j) - g_\alpha(X_k, X_k))$ is the Energy distance (ε_α -distance). For $0 < \alpha \leq 2$, the decomposition $T_\alpha = W_\alpha + S_\alpha$ holds and W_α and S_α are non-negative (Rizzo and Székely, 2010; Székely and Rizzo, 2013). For $K \geq 2$ and $0 < \alpha \leq 2$, and X_1, \dots, X_K independent and identically distributed (i.i.d.), the following statements about S_α hold:

- $S_\alpha(X_1, \dots, X_K) \geq 0$;
- for $0 < \alpha < 2$, $S_\alpha(X_1, \dots, X_K) = 0$ if $X_1 = \dots = X_K$;
- $\alpha = 2$, $S_2(X_1, \dots, X_K) = 0$, if and only if X_1, \dots, X_K have equal means.

For proof and details see Theorem 1 and Corollary 1 in (Rizzo and Székely, 2010).

Given the properties of S_α , Rizzo and Székely (2010) proposed the following statistic for testing equal distributions:

$$F_\alpha = \left(\frac{S_\alpha}{K-1} \right) \cdot \left(\frac{N-K}{W_\alpha} \right) \quad (4.5)$$

F_α does not have an F-distribution, but it is non-negative and takes large values when the samples X_1, \dots, X_K are drawn from non-equal distribution, supporting the alternative hypothesis (Rizzo and Székely, 2010).

Here, we implemented the test considering two values of the index α : $\alpha = 1$ to test the null-hypothesis of equal distributions between pairs of time series, and $\alpha = 2$ to test the null-hypothesis of equal means between pairs of time series. The former choice corresponds to the Euclidean distance and allows g_α (eq. 4.1) to be linearized, reducing the computational effort (Rizzo and Székely, 2010). The latter choice adds information about the mean of the two samples.

4.3.2 Extreme Value Analysis for IDF curves

Precipitation-based IDF curves estimation involves fitting a representative distribution function to observed extreme precipitation (Bonnin et al., 2006). Extreme value analysis is widely used in hydrological design and risk assessment for a statistical representation of rare events (Coles, 2001). Time series of annual maxima are commonly described by the Generalized

Extreme Value (GEV) distribution. The cumulative distribution function of the GEV distribution is (Cheng et al., 2014):

$$\Psi(x) = \exp\left\{-\left(1 + \xi \cdot \left(\frac{x - \mu}{\sigma}\right)\right)^{-\frac{1}{\xi}}\right\} \quad (4.6)$$

for $\xi \cdot \left(\frac{x - \mu}{\sigma}\right) > 0$. μ , σ , and ξ are the statistics of the distribution: μ is the location parameter and represents the center of the distribution; σ is the scale parameter and describes the distribution of the data around μ ; ξ is the shape parameter and defines the tail behavior of the distribution. Current IDF curves in the United States, available through the National Oceanic and Atmospheric Administration (NOAA), are derived based on the stationary GEV distribution (i.e., time independent parameters) shown in equation 4.6. The stationary GEV model can be adapted for time-dependent series by letting the parameters of the distribution be a function of time ($\mu(t)$, $\sigma(t)$, $\xi(t)$), (Coles, 2001), for a more realistic representation of the time series behavior (Cheng et al., 2014).

Here, we derived future IDF curves of precipitation based on a GEV distribution with time-dependent statistics only upon detection of a statistically significant trend in the data (Mann-Kendall trend test (Mann, 1945) with a 0.05 level of significance). We used the Nonstationary Extreme Value Analysis (NEVA) framework proposed by Cheng et al. (2014) to estimate the distribution parameters because it has two main advantages:

- (i) it is versatile enough to deal with temporally stationary and nonstationary extremes (including annual maxima and extremes over a particular threshold);
- (ii) it is based on Bayesian inference and Differential Evolution Markov Chain (DE-MC), which provide both parameter estimation and uncertainty quantification (Cheng et al., 2014).

Let θ be the parameter of a given distribution and let $\mathbf{Y} = \{y_1, \dots, y_n\}$ be the set of

n observations. Following the Bayes theorem, the probability of θ given \mathbf{Y} (posterior) is proportional to the product of the probability of θ (prior) and the probability of \mathbf{Y} given θ (likelihood function). Assuming independence between the observations \mathbf{Y} :

$$p(\theta|\mathbf{Y}) \propto \prod_{i=1}^n p(\theta) \cdot p(y_i|\theta) \quad (4.7)$$

In NEVA, the likelihood function is the GEV distribution, and θ is the vector containing the parameters of the GEV distribution to be estimated. In the stationary case, $\theta = \{\mu, \sigma, \xi\}$. Hence, considering independent GEV parameters:

$$p(\mu, \sigma, \xi|\mathbf{Y}) \propto \prod_{i=1}^n p(\mu) \cdot p(\sigma) \cdot p(\xi) \cdot p(y_i|\mu, \sigma, \xi) \quad (4.8)$$

In the case of a nonstationary analysis, θ contains additional parameters, which are the coefficients of the time-dependent functions, e.g., $\mu(t)$, $\sigma(t)$, and $\xi(t)$.

$$p(\theta|Y, t) \propto \prod_{i=1}^n p(\theta) \cdot p(y_i|\theta, t) \quad (4.9)$$

In NEVA, the priors are non-informative normal distributions, for location and scale parameters, while the prior for the shape parameter is a normal distribution, with a standard deviation of 0.3, as suggested by Renard et al. (2013), (Cheng et al., 2014). The DE-MC algorithm is then implemented to sample a large number of realizations of θ over the parameter space, (Cheng et al., 2014). The \hat{R} criterion (Gelman and Shirley, 2011) is used to assess convergence, where \hat{R} should remain below 1.1 (Cheng et al., 2014). Moreover, Bayes factor is implemented as a test for model selection: it compares the posterior distributions of two alternative models (e.g. stationary model vs. non-stationary model) (Cheng et al., 2014; Renard et al., 2013). For further details about the Bayesian parameter estimation approach, the reader is referred to Cheng et al. (2014) and Cheng and AghaKouchak (2014).

In this study, the nonstationary GEV distribution refers to a GEV distribution with either

the location parameter or location and scale parameters as a function of time. Hence, θ is in the former case $\theta = \{\mu_1, \mu_0, \sigma, \xi\}$, and in the latter $\theta = \{\mu_1, \mu_0, \sigma_1, \sigma_0, \xi\}$. The selection of the nonstationary model versus a stationary model depends on the Mann-Kendall trend (MK, with 5% significance level) test, which characterizes the average behavior (mean) of the data over time. The mean can be regarded as an approximation of the location parameter of the GEV distribution. Hence, we modeled $\mu(t)$ to reproduce the observed trend. We assumed $\mu(t) = \mu_1 \cdot t + \mu_0$, because a more complex trend could likely result in an overfitting of the observation period and lead to an unrealistic representation of the future (Serinaldi and Kilsby, 2015). Even though more complex models are considered in the literature to be more accurate (e.g., Kwon and Lall, 2016; Sarhadi et al., 2016), parsimonious models (i.e., models showing desired level of performance efficiency with a minimum number of parameters) have shown to perform better (Serinaldi and Kilsby, 2015; Luke et al., 2017; Serago and Vogel, 2018). In the case of a time-dependent location parameter, the White test (White, 1980) for homoscedasticity is performed; if the null-hypothesis of constant variance in the residuals is rejected (with 5% significance level), we assumed a non-stationary model with time-dependent location and scale parameters. The scale parameter is modeled as $\log(\sigma(t)) = \sigma_1 \cdot t + \sigma_0$, as suggested by Coles (2001) to ensure positivity. Finally, ξ was kept constant given the difficulties to precisely estimate it, (Coles, 2001), especially for short time series, (Papalexiou and Koutsoyiannis, 2013).

4.3.3 Incorporating Multi-Model Simulations for IDF curve Analysis

GCM projections can provide information on characteristics of future extremes. Consequently, we propose a new framework for deriving IDF curves of precipitation based on multi-model simulations. First, we derived the IDF curves for the climate models using the aforementioned Bayesian inference approach (i.e., NEVA). Since there is significant variabil-

ity across the climate models, we chose to estimate the IDF curves for each model separately (Figure 4.1). We then merged the resulting IDF curves from each model to derive multi-model IDF curves. The final result is the expected IDF curve along with its uncertainty bounds, which summarize the variability due to both the parameter estimation approach (variability within each model) and the diversity of climatic models (variability across models).

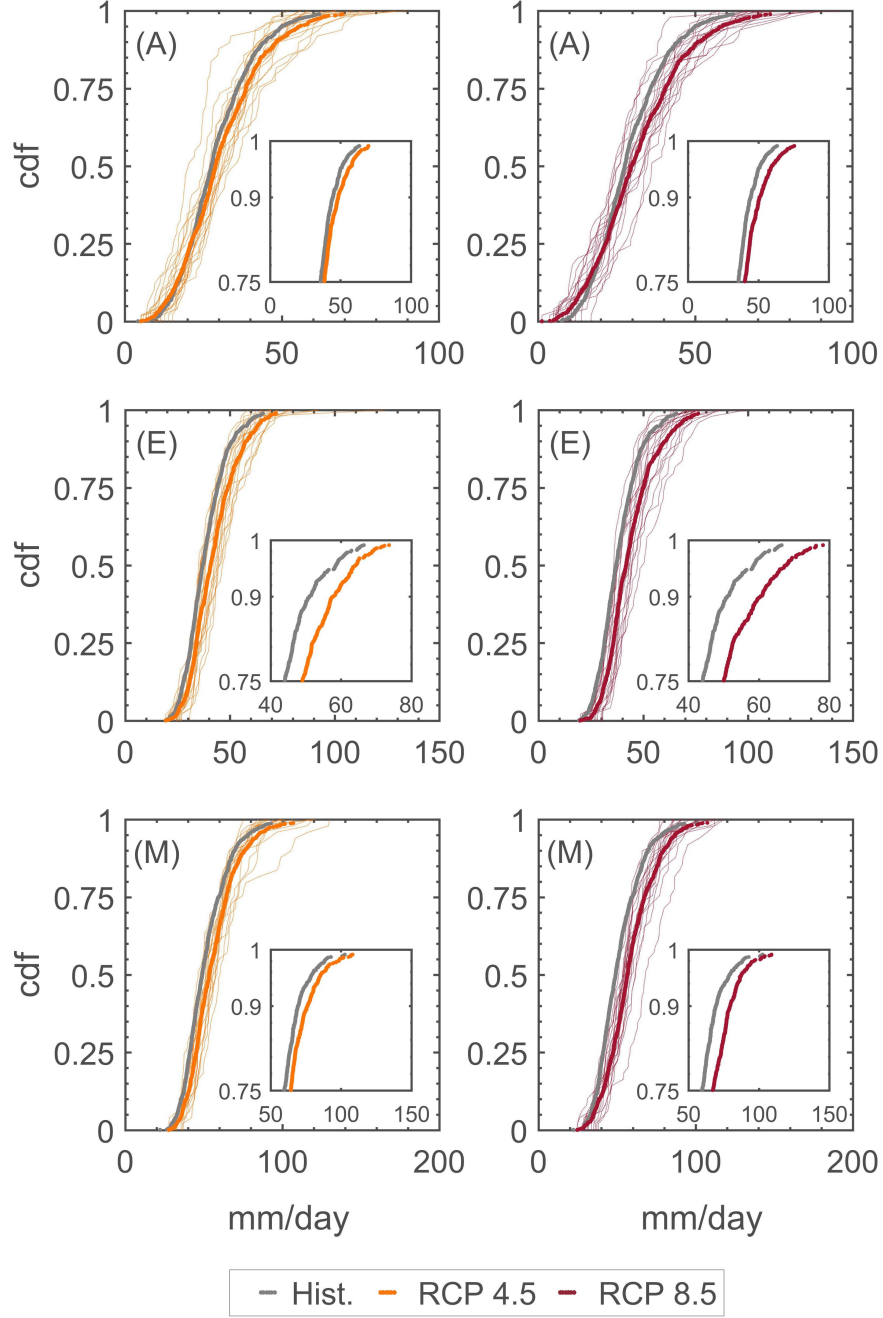


Figure 4.1: Comparison between 1-day extreme historical records (grey dotted line) and future climate (RPC4.5 orange and RCP8.5 red dotted line) ECDFs. The shaded dotted lines represent the uncertainty on the future climate. The inner boxes show the right tail behavior of the distributions. A) San Diego - CA, E) Chicago - IL, M) Atlanta - GA.

Here, we applied the proposed framework to annual precipitation maxima intensities from historical simulations $HE_{m,d}^s$ and future climate $FE45_{m,d}^s$ and $FE85_{m,d}^s$. Consequently, for

each station, we derived the historical multi-model IDF curves and future multi-model IDF curves based on RCP4.5 and RCP8.5 scenarios. We derived historical IDF curves imposing a stationary GEV model without performing a trend test, to be consistent with NOAA's IDF curves. We then derived IDF curves from future climate projections RCP4.5 and RCP8.5 separately; the GEV model selected (stationary/nonstationary) depends upon the result of the Mann-Kendall trend test, and subsequent White test. GCMs provide gridded area average simulations while the current IDF curves available from NOAA are mainly based on point observations. Gridded area averaged observations are always smoother compared to point observations. Hence, we identified a bias by comparing historical IDF curves and NOAA IDF curves, which implies assuming a quantile-based bias. We then applied the same correction to historical and projected IDF curves.

In the case of a nonstationary GEV model, the GEV distribution function is time-dependent. The intensity of the p -event is then given by equation 4.10:

$$q_p = \left(\left(-\frac{1}{\ln(p)} \right)^\xi - 1 \right) \cdot \frac{\hat{\sigma}}{\xi} + \hat{\mu} \quad (4.10)$$

where $\hat{\mu}$ is $\hat{\mu} = \text{median}(\mu(t))$ and $\hat{\sigma}$ is $\hat{\sigma} = \text{median}(\sigma(t))$. We selected $\hat{\mu}$ and $\hat{\sigma}$ within the period of the simulations to avoid any further projections of future climate. Finally, we investigate how the frequency of past events is expected to change. Given the i th set of GEV parameters (μ_i , σ_i , and ξ_i) from the ensemble of solution, the expected return period T_i is given by $\frac{1}{1-\Psi(I_T)}$, where $\Psi(I_T)$ is as follows:

$$\Psi(I_T) = \exp \left\{ - \left(1 + \xi_i \cdot \left(\frac{I_T - \mu_i}{\sigma_i} \right) \right)^{-\frac{1}{\xi_i}} \right\} \quad (4.11)$$

Consequently, a sample of the return periods T_i of an event of intensity I_T can be retrieved, Figure 4.2, and inference can be made.

In this study, we selected the intensity of a 1-day event with return period T , I_T , from the

current NOAA precipitation frequency estimates for a specific location. To assess whether the recurrence of an event with intensity I_T is projected to change under future climate scenarios, we used the ensemble of return level curves retrieved via Bayesian inference to define IDF curves, and we derived the 0.25-, 0.50-, and 0.75-percentile of the ensemble. We then evaluated the expected future return period, along with its inter-quartile variability as the intersection between I_T and the 0.25-, 0.50-, and 0.75-percentile curves.

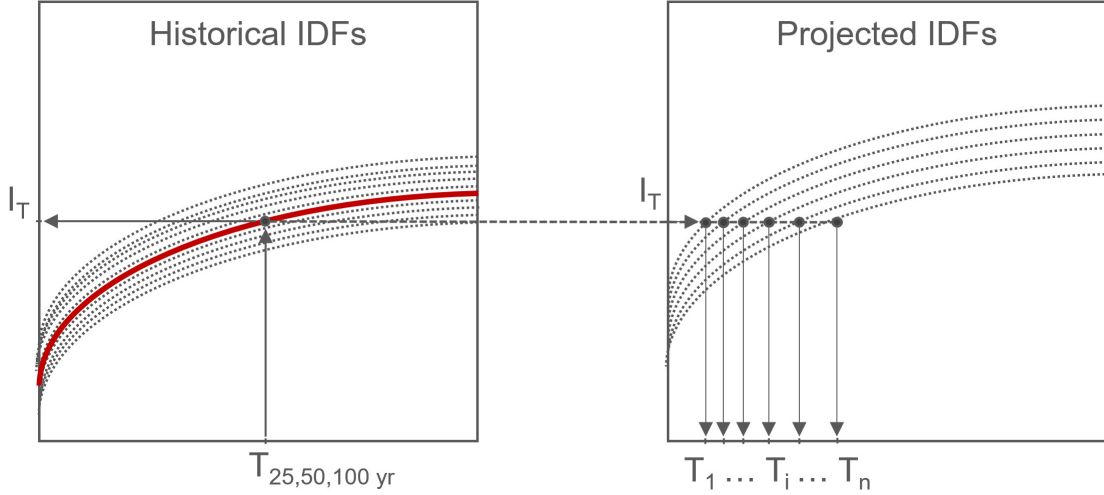


Figure 4.2: Conceptual explanation of the methodology adopted to quantify changes in the occurrences of historical events under future climate.

4.4 Results

The null-hypotheses of equal distributions ($\alpha = 1$) and equal means ($\alpha = 2$) between the median of historical records and the future climate projections are rejected ($p_{value} \sim 0$), indicating that the occurrence of future extreme precipitation intensities are likely to diverge from historical ones. This contradicts the commonly-used stationary assumption in infrastructure design and risk assessment. Figure 4.1 shows the Empirical Cumulative Distribution Functions (ECDFs) of 1-day extreme precipitation for 3 of the selected stations; Table 4.2 summarizes the percent change in the median and in the 90th quantile of the simulated 1-day

extreme precipitation intensity. The ECDFs of future climate precipitation extremes (Figure 4.1) display a shift towards the right, indicating that these cities may face an increase in severe rare events in the near future, even though there is high variability across the models. Overall, the RCP 8.5 scenario seems to lead to more severe events. In the western U.S., the percent change in the median and the 90th quantile is around 10% for RCP4.5 and 10-15 % RCP 8.5. Sacramento (CA) and Salt Lake City (UT) are the exception, as they display a percent change around 20% for both scenarios (Table 4.2). In the eastern U.S., Chicago (IL), Nashville (TN), and New York (NY) display a 15-20% change in the median and 90th quantile for RCP 8.5, while the remaining cities exhibit a change around 10% or below for both scenarios (Table 4.2). IDF curves provide information on the magnitude and recurrence of extreme events based on frequency analysis. For this reason, shifts in extreme rainfall distribution will affect how the IDF curves are defined, and will also affect the intensity of the design value for the event. Therefore, the resilience of infrastructures and natural and engineered slopes can be compromised. Figures 4.3, 4.4, and 4.5 illustrate pairs of current and projected IDF curves along with the 90% Confidence Interval (or Credible Interval) within and across climatic models based on RCP 8.5 scenario (see Figures 4.8 - 4.10 for RCP 4.5) Under the future scenarios chosen, our results show an overall upward shift of the IDF curves, indicating that more severe events are expected to occur. Assuming that climate model simulations provide reasonable estimates of future extremes, Figure 4.6b and Figure S4 show the so-called safety factors C (i.e., ratio of medians of the future relative to the past IDF curves), if one is interested in adjusting current design values to cope with a changing climate. In western U.S., the intensity of extreme events could potentially experience a 20% increase, e.g. Salt Lake City and Sacramento, Figure 4.6b. After investigating the change in extreme event intensity for a fixed return period, we explored changes in the frequency of extreme events of 1-day duration for a given event magnitude. Specifically, we chose the intensity of three baseline events corresponding to 25-, 50- and 100-year events (retrieved from current NOAA IDF curves) to estimate their expected occurrence in the future, along

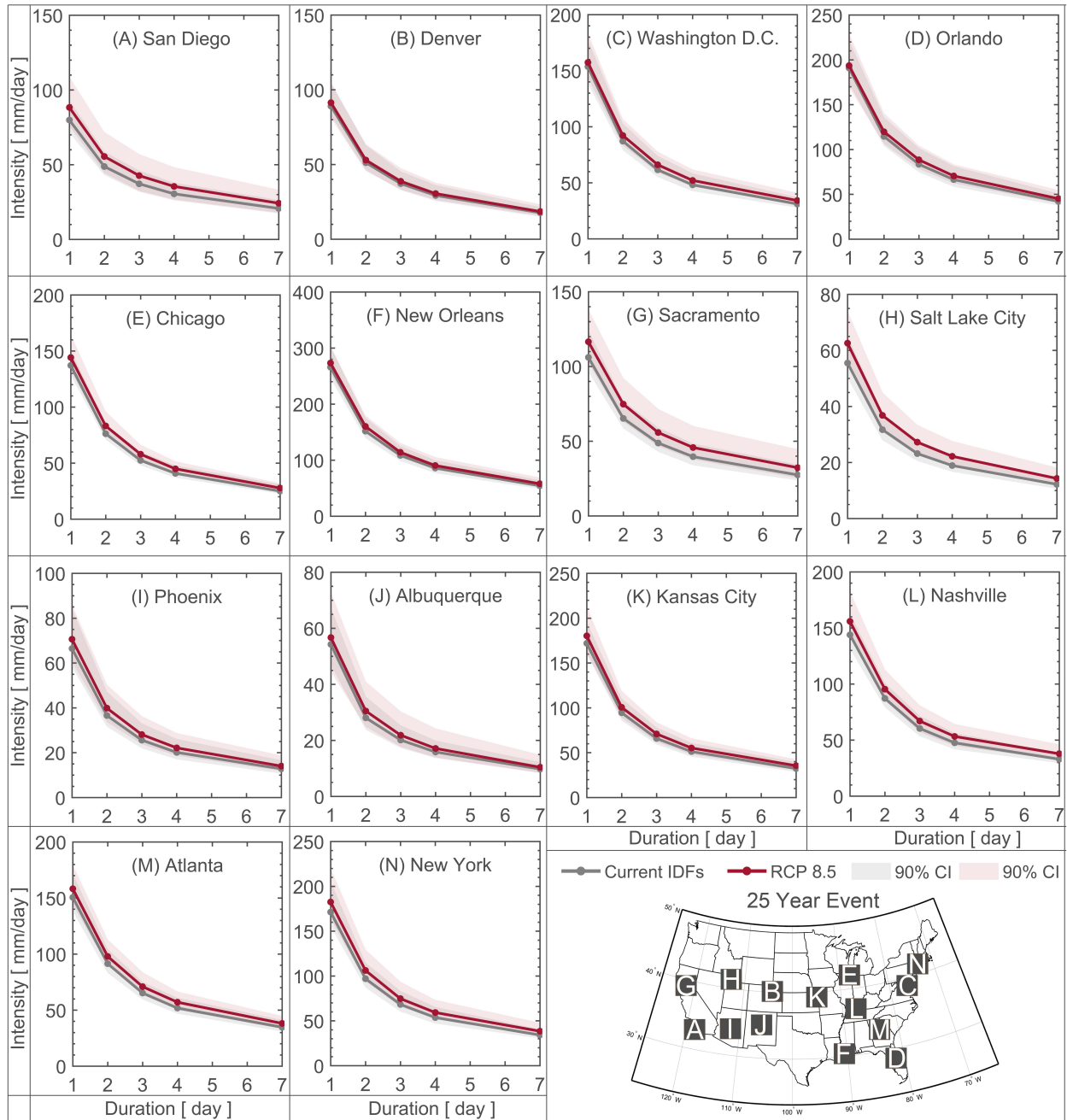


Figure 4.3: RCP 8.5 - Comparison between current (grey lines) and future climate scenario (red lines) IDF curves, along with 90 % confidence intervals, given an average return interval of 25 years.

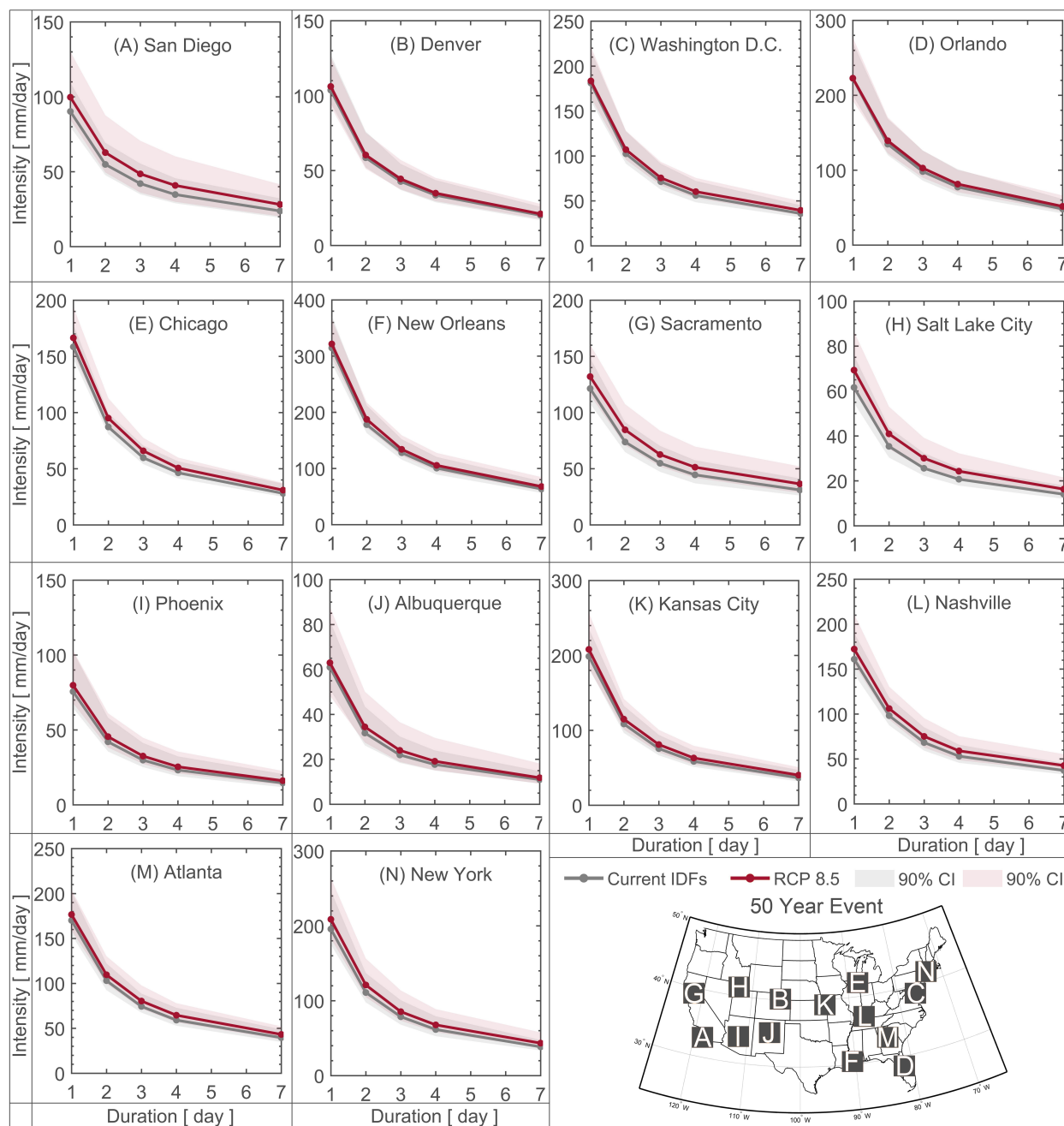


Figure 4.4: RCP 8.5 - Comparison between current (grey lines) and future climate scenario (red lines) IDF curves, along with 90 % confidence intervals, given an average return interval of 50 years.

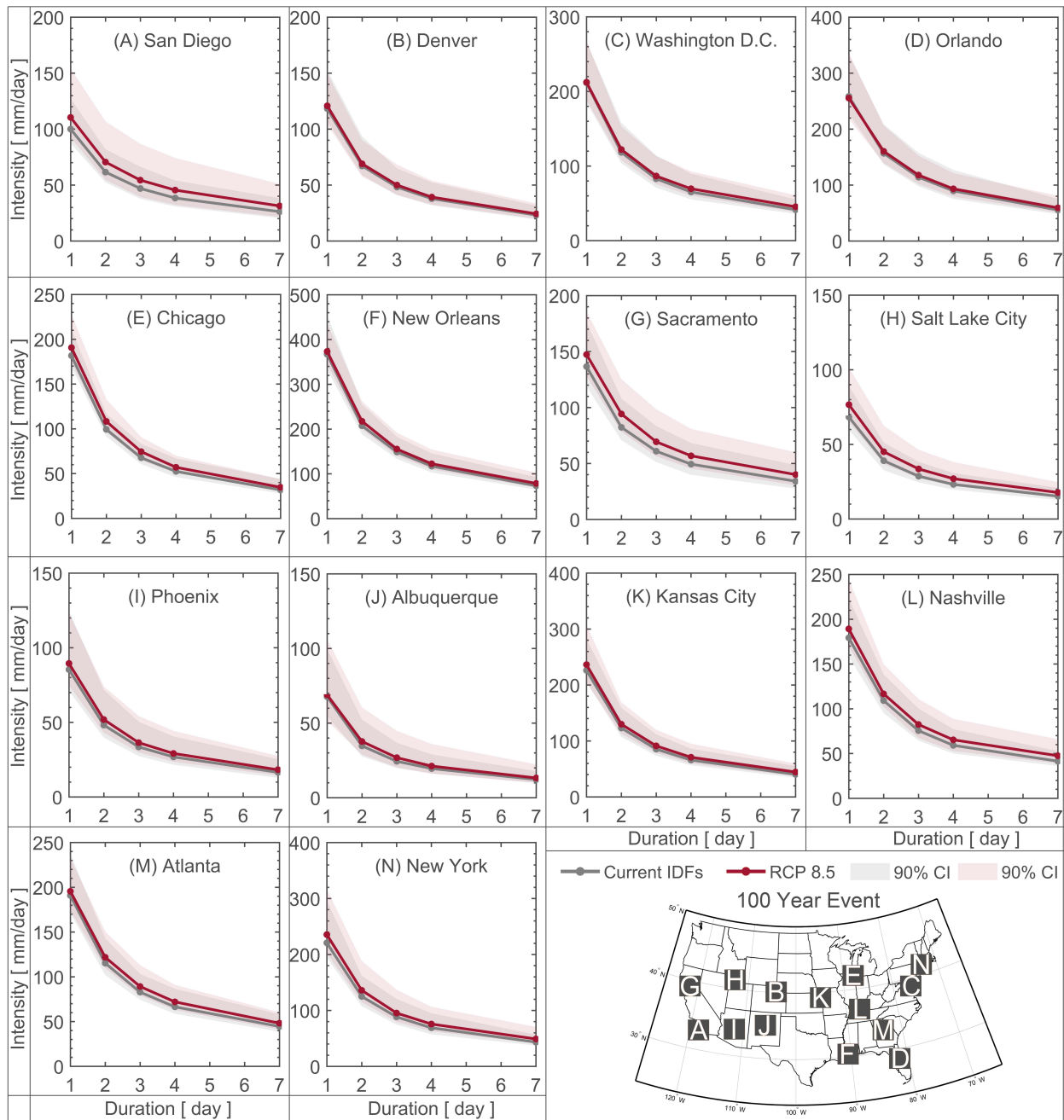


Figure 4.5: RCP 8.5 - Comparison between current (grey lines) and future climate scenario (red lines) IDF curves, along with 90 % confidence intervals, given an average return interval of 100 years.

with their inter-quartile range (IQR). Figure 4.6a illustrates the return periods expected in the future of the baseline events (dots), along with the IQR (gray lines). Events expected to occur every 50, or 100 years are becoming more frequent, raising public safety concerns within anthropized environments, especially in the western U.S.. For example, climate model simulations project that the frequency of a 50-year event in the future will double in San Diego (CA) and Salt Lake City (UT). Although the future scenarios predict changes in magnitude and frequency of extreme precipitation events, total annual mean rainfall is expected to remain the same. Figure 4.6c shows that locations in the eastern U.S. register an increase in mean total annual precipitation and moderate changes in extreme events, whereas locations in the western U.S. do not expect to receive more water overall than in the past, even though extreme events are predicted to become more severe and more likely. A recent study argues that drought conditions in California, linked to warmer temperatures, have been worsened over the past decades, even though negative precipitation anomalies have not shown any change (Diffenbaugh et al., 2015). Analogously, in California we observed total annual precipitation in a future climate consistent with the past. Consequently, to better characterize meteorological extremes over the state, we analyzed a number of urban locations mainly along California’s coast (Table 4.3), adopting the same procedures used for the other urban stations across the U.S.. California’s IDF curves are shown in Figures 4.17 - 4.22. However, we only used the four GCMs as recommended by the guidelines for originating the California’s Fourth Climate Change Assessment Report (Table 4.4) that offer much higher spatial resolution (1/16 degree). Our results suggest a substantial increase in the severity of future extreme precipitation events for RCP 8.5 scenario (Figure 4.7). The results indicate an approximately threefold increase in occurrences of extremes relative to past events, particularly in southern California (Figure 4.7).

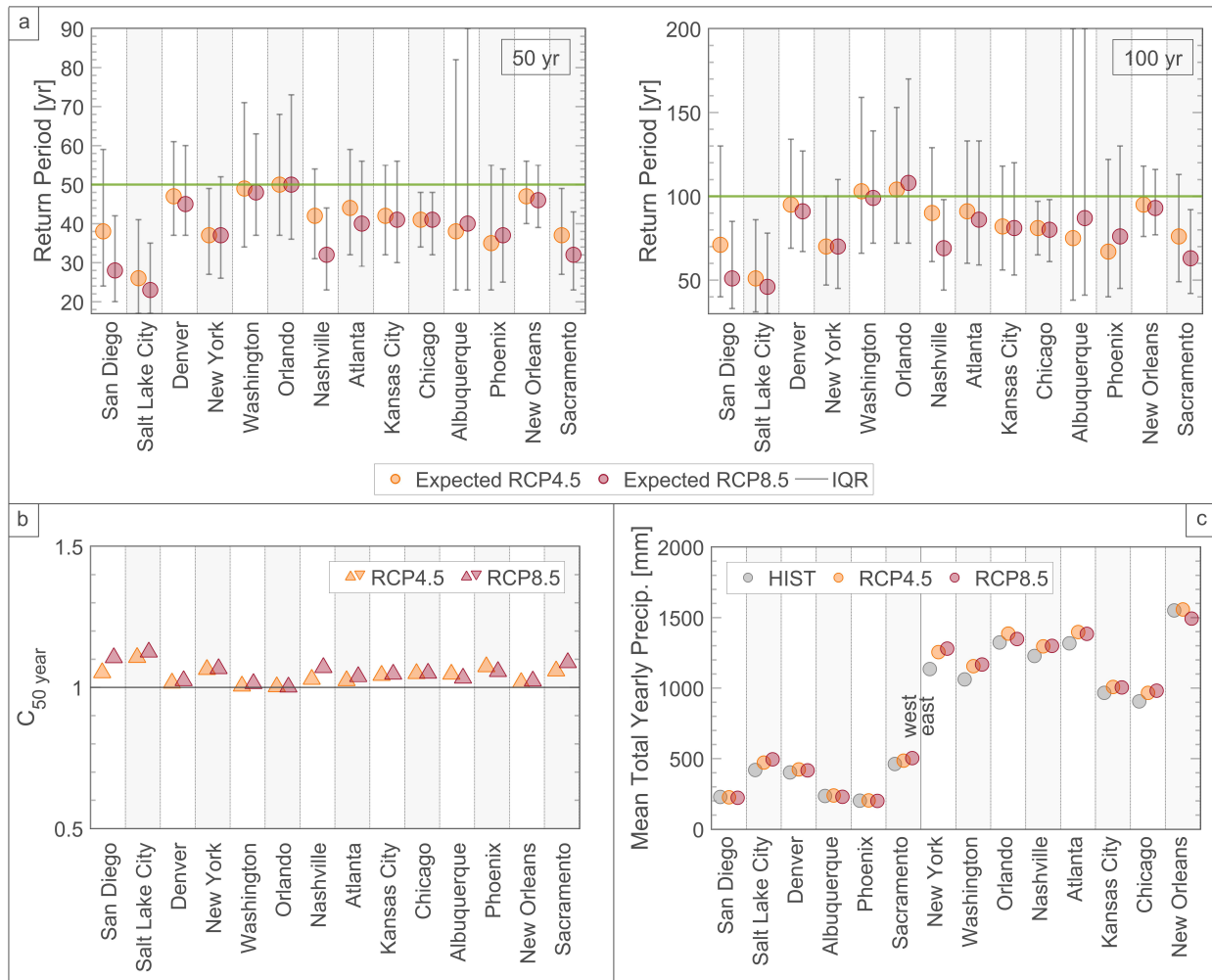


Figure 4.6: a) Return periods under future climate of events currently associated with return periods of 50-, and 100-year in urban locations across the U.S.: expected projected return periods (dots) along with inter-quartile range (IQR - grey lines). b) Safety factors (i.e., ratio of medians of the future relative to the past IDF curves). c) Total annual mean precipitation of historical records.

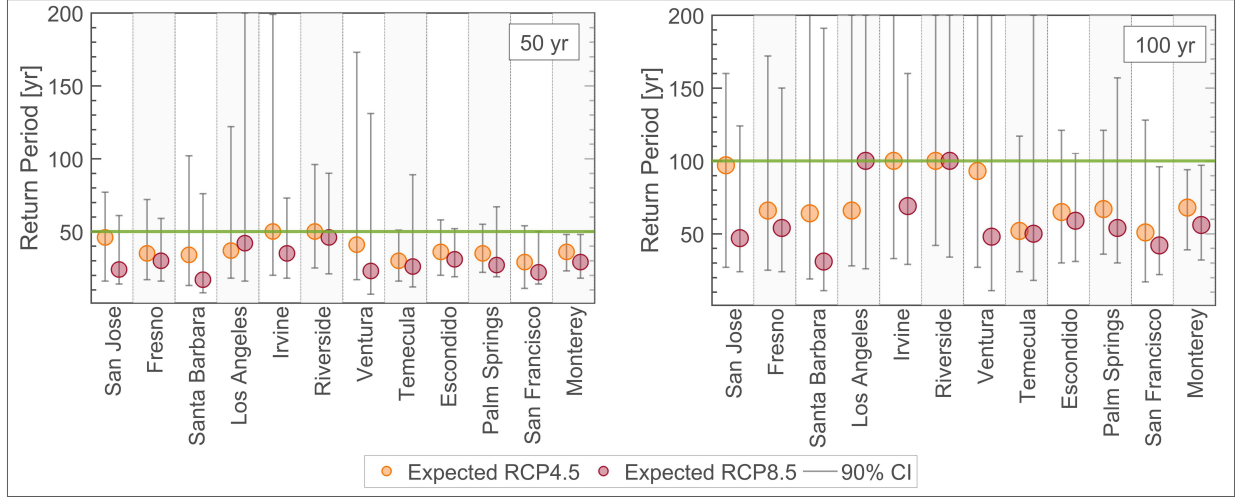


Figure 4.7: Return periods under future climate of events historically associated with return periods of 50-, and 100-year in California. Expected projected return periods (dots) and 90 % confidence interval (gray lines).

4.5 Conclusion and Discussion

In this study, we have shown the potential impacts of a warming climate on extreme precipitation intensity and recurrence interval. Urban areas, especially in the western U.S., may struggle against increases in severity and frequency of rare events. Increase in intensity, duration, and frequency of extreme precipitation can adversely impact the integrity of infrastructure and natural and engineered slopes. Infrastructure built with soil (e.g., earthen dams, levees, embankments), or that interface with soil (e.g., roads, bridge, pipelines, foundations), are more vulnerable because severe rainfall causes soil erosion and, upon infiltration, can significantly reduce the strength of soil. The topic of infrastructure resilience is even more important in regions where multiple drivers of change coincide. Coastal cities, for example, are even more vulnerable due to the compounding effects of sea level rise and change in climate (Hallegatte et al., 2013). By 2070, the population jeopardized by extreme floods is expected to increase threefold with exposed assets increasing by approximately 9% of the projected global GPD of the same period (Hanson et al., 2011).

We argue that better infrastructure planning and maintenance is fundamental for a resilient society. The proposed method for addressing nonstationarity in future climate scenarios can reduce the risk of underestimating future extreme precipitation events and their severity. The adaptation of existing infrastructure, which were designed assuming a stationary climate, requires assessing their performance under future climate scenarios. Further, it requires revisiting design guidelines for infrastructure to employ nonstationary IDF curves in future design procedures.

4.6 Supporting Information

Appendix based on the Supporting Information of the following published work:

Ragno, E., AghaKouchak, A., Love, C. A., Cheng, L., Vahedifard, F., and Lima, C. H. R. (2018). Quantifying changes in future IntensityDurationFrequency curves using multimodel ensemble simulations. Water Resources Research, 54, 17511764. <https://doi.org/10.1002/2017WR021975>.

RCP 4.5	RCP 8.5
access1-0.1.rcp45	ccess1-0.1.rcp85
bcc-csm1-1.1.rcp45	bcc-csm1-1.1.rcp85
canesm2.1.rcp45	canesm2.1.rcp85
ccsm4.1.rcp45	ccsm4.1.rcp85
cesm1-bgc.1.rcp45	cesm1-bgc.1.rcp85
cnrm-cm5.1.rcp45	cnrm-cm5.1.rcp85
csiro-mk3-6-0.1.rcp45	csiro-mk3-6-0.1.rcp85
gfdl-esm2g.1.rcp45	gfdl-esm2g.1.rcp85
gfdl-esm2m.1.rcp45	gfdl-esm2m.1.rcp85
inmcm4.1.rcp45	inmcm4.1.rcp85
ipsl-cm5a-lr.1.rcp45	ipsl-cm5a-lr.1.rcp85
ipsl-cm5a-mr.1.rcp45	ipsl-cm5a-mr.1.rcp85
miroc-esm.1.rcp45	miroc-esm.1.rcp85
miroc-esm-chem.1.rcp45	miroc-esm-chem.1.rcp85
miroc5.1.rcp45	miroc5.1.rcp85
mpi-esm-lr.1.rcp45	mpi-esm-lr.1.rcp85
mpi-esm-mr.1.rcp45	mpi-esm-mr.1.rcp85
mri-cgcm3.1.rcp45	mri-cgcm3.1.rcp85
noresm1-m.1.rcp45	noresm1-m.1.rcp85

Table 4.1: List of Global Climate Models used

Location	State	Lat.	Long.	Change in Median		Change in 90th	
		°N	° W	%		%	
				RCP 4.5	RCP 8.5	RCP 4.5	RCP 8.5
San Diego	CA	32.71	117.16	5.9	8.8	8.0	14.4
Salt Lake City	UT	45.51	122.68	17.0	22.2	20.1	20.2
Denver	CO	39.71	105.01	4.8	4.5	1.8	0.5
New York	NY	40.71	74.03	9.8	13.5	10.0	10.7
Washington D.C.		38.93	77.04	10.1	11.2	10.7	8.8
Orlando	FL	28.55	81.36	4.6	7.0	5.6	9.2
Nashville	TN	36.16	86.81	11.7	18.8	10.1	18.9
Kansas City	MO	39.09	94.58	8.2	10.4	7.8	11.7
Atlanta	GA	33.75	84.39	8.8	13.3	9.13	14.1
Chicago	IL	41.87	87.63	10.4	13.9	12.9	18.3
Albuquerque	NM	35.09	106.60	9.0	9.4	12.0	11.2
Phoenix	AZ	33.43	112.05	7.8	9.2	11.6	10.5
New Orleans	LA	29.94	90.06	5.3	7.3	5.9	5.1
Sacramento	CA	38.57	121.49	11.9	16.1	12.8	18.2

Table 4.2: Observed Changes in Median and 90th quantile of 1-day precipitation event.

City	Lat.	Long.
	°N	° W
San Jose	37.34	58.11
Fresno	36.74	60.22
Santa Barbara	34.42	60.30
Los Angeles	34.04	61.78
Irvine	33.67	62.20
Riverside	33.95	62.61
Ventura	34.28	60.78
Temecula	33.49	62.85
Escondido	33.12	62.91
Palm Springs	33.84	63.47
San Francisco	37.78	57.58
Monterey	36.59	58.10

Table 4.3: Cities in California investigated in the study.

RCP 4.5	RCP 8.5
HadGEM2-ES.rcp45	HadGEM2-ES.rcp85
CNRM-CM5.rcp45	CNRM-CM5.rcp85
CanESM2.rcp45	CanESM2.rcp85
MIROC5.rcp45	MIROC5.rcp85

Table 4.4: List of LOCA downscaled Global Climate Models used for California

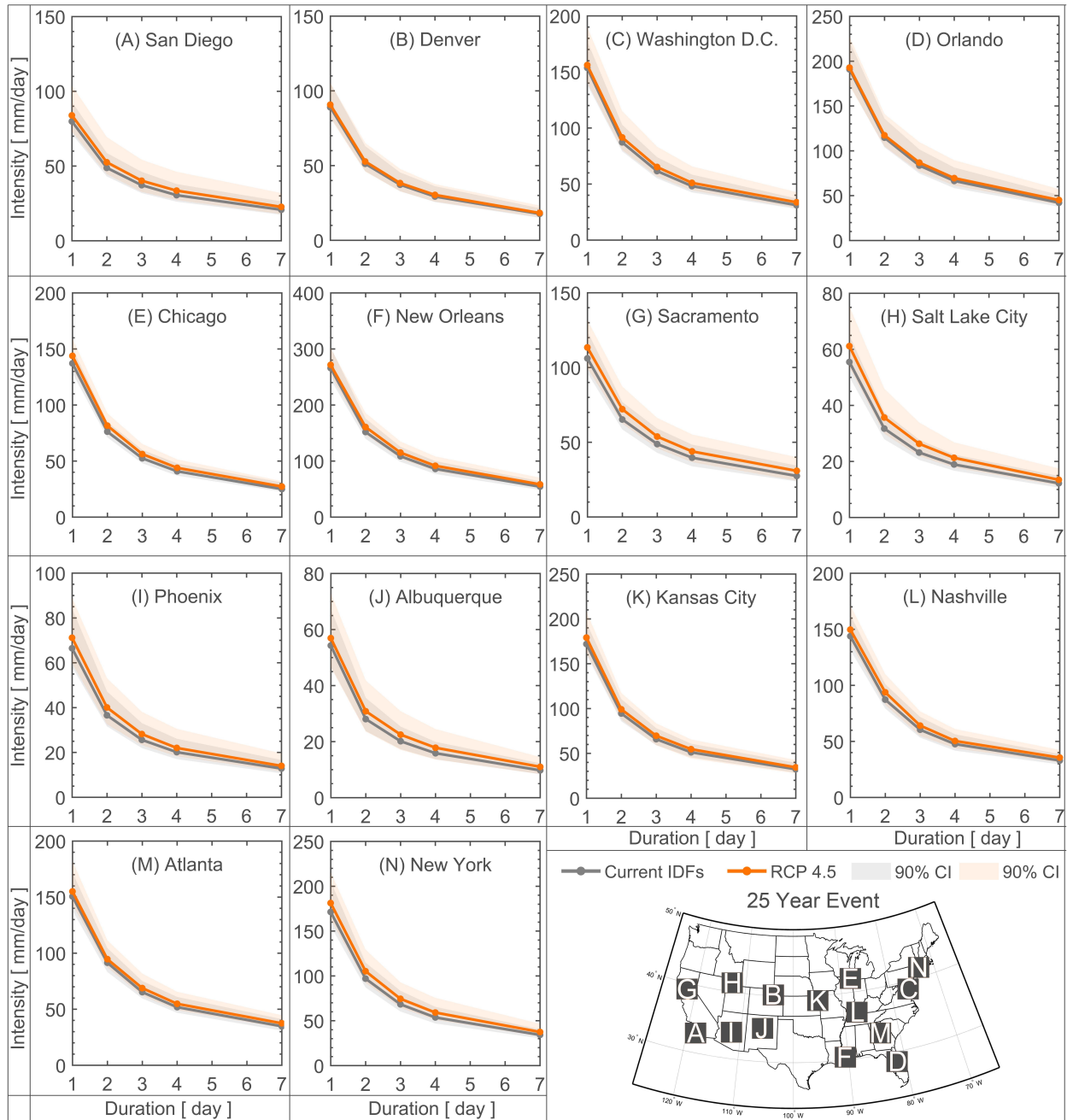


Figure 4.8: RCP 4.5 - Comparison between current (grey lines) and future climate scenario (orange lines) IDF curves, along with 90 % confidence intervals, given an average return interval of 25 years.

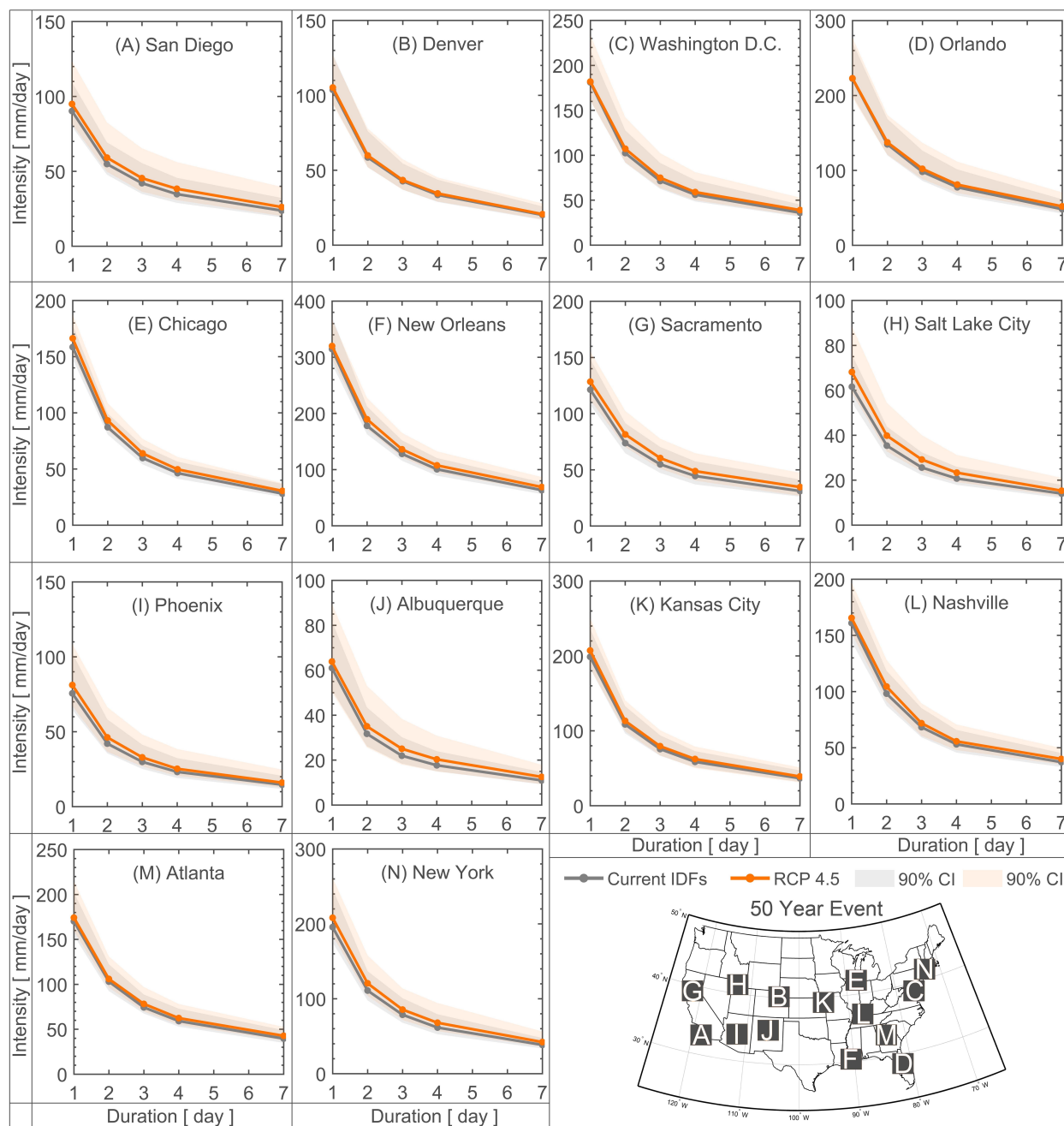


Figure 4.9: RCP 4.5 - Comparison between current (grey lines) and future climate scenario (orange lines) IDF curves, along with 90 % confidence intervals, given an average return interval of 50 years.

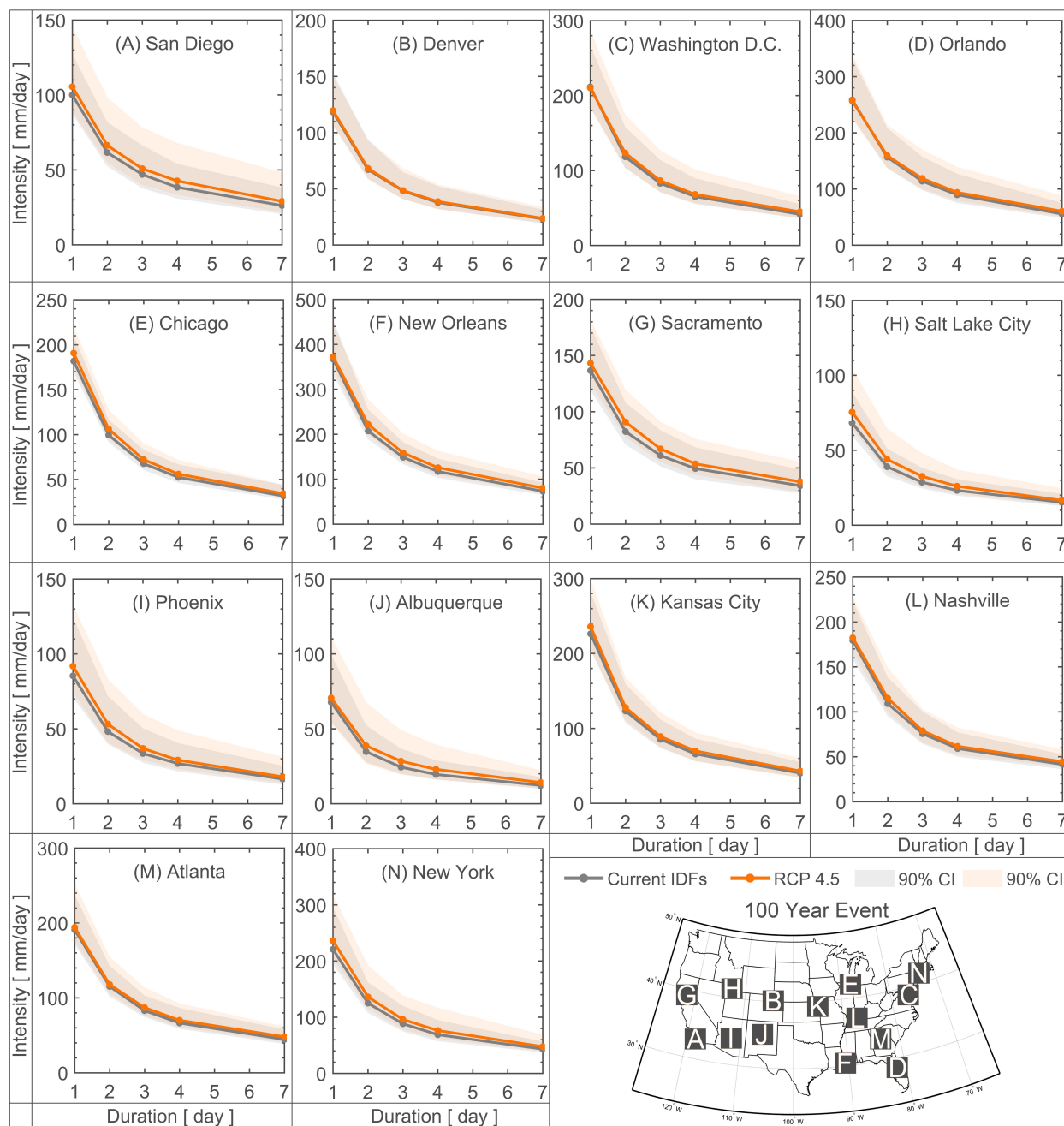


Figure 4.10: RCP 4.5 - Comparison between current (grey lines) and future climate scenario (orange lines) IDF curves, along with 90 % confidence intervals, given an average return interval of 100 years.

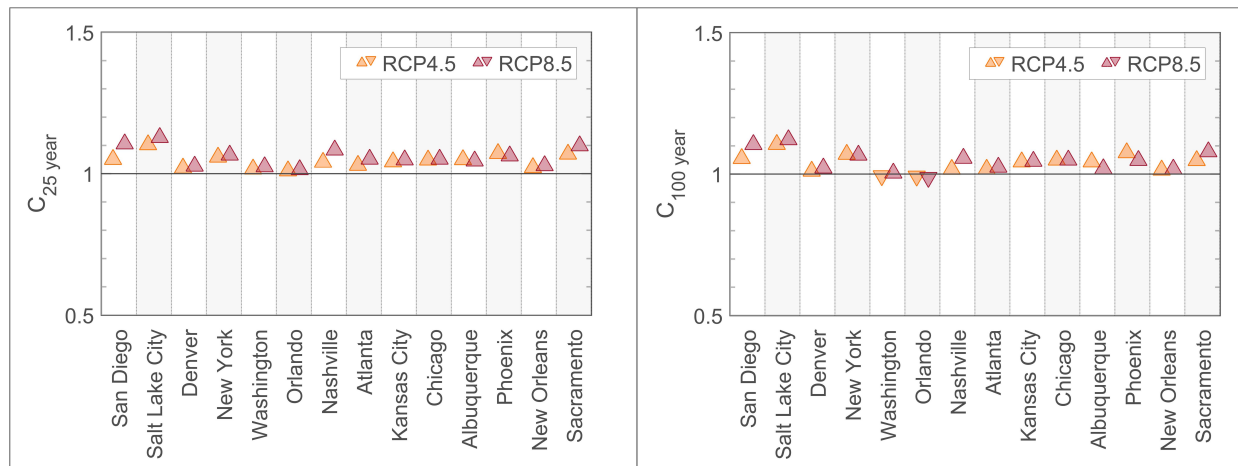


Figure 4.11: So-called safety factor (i.e., the ratio of medians of the future relative to the past IDF curves) for 25- and 100-year events.

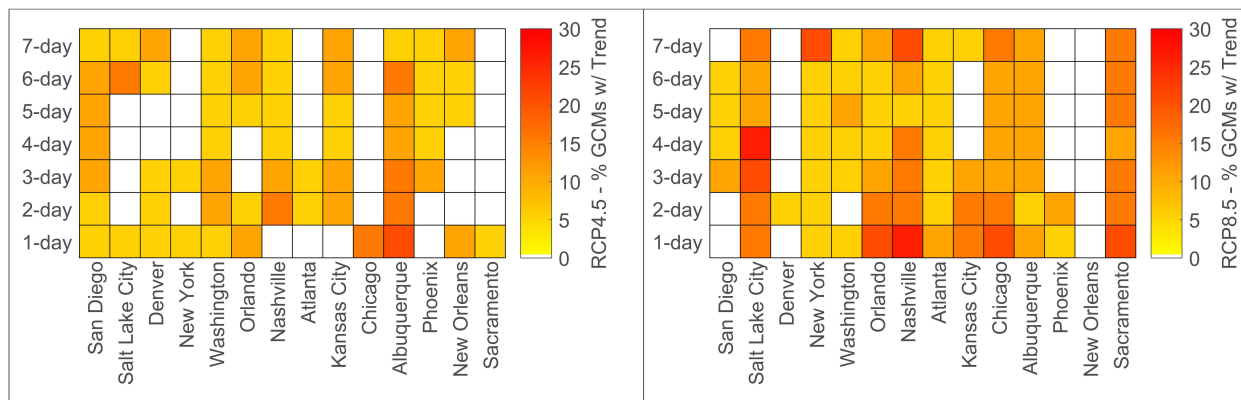


Figure 4.12: Percent of GCMs showing a statistical significant trend in the time series of extreme maxima precipitation intensities based on Mann - Kendall trend test. Significance level 5%.

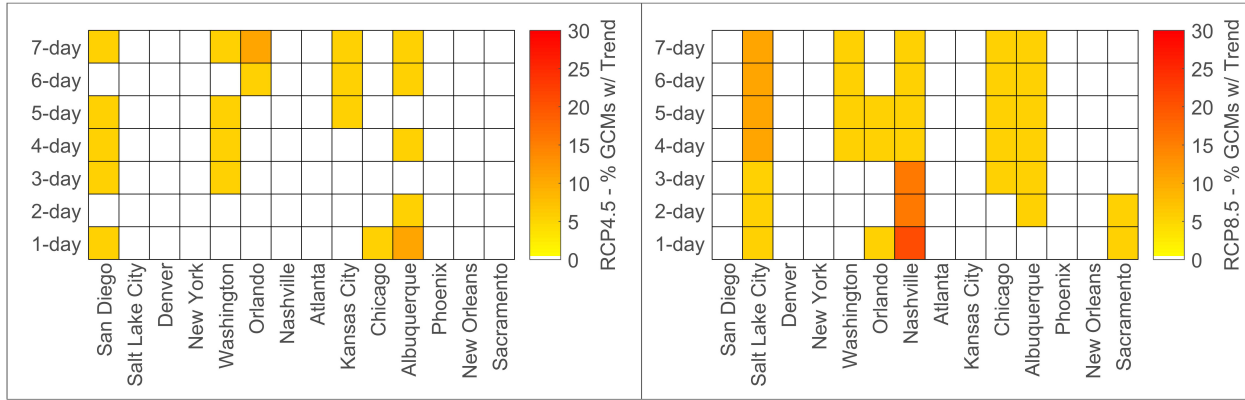


Figure 4.13: Percent of GCMs showing a statistical significant trend in the time series of extreme maxima precipitation intensities based on Mann - Kendall trend test. Significance level 1%.

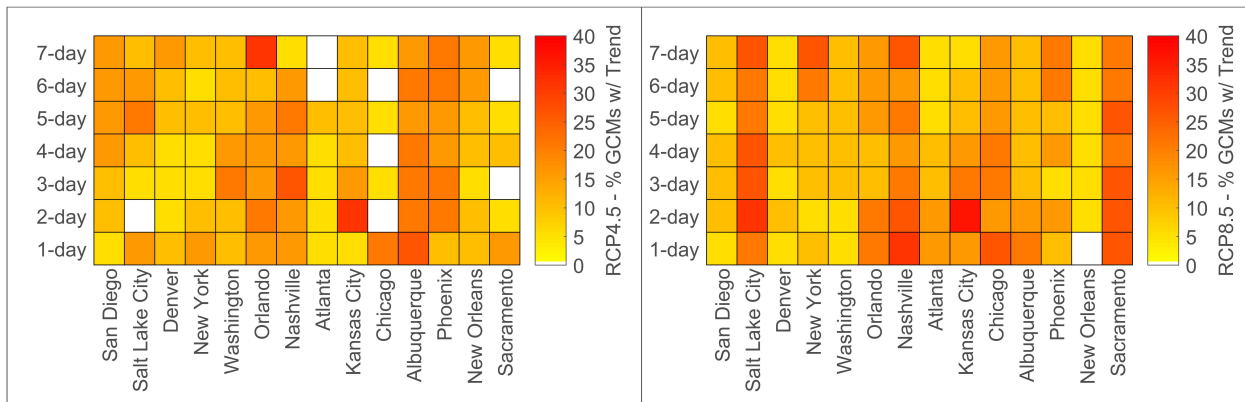


Figure 4.14: Percent of GCMs showing a statistical significant trend in the time series of extreme maxima precipitation intensities based on Mann - Kendall trend test. Significance level 10%.

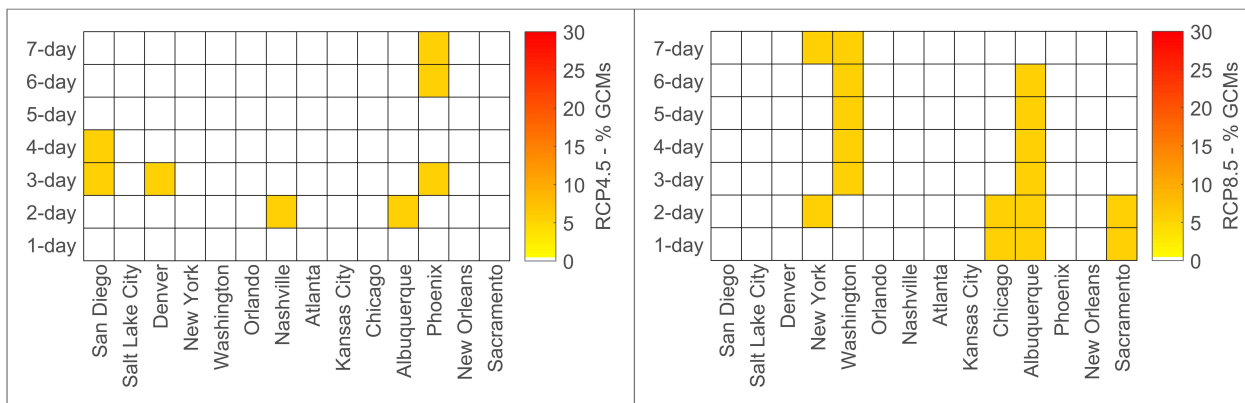


Figure 4.15: Percent of GCMs showing a statistical significant trend in the time series of extreme maxima precipitation intensities (Mann-Kendall trend test, significance level 5%) and statistical significant variability in the residuals (White test, significance level 5%).

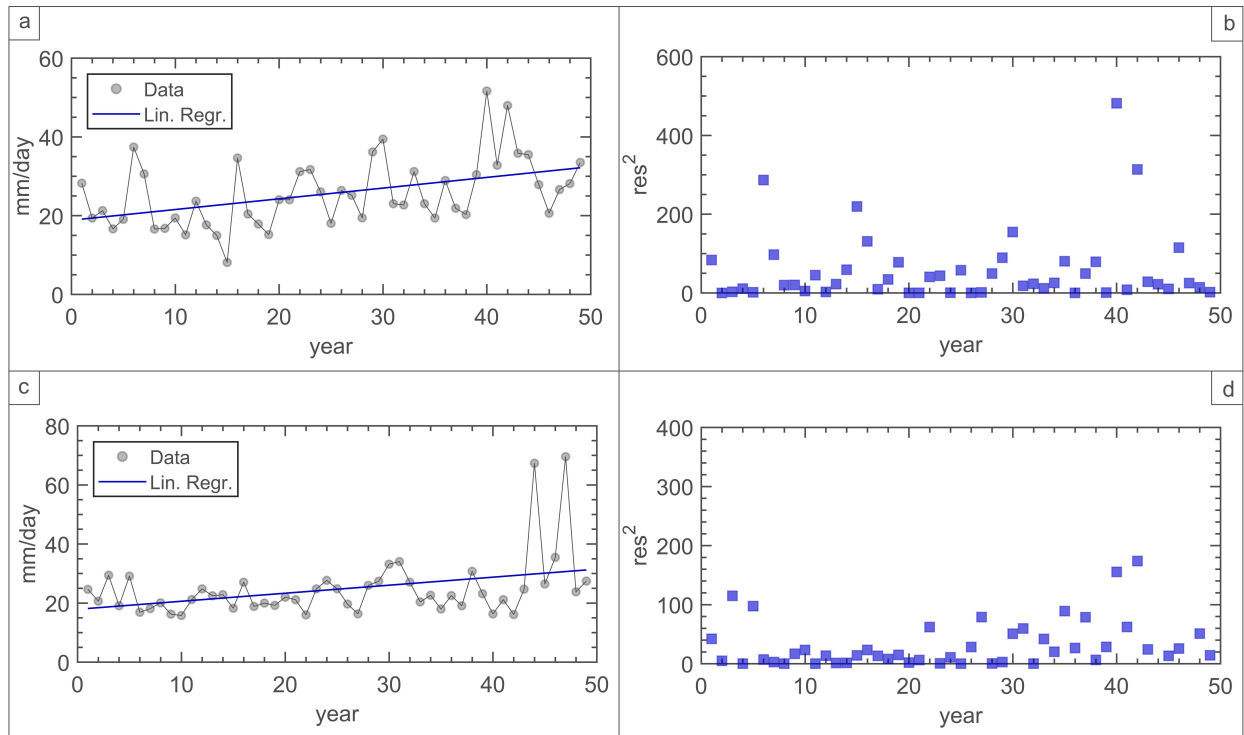


Figure 4.16: a) Example of annual time series with a significant trend and b) constant variance of the residuals - RCP8.5 Salt Lake City ; c) example of annual time series with a significant trend and d) time dependent variance of the residuals - RCP8.5 Washington D.C..

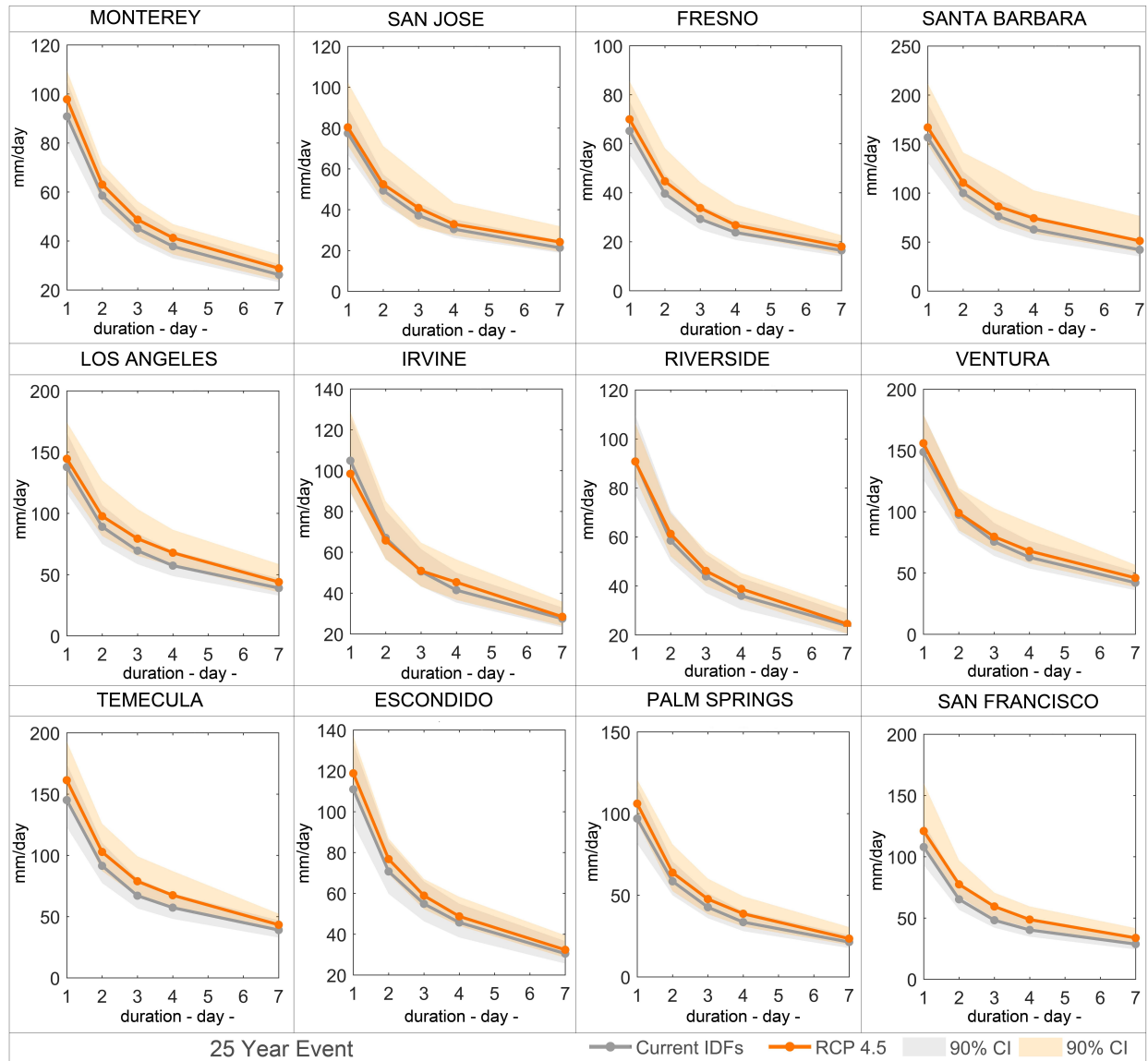


Figure 4.17: RCP 4.5 - California - Comparison between current (grey lines) and future climate scenario (orange lines) IDF curves, along with 90 % confidence intervals, given an average return interval of 25 years.

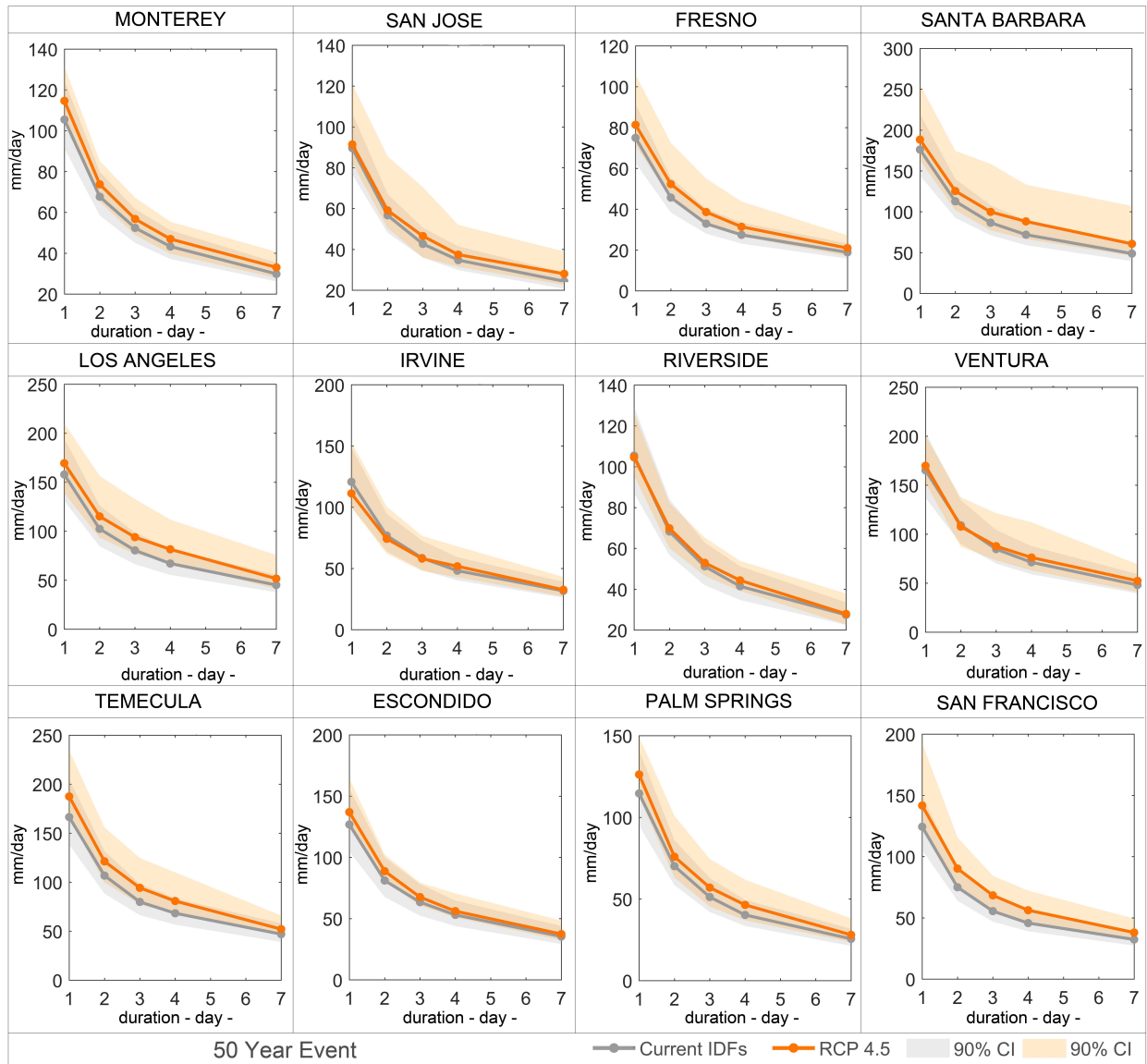


Figure 4.18: RCP 4.5 - California - Comparison between current (grey lines) and future climate scenario (orange lines) IDF curves, along with 90 % confidence intervals, given an average return interval of 50 years.

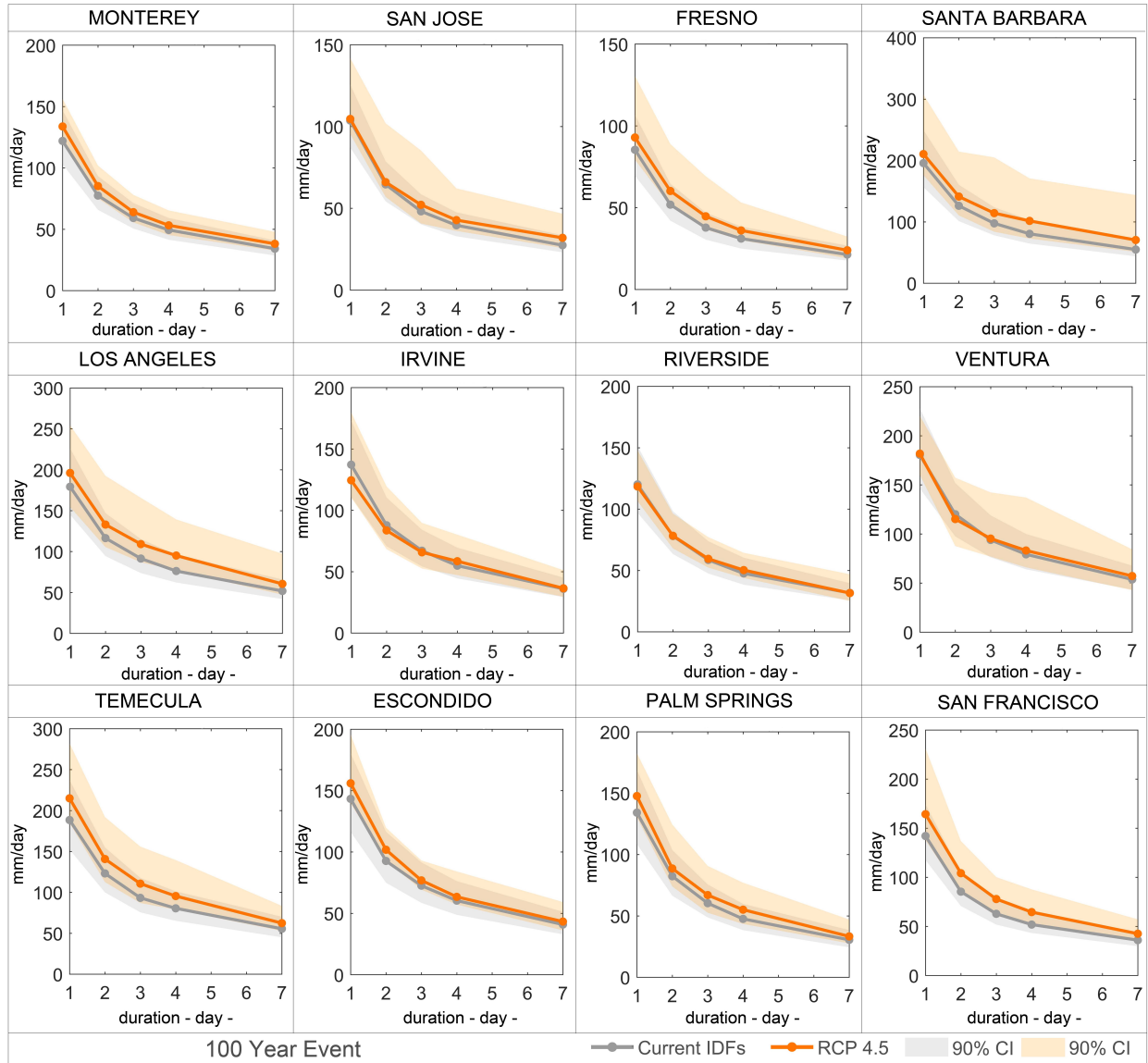


Figure 4.19: RCP 4.5 - California - Comparison between current (grey lines) and future climate scenario (orange lines) IDF curves, along with 90 % confidence intervals, given an average return interval of 100 years.

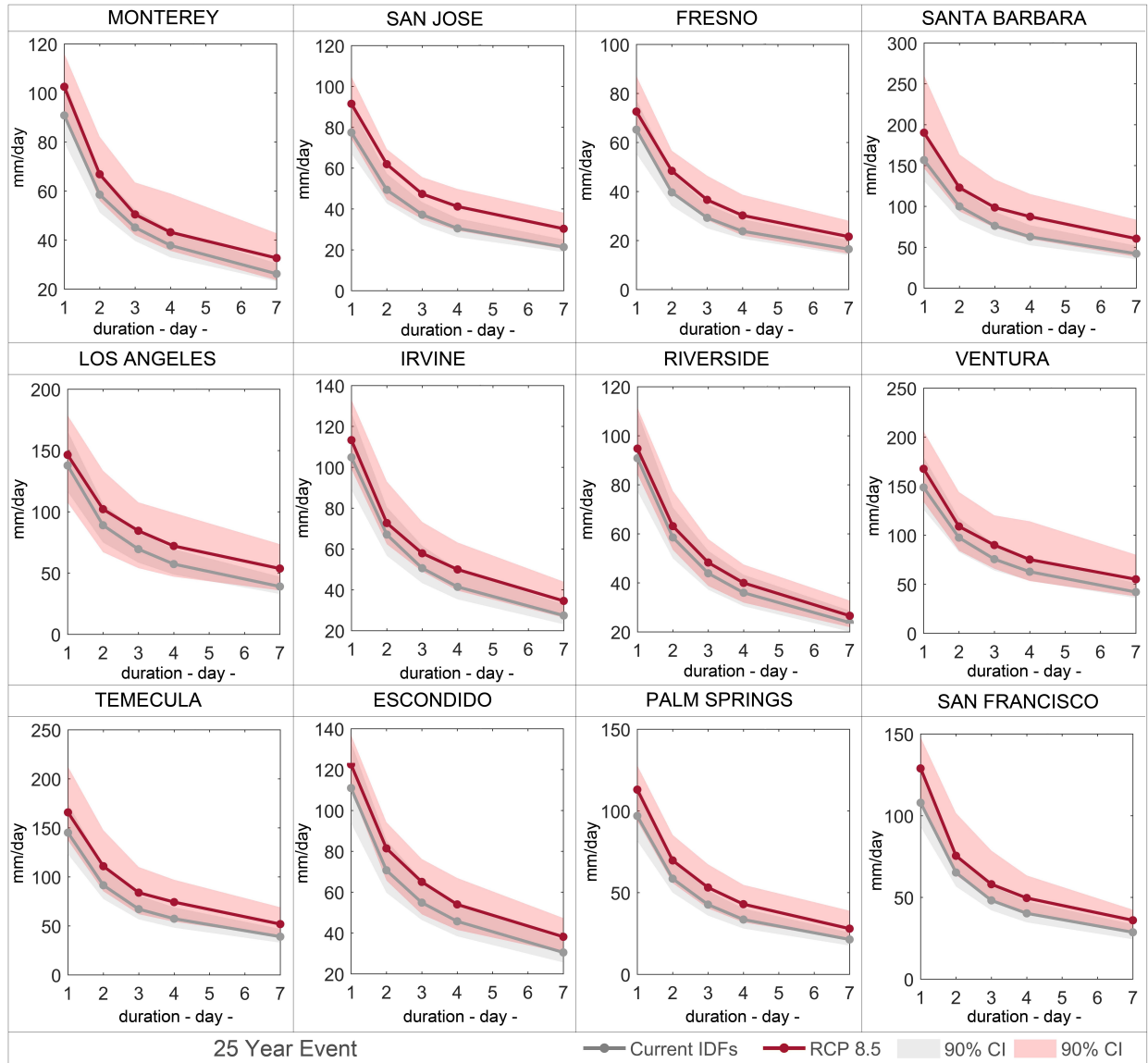


Figure 4.20: RCP 8.5 - California - Comparison between current (grey lines) and future climate scenario (red lines) IDF curves, along with 90 % confidence intervals, given an average return interval of 25 years.

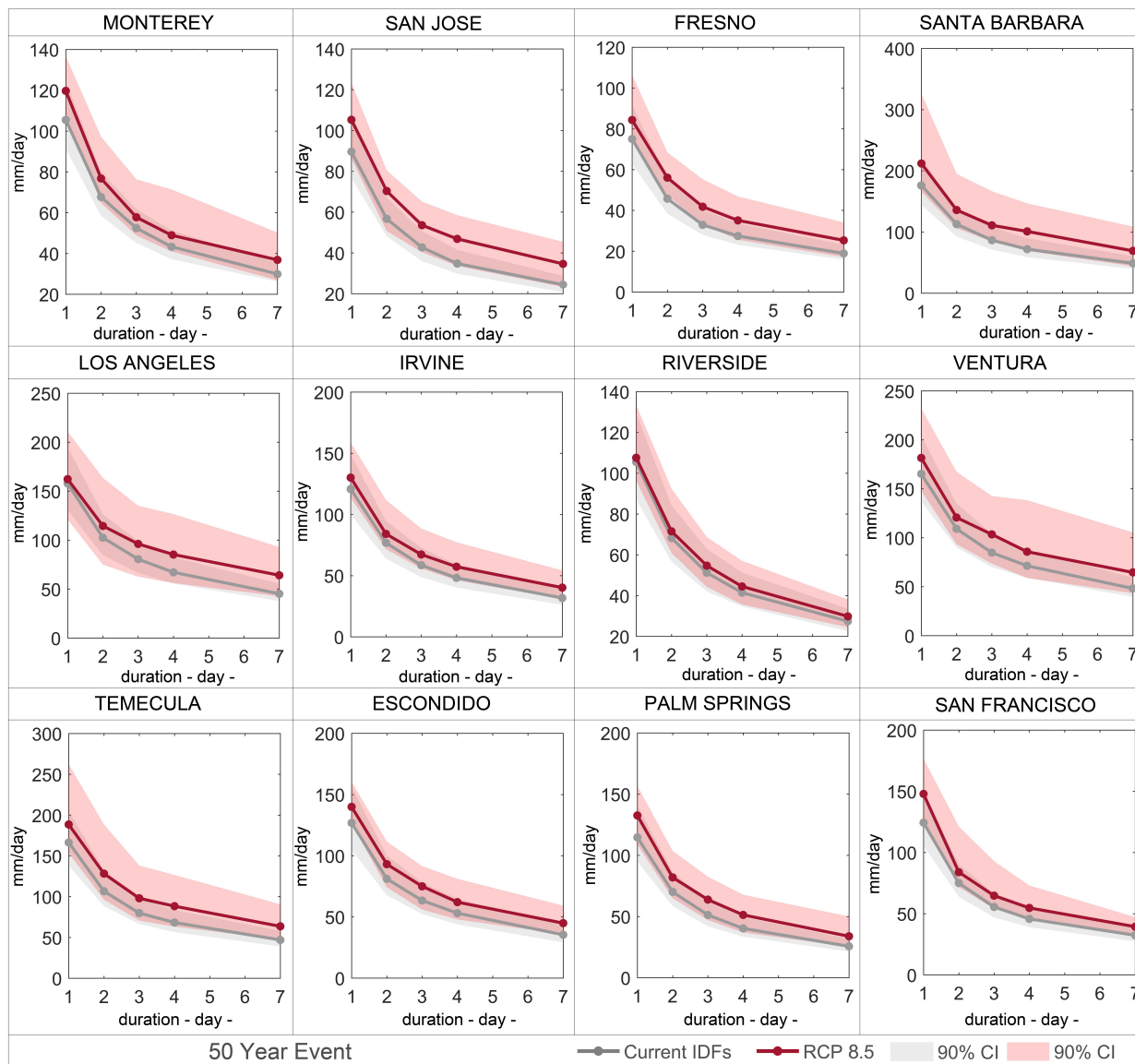


Figure 4.21: RCP 8.5 - California - Comparison between current (grey lines) and future climate scenario (red lines) IDF curves, along with 90 % confidence intervals, given an average return interval of 50 years.

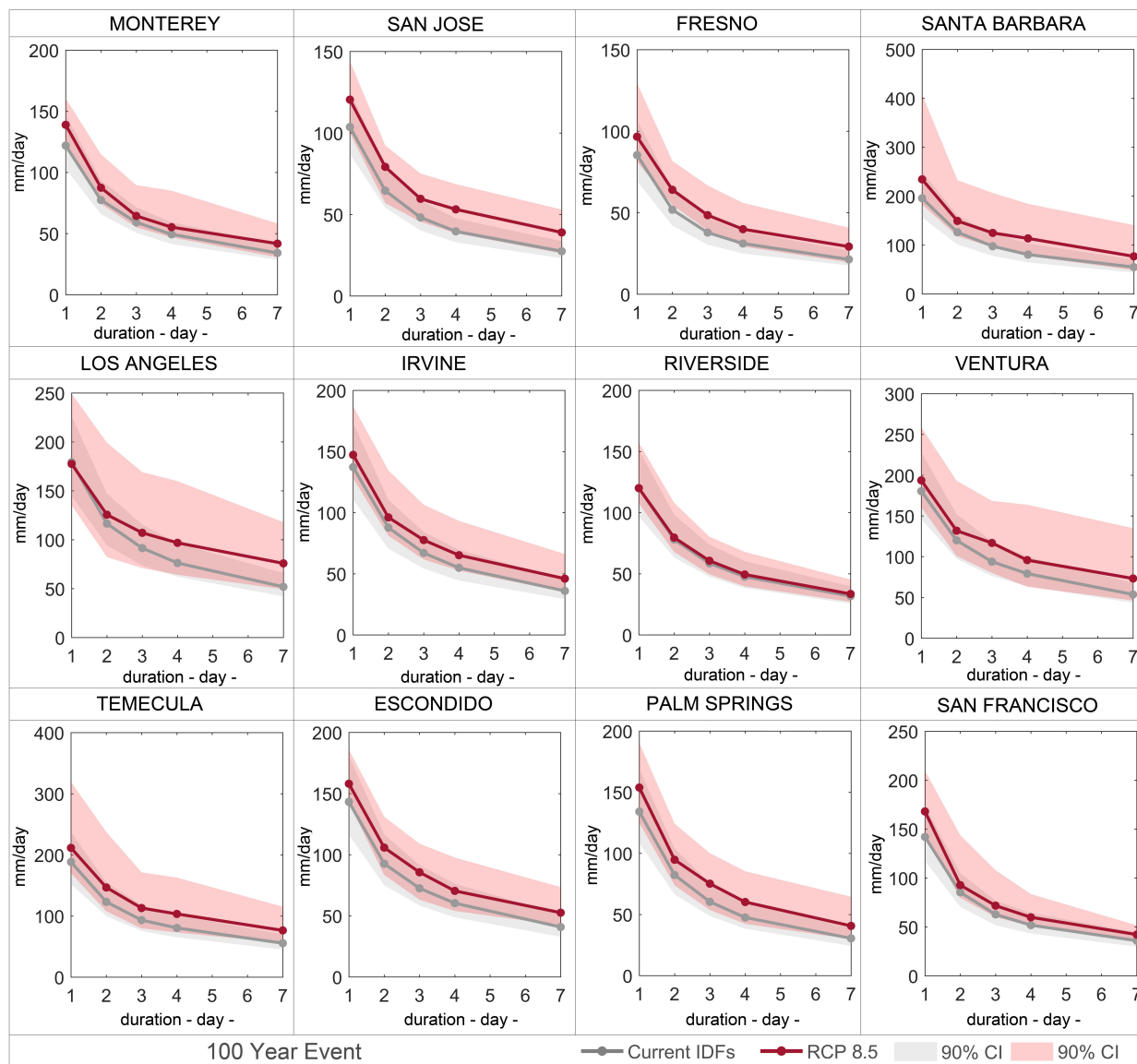


Figure 4.22: RCP 8.5 - California - Comparison between current (grey lines) and future climate scenario (red lines) IDF curves, along with 90 % confidence intervals, given an average return interval of 100 years.

Chapter 5

Multivariate Attribution of Extremes Using Copulas

In recent years, understanding the role of human activities on observed extreme events and climatic changes has received a great deal of attention. Studies investigating the causes of observed climatic changes use two main terms: detection and attribution. *Detection* of change is “[...] the process of demonstrating that climate or a system affected by climate has changed in some defined statistical sense without providing a reason for that change,” (IPCC, 2014a). *Attribution* is “[...] the process of evaluating the relative contributions of multiple causal factors to a change or event with an assignment of statistical confidence,” (IPCC, 2014a).

Examples included understanding effect of anthropogenic emissions and/or land cover changes on the observed increases in surface temperatures (e.g., Barnett et al., 1999; Villarini et al., 2010; Melillo et al., 2014; Diffenbaugh et al., 2015; Fischer and Knutti, 2015; Mazdiyasni and AghaKouchak, 2015) and extreme precipitation events (e.g., Zhang et al., 2007; Villarini et al., 2010; Min et al., 2011; Marvel and Bonfils, 2013; Westra et al., 2013; Cheng et al.,

2014; Fischer and Knutti, 2016; Mallakpour and Villarini, 2017), with the aim of improving risk assessment, adaptation planning and management (Hegerl et al., 2010).

Different methodologies have been developed and adopted in attribution studies. In regression-based fingerprint methods (e.g. Hasselmann, 1993; Hegerl et al., 1996; Zhang et al., 2007; Santer et al., 2013) observations are regressed onto a pattern derived from a numerical simulation with known external forcings. If the scale factor is significantly different than zero, the detected change is attributed to the forcings of the numerical model (Knutson, 2017) (e.g., a model simulation with anthropogenic emissions as forcing). Non-fingerprint methods (e.g. Kolmogorov-Smirnov test, Cramer Von Mises test) similarly rely on running a global climate model with known forcings to reproduce a hypothetical alternative world, and then detect changes by analyzing whether observations are consistent with simulations (Knutson, 2017). Attribution studies can also rely on causality tests, such the Granger causality test (Granger, 1960), where the aim is to infer the causal relationship between external forcings, e.g. CO₂ emissions, and the observed pattern in a climate data record (Stern and Kaufmann, 2014). In general, identifying and quantifying to what extent human activities have resulted in significant changes in climate variables is a major challenge (Fischer and Knutti, 2015) because the outcome often relies on the suitability of the methodologies used to evaluate change.

For extreme events, attribution studies can be carried out considering the concept of frequency analysis. For example, the Fraction of Attributable Risk (FAR) is a measure of the change in the risk associated with an event caused by external forcings. FAR is defined as $FAR = 1 - p_0/p_1$, where p_0 is the probability of an event given its natural variability (e.g., a climate model forced with solely natural forcings), and p_1 is the probability of the same event in the case of anthropogenic forcings (Knutson, 2017; Fischer and Knutti, 2015) (e.g., a climate model forced with the observed anthropogenic emissions). Observed changes can also be attributed to changes in environmental conditions, which can be themselves at-

tributed to the external/anthropogenic forcings, i.e. multistep attribution, (Knutson, 2017). An example could be the intensification of the water cycle, which is mainly attributed to the increase in atmosphere temperature, which in turn is caused by higher CO₂ concentration in the atmosphere as a result of human activities (Trenberth, 2011).

The methodologies available and commonly used for detection and attribution studies rely on a modeling assumption of independence between climate variables or different features of a climate variable (e.g., intensity and duration). However, in the real world, climatic variables or features of natural phenomena are interdependent, such as the dependence between intensity and duration of extreme precipitation events (i.e. more intense storms have shorter durations and vice versa). To overcome this limitation, we present a new multivariate methodological framework to investigate changes between characteristics of climate variables considering their interdependencies (here, precipitation intensity and duration). The methodology, based on copula functions (Nelsen, 2006), is able to capture changes in both the occurrences (or return periods) of baseline events and the dependence structure of the two characteristics/variables. The capability of detecting changes in all the aspects of extreme precipitation is of great importance especially for water-related risk reduction strategies, climate change adaptation measures, and infrastructure design procedure.

We apply the methodology to pairs of intensity and duration associated with precipitation events from the Coupled Model Intercomparison Project 5 (CMIP5) simulations. We consider two types of runs: the historical run (HR) and the historical natural run (HNR). The former represents a hypothetical “natural world” driven only by natural variability (excluding the observed increase in anthropogenic emissions), whereas the latter includes both natural and anthropogenic forcings. From the numerical perspective, the two simulations are identical and they only differ in the anthropogenic emissions component. The difference between the two simulations (e.g., change in extreme precipitation in the two sets of simulations) is then attributed to anthropogenic activities.

In the reminder of the chapter, we will introduce the proposed multivariate detection and attribution framework. We will then provide a comprehensive description of the precipitation data used for testing the proposed method. Finally, we will present and discuss the results.

5.1 Methodology

5.1.1 Copula and Conditional Copula

The bivariate joint distribution function F_{XY} of two time-independent variables X and Y can be greatly simplified by expressing it in terms of its one-dimensional uniform marginals, F_X and F_Y , and the dependent function C , called copula (Salvadori and De Michele, 2004). Following Sklar's theorem (Sklar, 1959) and the notation in Salvadori and De Michele (2004), let F_{XY} be a joint distribution function with marginals F_X and F_Y . Then, there exists a copula function C such that

$$F_{XY}(x, y) = C(F_X(x), F_Y(y)) \quad (5.1)$$

for all $x, y \in \mathbb{R}$. If F_X and F_Y are continuous, C is uniquely defined; otherwise, C is uniquely defined on $Ran(F_X) \times Ran(F_Y)$, where Ran denotes their range. Conversely, if C is a copula and F_X and F_Y are distribution functions, then F_{XY} is given by equation 5.1. $C : [0, 1] \times [0, 1] \rightarrow [0, 1]$ such that for all $u, v \in [0, 1]$ $C(u, 0) = 0$, $C(u, 1) = u$, $C(0, v) = 0$, $C(1, v) = v$, and C is a 2-increasing function (Salvadori 2004). The pair (X, Y) represents the variables of interest in their original domain, i.e. precipitation intensity and duration, while the pair $(U = F_X, V = F_Y)$ represents their uniform marginals in $[0, 1] \times [0, 1]$ (Salvadori and De Michele, 2004).

The copula conditional probability can be retrieved by differentiating equation 5.1 (Nelsen,

2006).

$$P\{U \leq u|V = v\} = \frac{\partial}{\partial v}C(u, v) \quad (5.2)$$

$$P\{V \leq v|U = u\} = \frac{\partial}{\partial u}C(u, v) \quad (5.3)$$

In the following study, we are interested in a comprehensive characterization of the simultaneous changes in intensity and duration of extreme precipitation events. In common practice, the relationship between precipitation intensity, duration, and frequency is represented by Intensity-Duration-Frequency (IDF) curves, which summarize the expected maximum intensity of a rainfall event for a fixed storm duration and frequency. IDF curves are traditionally derived based on univariate frequency analysis because of the intrinsic difficulty of deriving the joint distribution of precipitation characteristics (Singh and Zhang, 2007). However, copula method provides a venue to overcome the limitation of standard bivariate distributions, such that IDF curves can be derived based on conditional copula (Singh and Zhang, 2007; De Michele and Salvadori, 2003b; Morales-Nápoles et al., 2017).

Frank copula function has been shown to be the most flexible to represent the relationship between intensity and duration of precipitation events (Singh and Zhang, 2007; De Michele and Salvadori, 2003b), and it provides a good fit for the pairs in this study.

The Frank copula C_δ belongs to the Archimedean family, and it is defined as

$$C_\delta(u, v) = -\frac{1}{\delta} \ln \left(1 + \frac{(e^{-\delta u} - 1) \cdot (e^{-\delta v} - 1)}{e^{-\delta} - 1} \right) \quad (5.4)$$

where $u, v \in [0, 1]$ and $\delta \in \mathbb{R}$. The parameter δ can be expressed as a function of Kendall's τ :

$$\tau(\delta) = 1 + 4 \frac{D_1(\delta) - 1}{\delta} \quad (5.5)$$

where $\delta' = e^{-\delta}$ and D_1 is the first order Debye function (De Michele and Salvadori, 2003b). Negative values of the parameter δ corresponds to negative dependence ($\tau < 0$), while positive values of δ correspond to positive dependence ($\tau > 0$); the limit case of $\delta = 0$ corresponds to independence (De Michele and Salvadori, 2003b). Therefore, Frank copula is flexible enough to model both positive and negative dependence (De Michele and Salvadori, 2003b).

The conditional probability for the Frank copula can be expressed as:

$$C_\delta(U|V = v_0) = \frac{(e^{-\delta u} - 1)e^{-\delta v_0}}{(e^{-\delta u} - 1)(e^{-\delta v_0} - 1) + (e^{-\delta} - 1)} \quad (5.6)$$

where $v = v_0$ is the conditioning variable (Singh and Zhang, 2007). Given the symmetry of the Frank copula, $C_{\delta,V|U=u_0}$, can be derived from equation 5.6 by exchanging the variables u and v .

The conditional return period can be estimated as

$$T_{C_\delta(U|V=v_0)} = \frac{1}{1 - C_\delta(U|V = v_0)} \quad (5.7)$$

5.1.2 Detection of Changes

Extreme events are commonly identified among experts and non-experts in relation to their occurrence probability, recurrence interval or return period. For example, an event with a 0.01 probability of being exceeded each year is called a 100-year event, where 100 years is the return period. Generalizing, an event with a q -probability of being exceeded each year is referred to as the $(1/q)$ -year event. One way to express changes in extreme events is to estimate the expected return period of a baseline event when an alternative climate scenario is considered (Ragno et al., 2018). In other words, we are interested in estimating the

expected return period of the historical 25-, 50-, 100-year events, hereafter baseline events, in a hypothetically alternative world, the “natural world”, characterized only by natural variability. The difference would then explain the contribution of anthropogenic activities on changes in the frequency of extremes.

Let (I_{HNR}, D_{HNR}) and (I_{HR}, D_{HR}) be the two bivariate time series of simulated precipitation intensity (I) and duration (D), respectively, from HNR (natural only) and HR (baseline or historical) runs. Let $F_{I_{HNR}}$, $F_{D_{HNR}}$, $F_{I_{HR}}$, and $F_{D_{HR}}$ be their respective marginal distributions. Let (I_{HNR}, D_{HNR}) and (I_{HR}, D_{HR}) be represented by the Frank copulas, $C_{\delta_{HNR}}$ and $C_{\delta_{HR}}$, respectively. Let $I_{HR,d}^T$ be the intensity of a baseline T -year event given a storm duration d . Therefore, the expected return period in the alternative “natural world” is defined based on equation 5.6 such as:

$$T^{HNR} = \frac{1}{1 - P(I \leq I_{HR,d}^T | D = d)} \quad (5.8)$$

where $P(I \leq I_{HR,d}^T | D = d) = C_{\delta_{HNR}}(F_{HNR}(I_{HR,d}^T) | F_{HNR}(d))$. The changes in return period will account for changes in both the dependence structure between I and D , and the magnitude of precipitation events.

For a comprehensive characterization of changes in precipitation I and D , we suggest to isolate the changes in their dependence structure. The advantage in the use of copula functions resides in the possibility of representing the correlation structure in a simplified domain, $[0, 1] \times [0, 1]$, where the effect of the absolute value of the two variables is removed. By numerically inverting the equation 5.6, it is possible to express u as a function of the conditioning variable v and fixed conditional probability $C_{u|v}$ (Figure 5.1). Once the value of the joint conditional probability is chosen, the dependence structure controls the associated marginal distribution u : for negative dependence, lower values of the conditioning variable v are associated with $u \geq C_{u|v}$ (Figure 5.1 top panels); for positive dependence, higher values

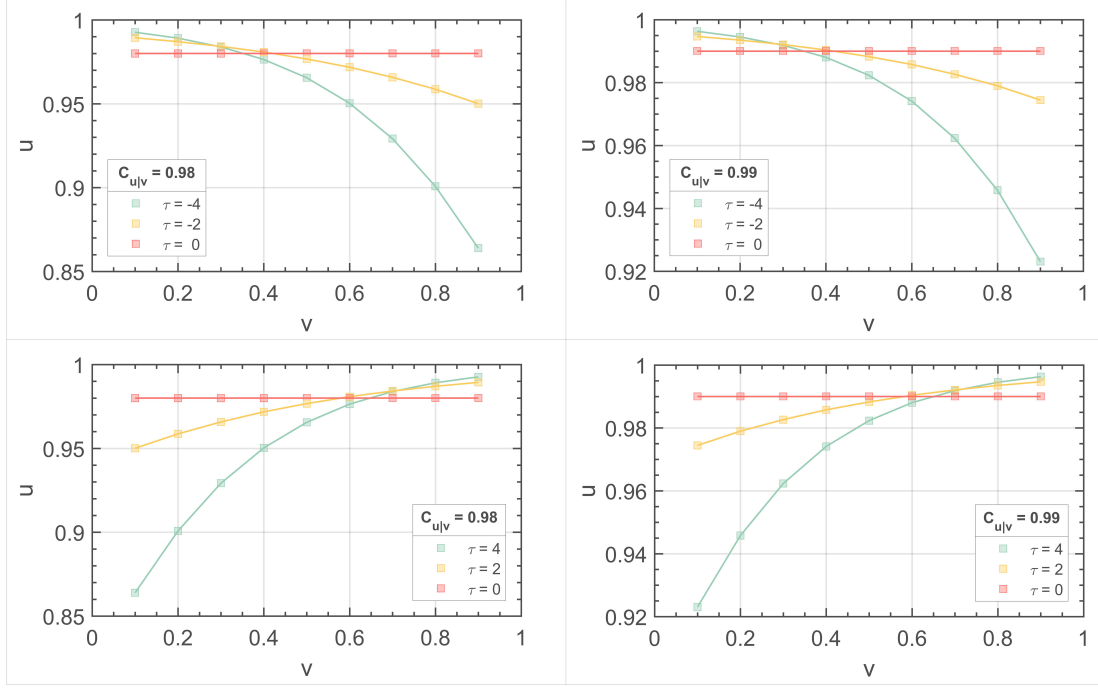


Figure 5.1: Effect of the dependence structure of the copula model (τ) on the marginal distribution u for fixed value of the joint conditional probability $C_{u|v}$.

of the conditioning variable v are associated with $u \geq C_{u|v}$ (Figure 5.1 bottom panels). Because of the upper limit inherent in the cumulative density function, $C_{u|v} \rightarrow 1$, $u \rightarrow 1$ for $v \rightarrow 0$ (negative dependence) or for $v \rightarrow 1$ (positive dependence). It is worth noting that the relation between u and v , relative to the joint conditional probability $C_{u|v}$, is fully defined by the copula family and its parameter(s), while it is independent from the marginal distributions.

Let the marginal u be $u = F_I(i)$ and the marginal v of the conditioning variable be $v = F_D(d)$. The relation between u and v , given a joint conditional probability equal to the frequency of baseline events commonly used for risk assessment (e.g., 25-, 50-, 100-year), can reveal changes in extreme events induced by changes in the dependence structure between precipitation's characteristics, i.e. intensity and duration.

The above results can be extended to any copula family as well as any pair of dependent variables, even when they are not characteristics of the same phenomenon (i.e., two different

variables or sets of events such as droughts and heatwaves). This approach can provide insights to aspects of natural phenomena for further investigation and to improve our understanding of their sensitivity to external forcings.

5.2 Data

We apply the proposed approach for change detection of interdependent climate variables to simulated precipitation from the following Global Climate Models (GCMs): CCSM4, CNRM-CM5, and MIROC-ESM (Archive, 2018). We retrieve simulations from HNR and HR. The HNR is representative of an alternative “natural world” driven only by natural variability, in which the amount of CO₂ in the atmosphere attributed to human activities is removed (Taylor et al., 2009, 2012). The choice of these two runs enable us to attribute the detected changes to the human footprint. We consider 156 years of daily simulations, i.e. from 1850 to 2005, from a spatial grid cell geographically identified with Los Angeles (CA, USA). The precipitation unit is $kg/(sm^2)$, which corresponds to $1mm/s = 3600mm/hr$.

We then identify, in each given year, all storm events, and we characterize them in terms of intensity ($I - mm/hr$) and duration ($D - day$). We use a dry period of 1-day to separate storm events, the choice of which is justified by the temporal resolution of the simulations. Moreover, I is equal to the average precipitation intensity during the storm event. For example, for a D -day storm duration I will be given by:

$$I = \frac{1}{D} \cdot \sum_{d=1}^D p_i \quad (5.9)$$

where p_i is the precipitation intensity simulated for the i -th day.

Once the storms have been characterized in terms of I and D , for each year we sample only one event per duration, i.e. the event associate with the maximum intensity among events

Models	τ_{HNR}	τ_{HR}	δ_{HNR}	δ_{HR}
<i>CCSM4</i>	-0.16	-0.19	-1.41	-1.39
<i>CNRM-CM5</i>	-0.31	-0.30	-2.88	-2.68
<i>MIROC-ESM</i>	-0.14	-0.20	-1.20	-1.74

Table 5.1: List of Kendall’s τ and Frank copula parameter δ for the models, i.e. CCSM4, CNRM-CM5, MIROC-ESM, and runs, i.e. HNR, HR, investigated.

with the same duration. This sampling procedure guarantees a time series of independent elements, and it allows us to derive the 25-, 50-, and 100-year events as the inverse of the joint conditional exceedance probability, $C_\delta(F_I(I)|F_D(D))$. We assume a maximum storm duration of 7 days, to ensure a representative number of storm events for each duration.

After having processed the data, for each GCM we have two bivariate time series for each climate model: $(I_{\text{HNR}}, D_{\text{HNR}})$ and $(I_{\text{HR}}, D_{\text{HR}})$. Generally, the following negative dependence is observed between I and D : the lower D is, the higher I is.

5.3 Result

We first calculate the Kendall correlation coefficient τ to have an insight into the correlation structure between simulated precipitation characteristics. All the pairs (I, D) show a negative correlation, see Table 5.1.

Afterwards, we transform (I, D) into $[0, 1] \times [0, 1]$ domain, such as: $u = F_I(i)$ and $v = F_D(d)$, where F_I and F_D are the empirical cumulative distribution functions of the precipitation characteristics I and D respectively. Once the uniform marginals have been calculated, we estimate the parameter δ of the Frank copula based on the observed pair of (u, v) using the maximum likelihood estimate method (see *copulafit* built-in function of Matlab (Matlab, 2017)). Given a negative correlation structure between I and D , negative values of the Frank parameter δ are estimated. Figure 5.2.a, .c, and .e show the scatter plots of the pairs

(I, D) in \mathbb{R} and $[0, 1] \times [0, 1]$ domain. Figure 5.2.b, .d, and .f show the fitted Frank copulas. Both the Kendall correlation τ and the Frank copula parameter δ , Table 5.1 and Figure 5.2, reveal a minor sensitivity of precipitation characteristics on the CO_2 concentration in the atmosphere.

We further investigate the effect of the increase in greenhouse gas (GHG) emissions by looking at the tail behavior of the joint conditional probability. Indeed, the tail of a distribution is the aspect ruling water-related risk management and adaptation strategies.

Changes in the return period

We investigate changes in extreme events such as 25-, 50-, and 100-year precipitation events (corresponding to the conditional Frank copula $C_\delta(F_I|F_D(d))$ equal to 0.96, 0.98, and 0.99) following Ragno et al. (2018). We calculate the expected return period of baseline events (events simulated in the “real world” - HR) in the hypothesized alternative “natural world” (HNR), Figure 5.3.a, .c, and .e. As an example, we estimate the 25-year 1-day storm event, $I_{HR,1}^{25}$ such that $C_{\delta_{HR}}(I \leq I_{HR,1}^{25}|D = 1) = 0.96$. Subsequently, we calculate the corresponding return period in the “natural world” as $T^{HNR} = 1/(1 - C_{\delta_{HNR}}(I \leq I_{HR,1}^{25}|D = 1))$.

Even though there is disagreement across the models selected, the increase in CO_2 concentration in the atmosphere has made extreme events more frequent. For example, what is considered today to be a today 50-year event (Figure 5.3 c) of 1-day duration would have been, on average, a 60-year event in the alternative “natural world” (Figure 5.3.c red dot). The results summarized in Figure 5.3.a, .c, and .e, about the changes in the frequency of extreme events, account for the GHG effects on both the amount of precipitation and the interdependence between precipitation characteristics I and D .

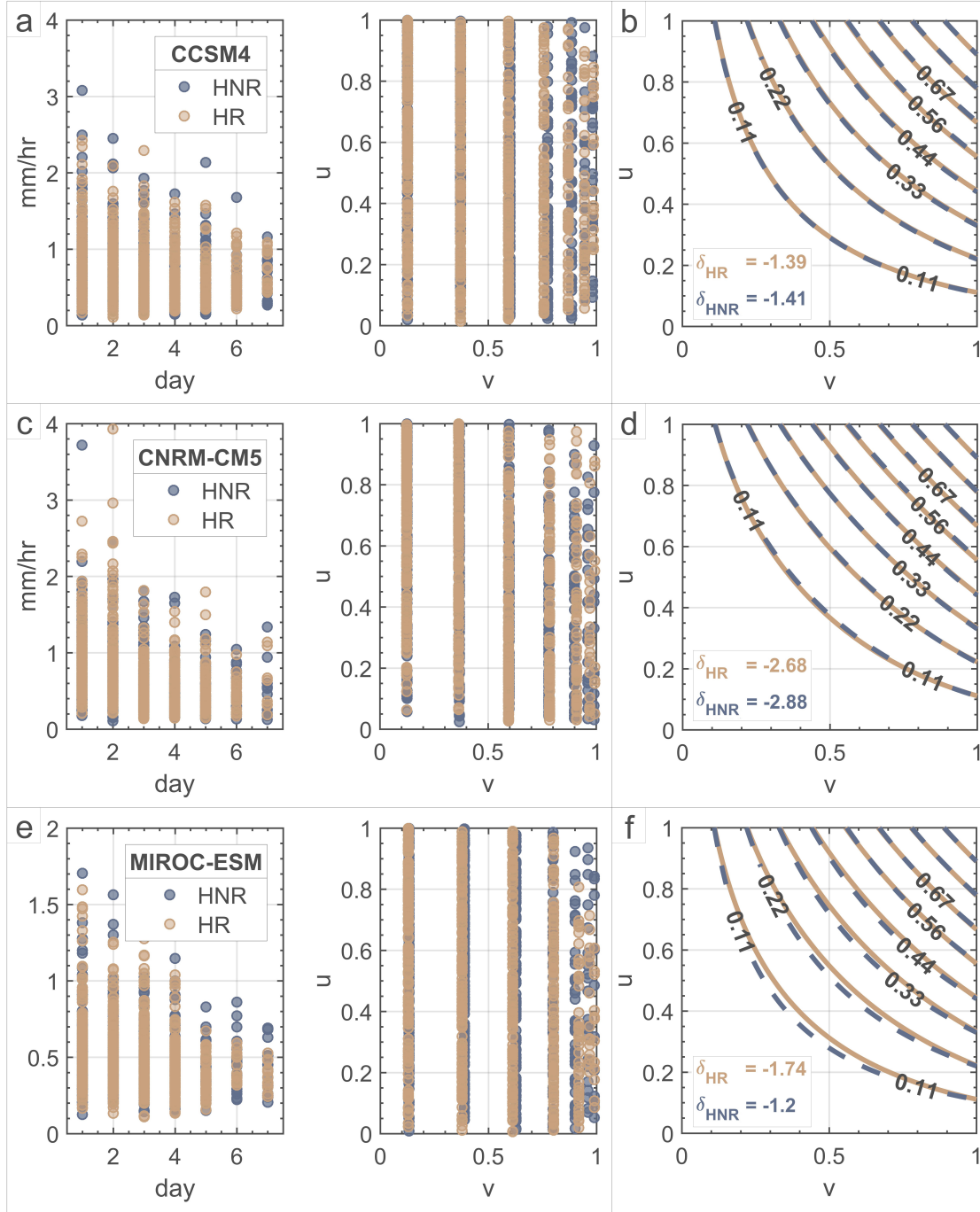


Figure 5.2: (I, D) scatter plots and Frank copulas. Model CCSM4: a) Scatter plot in \mathbb{R} and $[0, 1] \times [0, 1]$ domain and b) Fitted Frank Copulas. Model CNRM-CM5: c) Scatter plot in \mathbb{R} and $[0, 1] \times [0, 1]$ domain and d) Fitted Frank Copulas. Model MIROC-ESM: e) Scatter plot in \mathbb{R} and $[0, 1] \times [0, 1]$ domain and f) Fitted Frank Copulas.

Changes in the dependence structure

We want to isolate the changes in the dependence structure by focusing only on the $[0, 1] \times [0, 1]$ domain. Figure 5.3.b, .d, and .f show isolines corresponding to $C_\delta(F_I|F_D(d))$ equal to 0.96, 0.98, and 0.99, respectively. The negative dependence structure of the joint probability function acts on the value of marginal probability u corresponding to the conditional joint probability of interest: the marginal probability u decreases for increasing value of marginal probability v . This result confirms that the interdependence between precipitation characteristics adds valuable information in defining the frequency, and therefore the absolute value, of the variable, i.e. precipitation intensity, used for infrastructure design and risk assessment. It is possible to notice that MIROC-ESM (M3) is the most sensitive model to CO_2 concentration in terms of dependence structure, Figure 5.3.b, .d, and .f - diamonds, given that the two corresponding curves diverge for large v .

From a comparison between the changes observed in the return period and those observed in the dependence structure, we notice that in the \mathbb{R} domain the magnitude of precipitation intensity hides the changes occurring in the dependence structure. For example, the MIROC-ESM model exhibits the largest change in the dependence structure (see Table 5.1 and Figures 5.3.b, .d, and .f). However, in terms of return periods, it is the model that exhibits the smallest changes among the three (Figures 5.3.a, .c, and .e). Overall, when we average the three dependence structures, no changes are observed between HR and HNR.

5.4 Discussion and Conclusion

Most studies on attribution of extremes are univariate and focus on only one variable or one feature of a variable (e.g., annual precipitation maxima). In this study, we propose a multivariate attribution analysis framework that allows investigating changes in dependent

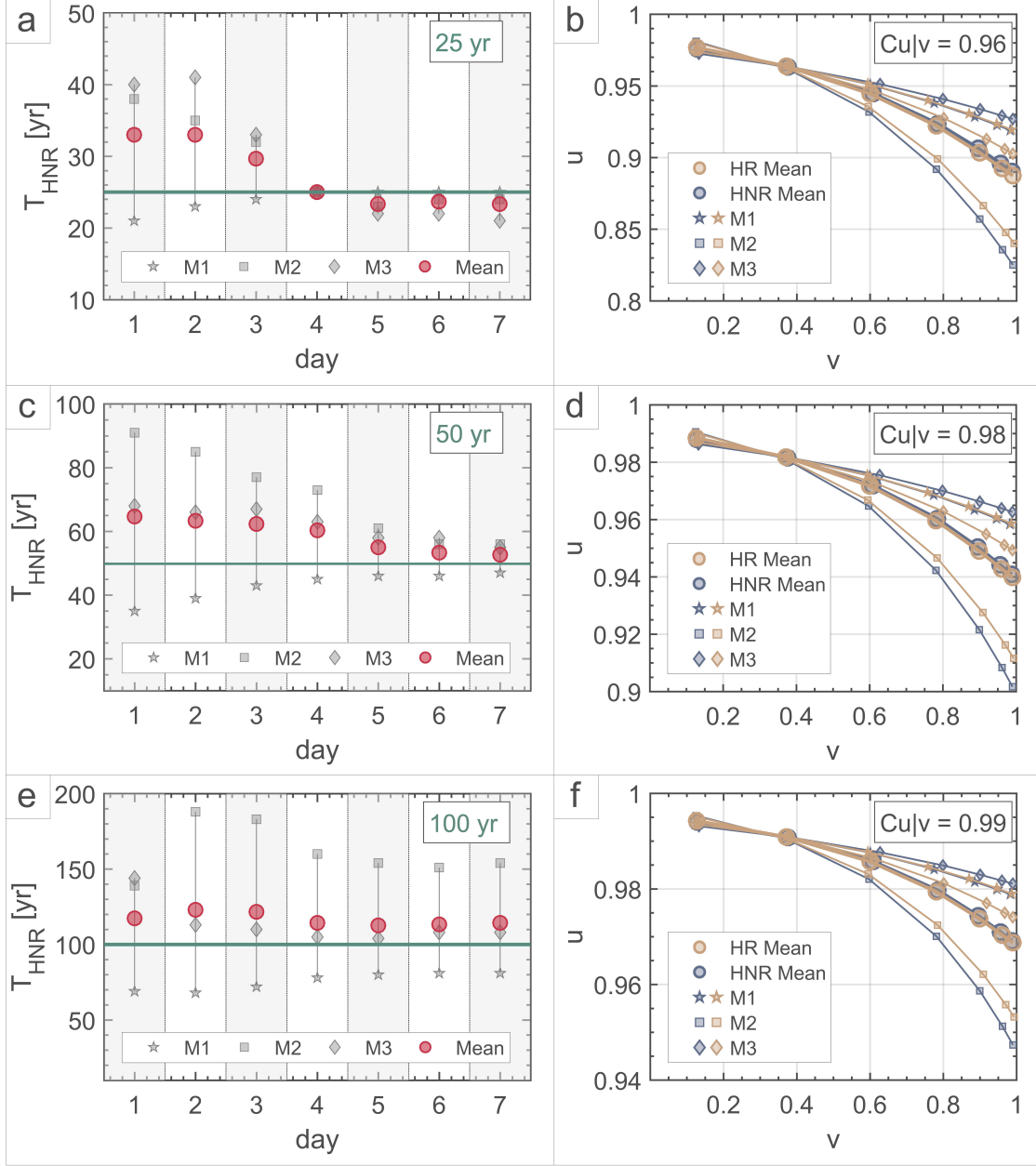


Figure 5.3: Detected changes in the precipitation characteristics (I, D). M1, M2, and M3 denote the models CCSM4, CNRM-CM5, and MIROC-ESM, respectively. Panel a, c, and e show the corresponding 25-, 50-, and 100-year events, respectively, in the alternative natural world. Panel b, d, and e represents the effect of the dependence structure on the marginal distribution $u = F_I(I)$ for a fixed value of the joint conditional probability, $C_\delta(F_I|F_D(d))$, equal to 0.96, 0.98, and 0.99 respectively

variables or multiple features of a climate data record.

We show that human footprint has altered the magnitude and frequency of extreme precipitation events. Comparing model simulations with and without anthropogenic emissions, we show that extreme precipitation events that we define as 25-, 50- and 100-year events in today’s climate (observed record) are occurring more frequently than under an alternative “natural” world, driven only by natural variability. These results mean that anthropogenic CO₂ emissions have contributed to more frequent storms, increasing the exposure of population and societies to natural hazards. Moreover, we showed that changes in the magnitude of events (e.g., amount of precipitation) can potentially affect changes in the dependence structure of different features of an event (e.g., duration vs intensity of rain event).

The method we proposed here addresses this issue through describing the potential dependencies in a unit domain independent of the magnitudes and marginals of the data. The approach proposed here can be extended for higher dimension problems. Future work in this direction will focus on developing a generalized metric linking the dependence structure of variables of interest to their marginals to facilitate extreme value analysis in a multivariate case.

Chapter 6

Conclusion

Today's society is extremely vulnerable to natural hazards because of the observed climatic changes and the higher exposure to them resulting from growth and urban development. When combined with other anthropogenic changes such as land use and land cover, these factors exacerbate the societal and economic impacts of natural hazards.

The ability to correctly model the expected magnitude and frequency of extreme events is fundamental for improving design concepts, risk assessment methods, and adaptation plans. This is particularly important for extreme events that have significant impacts on societies, infrastructure and human lives, such as extreme precipitation events which cause flooding and landslides. The scientific community, global organizations, and other stakeholders have all recognized the urgency of improving our understanding of both natural and human-induced climate variability.

In order to advance our understanding we propose a methodological framework for investigating hydroclimatic extremes over time and in response to a physical driver/covariate (Chapter 2) and we shed light on the uncertainty inherent in the estimation of climatic extremes and how it should be interpreted by planners and decision-makers under con-

ditions of uncertainty (Chapters 3). Using the method developed in this thesis, we show how extreme precipitation is expected to change in the future (Chapters 4). We also highlight the importance of merging information from observations and climate model simulations for risk assessment purposes (Chapters 4). Finally, we outline a methodological framework for attribution of multiple extremes or multiple features of an extreme event (Chapter 5). The key findings and conclusions are summarized below.

In Chapter 2, we propose a generalized framework for process-based nonstationary extreme value analysis. Most of the existing tools for implementing extreme value analysis under the nonstationary assumption lack of a generalized framework for incorporating physically based covariates and estimating parameters which depend on a generic physical covariate. To address the above limitations, we propose the *Process-based Nonstationary Extreme Value Analysis* (ProNEVA) framework in which the nonstationarity component is defined by a temporal or process-based dependence of the observed extremes on a physical driver (e.g., changes in runoff in response to urbanization, or changes in extreme temperatures in response to CO₂ emissions). ProNEVA offers temporal and process-based stationary and nonstationary extreme value analysis, parameter estimation, uncertainty quantification, and a comprehensive assessment of the goodness of fit. We freely provide the source code of ProNEVA and a graphical user interface (GUI) to facilitate its applications (Section 2.9) in the hope that an easily accessible ProNEVA motivates more physically-based nonstationary analysis of extreme events.

In Chapter 3, we propose a universal chart for improving how the risk of natural hazard is communicated. Given the variable likelihood of observing a rare event in a set of observations, predicting future rare events requires paying special attention to the confidence with which those predictions are made. Because predicting rare events does not depend solely on the number of observations or on the rarity of the event of interest, we propose a universal chart summarizing the likelihood of observing the rare event of interest within the available set

of observations (Figure 3.2). We recommend adopting the proposed chart to clarify and communicate the confidence of rare event inferences. To facilitate its proliferation within the scientific community, in this chart, the ratio between the length of records and the rarity of the extreme event is combined with the likelihood scale as determined by the Intergovernmental Panel on Climate Change (IPCC) Fifth Assessment Report guidance. This chart is a necessary tool for a more informative decision-making process related to natural hazard preparedness.

In Chapter 4 (Ragno et al., 2018), we show the potential impacts a warming climate has on extreme precipitation intensity and recurrence intervals. Urban areas, especially in the western U.S., are particularly impacted by increases in the severity and frequency of rare events. Increases in intensity, duration, and frequency of extreme precipitation can adversely impact the integrity of infrastructure and of natural and engineered slopes. Infrastructure built with soil (e.g., earthen dams, levees, embankments) or interfacing with soil (e.g., roads, bridges, pipelines, foundations) is vulnerable because severe rainfall causes soil erosion and can significantly reduce the strength of soil upon infiltration. The topic of infrastructure resilience is even more important in regions where multiple drivers of change coincide. Coastal cities, for example, are even more vulnerable due to the compounding effects of sea level rise and change in climate (Hallegatte et al., 2013). By 2070, the population jeopardized by extreme floods is expected to increase threefold with the exposed assets increasing by approximately 9% of the projected global GDP of the same period (Hanson et al., 2011). We argue that better infrastructure planning and maintenance is fundamental for a resilient society. The proposed method for addressing nonstationarity in future climate scenarios can reduce the risk of underestimating future extreme precipitation events and their severity. The adaptation of existing infrastructures, designed assuming a stationary climate, requires assessing their performance under future climate scenarios. Such adaptation also requires revisiting design guidelines for infrastructure and to employ nonstationary IDF curves in future design procedures.

In Chapter 5 we propose a multivariate attribution analysis framework which allows for investigating changes in dependent variables or in multiple features of a climate data record. We show that the human footprint has altered the magnitude and frequency of extreme precipitation events. A comparison of model simulations with and without anthropogenic emissions shows that extreme precipitation events (defined as 25-, 50- and 100-year events in the observed record) occurs more frequently in the human model than they do in the alternative “natural” model, which is driven only by natural variability. These results mean that anthropogenic CO₂ emissions have contributed to more frequent storms, increasing the exposure of population and societies to natural hazards. Moreover, we show that changes in the magnitude of events (e.g., amount of precipitation) can potentially affect changes in the dependence structure of different features of an event (e.g., duration versus intensity of rain event). The method we proposed here addresses this issue through describing the potential dependencies in a unit domain independent of the magnitudes and marginals of the data. The approach proposed here can be extended for higher dimension problems. Future work in this direction will focus on developing a generalized metric linking the dependence structure of variables of interest to their marginals to facilitate extreme value analysis in a multivariate case.

Bibliography

- AghaKouchak, A., Cheng, L., Mazdiyasni, O., and Farahmand, A. (2014a). Global warming and changes in risk of concurrent climate extremes: Insights from the 2014 California drought. *Geophysical Research Letters*, 41(24):8847–8852.
- AghaKouchak, A., Feldman, D., Stewardson, M. J., Saphores, J.-D., Grant, S., and Sanders, B. F. (2014b). Australia’s Drought: Lessons for California. *Science*, 343(March):1430–1431.
- Aho, K., Derryberry, D., and Peterson, T. (2014). Model selection for ecologists: the world-views of AIC and BIC. *Ecology*, 95(3):631–636.
- Akaike, H. (1974). A new look at the statistical model identification. *IEEE Transactions on Automatic Control*, 19(6):716–723.
- Akaike, H. (1998). Information Theory and an Extension of the Maximum Likelihood Principle BT - Selected Papers of Hirotugu Akaike. pages 199–213. Springer New York, New York, NY.
- Alexander, L. V. (2016). Global observed long-term changes in temperature and precipitation extremes: A review of progress and limitations in IPCC assessments and beyond. *Weather and Climate Extremes*, 11:4–16.
- Alexander, L. V., Zhang, X., Peterson, T. C., Caesar, J., Gleason, B., Klein Tank, A. M., Haylock, M., Collins, D., Trewin, B., Rahimzadeh, F., Tagipour, A., Rupa Kumar, K., Revadekar, J., Griffiths, G., Vincent, L., Stephenson, D. B., Burn, J., Aguilar, E., Brunet, M., Taylor, M., New, M., Zhai, P., Rusticucci, M., and Vazquez-Aguirre, J. L. (2006). Global observed changes in daily climate extremes of temperature and precipitation. *Journal of Geophysical Research Atmospheres*, 111(5):1–22.
- Allan, R. P. and Soden, B. J. (2008). Atmospheric Warming and the Amplification of Precipitation Extremes. *Science*, 321(5895):1481 LP – 1484.
- Anderson, M. C., Hain, C., Wardlow, B., Pimstein, A., Mecikalski, J. R., and Kustas, W. P. (2011). Evaluation of drought indices based on Thermal remote sensing of evapotranspiration over the continental United States. *Journal of Climate*, 24(8):2025–2044.
- Anderson, T. W. (1962). On the Distribution of the Two-Sample Cramer-von Mises Criterion. *The Annals of Mathematical Statistics*, 33(3):1148–1159.

Archive (2018). [https://cera-www.dkrz.de/WDCC/ui/cersearch/q?query=cmip5%20pr%20historicalNat%](https://cera-www.dkrz.de/WDCC/ui/cersearch/q?query=cmip5%20pr%20historicalNat%20)

Barnett, T. P., Hasselmann, K., Chelliah, M., Delworth, T., Hegerl, G., Jones, P., Rasmusson, E., Roeckner, E., Ropelewski, C., Santer, B., and Tett, S. (1999). Detection and attribution of recent climate change: A status report. *Bulletin of the American Meteorological Society*, 80(12):2631–2659.

Beniston, M. (2004). The 2003 heat wave in Europe: A shape of things to come? An analysis based on Swiss climatological data and model simulations. *Geophysical Research Letters*, 31(2).

Black, E., Blackburn, M., Harrison, G., Hoskins, B., and Methven, J. (2004). Factors contributing to the summer 2003 European heatwave. *Weather*, 59(8):217–223.

Boden, T., Marland, G., and Andres, R. (2017). Global, Regional, and National Fossil Fuel CO₂ Emissions. Carbon Dioxide Information Analysis Center. Oak Ridge National Laboratory, U.S. Department of Energy, Oak Ridge, Tenn., USA. http://cdiac.ess-dive.lbl.gov/trends/emis/meth_reg.html.

Bonnin, G., Perica, S., Dietz, S., Heim, S., Hiner, L., Maitaria, K., Martin Deborah Pavlovic, S., Roy, I., Trypaluk, C., Unruh, D., Yan, F., Yekta, M., Zhao, T., Brewer, D., Chen, L.-C., Parzybok, T., and Yarchoan, J. (2006). Precipitation - Frequency Atlas of the United States. *NOAA Atlas 14*, 1-10.

Bouwer, L. M., Crompton, R. P., Faust, E., Höppe, P., and Pielke, R. A. (2007). Confronting disaster losses. *Science*, 318(5851):753.

BP (2017). Statistical Review of World Energy. <http://www.bp.com/en/global/corporate/energy-economics.html>.

Bracken, C., Holman, K. D., Rajagopalan, B., and Moradkhani, H. (2018). A Bayesian Hierarchical Approach to Multivariate Nonstationary Hydrologic Frequency Analysis. *Water Resources Research*, pages 243–255.

Brands, S., Herrera, S., Fernández, J., and Gutiérrez, J. M. (2013). How well do CMIP5 Earth System Models simulate present climate conditions in Europe and Africa?: A performance comparison for the downscaling community. *Climate Dynamics*, 41(3-4):803–817.

Brekke, L., Thrasher, B. L., Maurer, E. P., and Pruitt, T. (2013). Downscaled CMIP3 and CMIP5 climate and hydrology projections: Release of downscaled CMIP5 climate projections, comparison with preceding information, and summary of user needs. *US Dept. of the Interior, Bureau of Reclamation, Technical Services Center, Denver*.

Cabanes, C., Cazenave, A., and Le Provost, C. (2001). Sea Level Rise During Past 40 Years Determined from Satellite and in Situ Observations. *Science*, 294(5543):840–842.

Cannon, A. J. (2010). A flexible nonlinear modelling framework for nonstationary generalized extreme value analysis in hydroclimatology. *Hydrological Processes*, 24(6):673–685.

- Cardona, O., van Aalst, M., Birkmann, J., Fordham, M., McGregor, C., Perez, R., Pulwarty, R., Schipper, E., and Sinh, B. (2012). Determinants of Risk: Exposure and Vulnerability. In Field, C., Barros, V., Stocker, T., Qin, D., Dokken, D., Ebi, K., Mastrandrea, M., Mach, K., Plattner, G.-K., Allen, S., Tignor, M., and Midgley, P., editors, *Managing the Risks of Extreme Events and Disasters to Advance Climate Change Adaptation: A Special Report of Working Groups I and II of the Intergovernmental Panel on Climate Change (IPCC)*, chapter 2, pages 65–108. Cambridge University Press, Cambridge, United Kingdom and New York, NY, USA.
- Cheng, L. and AghaKouchak, A. (2014). Nonstationary precipitation Intensity-Duration-Frequency curves for infrastructure design in a changing climate. *Scientific reports*, 4:7093.
- Cheng, L., AghaKouchak, A., Gilleland, E., and Katz, R. W. (2014). Non-stationary extreme value analysis in a changing climate. *Climatic Change*, 127(2):353–369.
- Clark, R. T., Brown, S. J., and Murphy, J. M. (2006). Modeling Northern Hemisphere summer heat extreme changes and their uncertainties using a physics ensemble of climate sensitivity experiments. *Journal of Climate*, 19(17):4418–4435.
- Cohn, T. A. and Lins, H. F. (2005). Nature’s style: Naturally trendy. *Geophysical Research Letters*, 32(23):1–5.
- Coles, S. and Pericchi, L. (2003). Anticipating Catastrophes Through Extreme Value Modeling. *Journal of the Royal Statistical Society - Series C - Applied Statistics*, 52(4):405–416.
- Coles, S. G. (2001). *An introduction to Statistical Modeling of Extreme Values*. Springer.
- Cooley, D. (2013). *Return Periods and Return Levels Under Climate Change*, chapter 4, pages 97–114. Springer Netherlands, Dordrecht.
- Cooley, D., Nychka, D., and Naveau, P. (2007). Bayesian Spatial Modeling of Extreme Precipitation Return Levels. *Journal of the American Statistical Association*, 102(479):824–840.
- Coumou, D. and Rahmstorf, S. (2012). A decade of weather extremes. *Nature Climate Change*, 2(7):491–496.
- Cueto, R. O., Martínez, A. T., and Ostos, E. J. (2010). Heat waves and heat days in an arid city in the northwest of México: Current trends and in climate change scenarios. *International Journal of Biometeorology*, 54(4):335–345.
- Dai, A. (2013). Increasing drought under global warming in observations and models. *Nature Climate Change*, 3(1):52–58.
- Damberg, L. and AghaKouchak, A. (2014). Global trends and patterns of drought from space. *Theoretical and Applied Climatology*, 117(3-4):441–448.

- Day, J. W., Katrina, R., Boesch, D. F., Clairain, E. J., Kemp, G. P., Laska, S. B., Mitsch, W. J., Orth, K., Mashriqui, H., Reed, D. J., Shabman, L., Simenstad, C. A., Streever, B. J., Twilley, R. R., and Watson, C. C. (2007). Restoration of the Mississippi Delta: Lessons from Hurricanes Restoration of the Mississippi Delta: Lessons from Hurricanes Katrina and Rita. *Science*, 315(March):1679–1685.
- De Michele, C. and Salvadori, G. (2003a). A Generalized Pareto intensity-duration model of storm rainfall exploiting 2-Copulas. *Journal of Geophysical Research Atmospheres*, 108:1–11.
- De Michele, C. and Salvadori, G. (2003b). A Generalized Pareto intensity-duration model of storm rainfall exploiting 2-Copulas. *Journal of Geophysical Research Atmospheres*, 108:1–11.
- DeGaetano, A. T. (2009). Time-dependent changes in extreme-precipitation return-period amounts in the continental united states. *Journal of Applied Meteorology and Climatology*, 48(10):2086–2099.
- Della-Marta, P. M., Haylock, M. R., Luterbacher, J., and Wanner, H. (2007). Doubled length of western European summer heat waves since 1880. *Journal of Geophysical Research Atmospheres*, 112(15):1–11.
- Di Baldassarre, G., Kooy, M., Kemerink, J. S., and Brandimarte, L. (2013). Towards understanding the dynamic behaviour of floodplains as human-water systems. *Hydrology and Earth System Sciences*, 17(8):3235–3244.
- Diffenbaugh, N. S., Swain, D. L., and Touma, D. (2015). Anthropogenic warming has increased drought risk in California. *Proceedings of the National Academy of Sciences*, 112(13):3931–3936.
- Donat, M. G., Lowry, A. L., Alexander, L. V., O’Gorman, P. A., and Maher, N. (2016). More extreme precipitation in the world’s dry and wet regions. *Nature Climate Change*, 6(5):508–513.
- Duan, Q. Y., Gupta, V. K., and Sorooshian, S. (1993). Shuffled complex evolution approach for effective and efficient global minimization. *Journal of Optimization Theory and Applications*, 76(3):501–521.
- Elsner, J. B., Kossin, J. P., and Jagger, T. H. (2008). The increasing intensity of the strongest tropical cyclones. *Nature*, 455(7209):92–95.
- Farajzadeh, M., Rahimi, M., Kamali, G. A., and Mavrommatis, T. (2010). Modelling apple tree bud burst time and frost risk in Iran. *Meteorological Applications*, 17(1):45–52.
- FEMA (2017). Historic Disaster Response to Hurricane Harvey in Texas.
- Field, C. B., Barros, V. R., Dokken, D. J., Mach, K. J., Mastrandrea, M. D., Bilir, T. E., Chatterjee, M., Ebi, K. L., Estrada, Y. O., Genova, R. C., and Others (2014). IPCC, 2014: Climate Change 2014: Impacts, Adaptation, and Vulnerability. Part A: Global and

- Sectoral Aspects. Contribution of Working Group II to the Fifth Assessment Report of the Intergovernmental Panel on Climate Change.
- Fink, A. H., Brucher, T., Kruger, A., Leckebusch, G. C., Pinto, J. G., and Ulbrich, U. (2004). The 2003 European summer heat waves and drought- synoptic diagnosis and impact. *Weather*, 59(d):209–216.
- Fischer, E. M. and Knutti, R. (2015). Anthropogenic contribution to global occurrence of heavy-precipitation and high-temperature extremes. *Nature Clim. Change*, 5(6):560–564.
- Fischer, E. M. and Knutti, R. (2016). Observed heavy precipitation increase confirms theory and early models. *Nature Climate Change*, 6(11):986–991.
- Fischer, E. M. and Schär, C. (2010). Consistent geographical patterns of changes in high-impact European heatwaves. *Nature Geoscience*, 3(6):398–403.
- Flato, G., Marotzke, J., Abiodun, B., Braconnot, P., Chou, S., Collins, W., Cox, P., Driouech, F., Emori, S., Eyring, V., Forest, C., Gleckler, P., Guilyardi, E., Jakob, C., Kattsov, V., Reason, C., and Rummukainen, M. (2013). Evaluation of Climate Models. In Stocker, T., Qin, D., Plattner, G.-K., Tignor, M., Allen, S., Boschung, J., Nauels, A., Xia, Y., Bex, V., and Midgley, P., editors, *Climate Change 2013: The Physical Science Basis. Contribution of Working Group I to the Fifth Assessment Report of the Intergovernmental Panel on Climate Change*, pages 741–866. Cambridge University Press, Cambridge, United Kingdom and New York, NY, USA.
- Flato, G. M. (2011). Earth system models: An overview. *Wiley Interdisciplinary Reviews: Climate Change*, 2(6):783–800.
- Frich, P., Alexander, L. V., Della-Marta, P., Gleason, B., Haylock, M., Tank Klein, A. M., and Peterson, T. (2002). Observed coherent changes in climatic extremes during the second half of the twentieth century. *Climate Research*, 19(3):193–212.
- Funk, C., Hoell, A., and Stone, D. (2014). Examining the contribution of the observed global warming trend to the california droughts of 2012/13 and 2013/14. *Bulletin of the American Meteorological Society*, 95(9):S11.
- Gariano, S. L. and Guzzetti, F. (2016). Landslides in a changing climate. *Earth-Science Reviews*, 162:227–252.
- Gelman, A. and Shirley, K. (2011). Inference from simulations and monitoring convergence. *Handbook of Markov Chain Monte Carlo*, pages 163–174.
- Gençay, R. and Selçuk, F. (2004). Extreme value theory and Value-at-Risk: Relative performance in emerging markets. *International Journal of Forecasting*, 20(2):287–303.
- Gilks, W., Roberts, G., and George, E. (1994). Adaptive Direction Sampling. *Journal of the Royal Statistical Society. Series D (The Statistician)*, 43(1):179–189.

- Gilleland, E. and Katz, R. W. (2016). **extRemes** 2.0: An Extreme Value Analysis Package in *R*. *Journal of Statistical Software*, 72(8).
- Gilleland, E., Ribatet, M., and Stephenson, A. G. (2013). A software review for extreme value analysis. *Extremes*, 16(1):103–119.
- Gleick, P. H. (2016). Impacts of California ’ s Ongoing Drought: Hydroelectricity Generation. Technical Report February.
- Gloor, M., Brien, R. J., Galbraith, D., Feldpausch, T. R., Schöngart, J., Guyot, J. L., Espinoza, J. C., Lloyd, J., and Phillips, O. L. (2013). Intensification of the Amazon hydrological cycle over the last two decades. *Geophysical Research Letters*, 40(9):1729–1733.
- Granger, C. W. J. (1960). Investigating Causal Relations by Econometric Models and Cross-spectral Methods. *Econometrica*, 37(3):424–438.
- Griffis, V. W., Asce, M., Stedinger, J. R., and Asce, M. (2007). Log-Pearson Type 3 Distribution and Its Application in Flood Frequency Analysis . I : Distribution Characteristics. *Journal of Hydrologic Engineering*, 12(October):482–491.
- Griffis, V. W. and Stedinger, J. R. (2007). Incorporating Climate Change and Variability into Bulletin 17B LP3 Model.
- Groisman, P. Y., Knight, R. W., Easterling, D. R., Karl, T. R., Hegerl, G. C., and Razuvaev, V. N. (2005). Trends in intense precipitation in the climate record. *Journal of Climate*, 18(9):1326–1350.
- Groisman, P. Y., Knight, R. W., Karl, T. R., Easterling, D. R., Sun, B., Lawrimore, J. H., Groisman, P. Y., Knight, R. W., Karl, T. R., Easterling, D. R., Sun, B., and Lawrimore, J. H. (2004). Contemporary Changes of the Hydrological Cycle over the Contiguous United States: Trends Derived from In Situ Observations. *Journal of Hydrometeorology*, 5(1):64–85.
- Gu, D., Gerland, P., Pelletier, F., and Cohen, B. (2015). Risk of Exposure and Vulnerability to Natural Disasters at the City Level: A Global Overview. Technical report.
- Gupta, H. V., Wagener, T., and Liu, Y. (2008). Reconciling theory with observations: elements of a diagnostic approach to model evaluation. *Hydrological Processes*, 22(November 2008):3802–3813.
- Gupta, I. D. and Deshpande, V. C. (1994). Application of Log-Pearson Type-3 Distribution for Evaluation of Design Earthquake Magnitude. *Journal of the Institution of Engineers (India), Civil Engineering Division*, 75:129–134.
- Haario, H., Saksman, E., and Tamminen, J. (1999). Adaptive proposal distribution for random walk Metropolis algorithm. *Computational Statistics*, 14(3):375–395.

- Haario, H., Saksman, E., and Tamminen, J. (2001). An adaptive Metropolis algorithm. *Bernoulli*, 7(2):223–242.
- Haigh, I., Nicholls, R., and Wells, N. (2010). Assessing changes in extreme sea levels: Application to the English Channel, 1900–2006. *Continental Shelf Research*, 30(9):1042–1055.
- Hallegatte, S., Green, C., Nicholls, R. J., and Corfee-Morlot, J. (2013). Future flood losses in major coastal cities. *Nature Climate Change*, 3(9):802–806.
- Hanson, S., Nicholls, R., Ranger, N., Hallegatte, S., Corfee-Morlot, J., Herweijer, C., and Chateau, J. (2011). A global ranking of port cities with high exposure to climate extremes. *Climatic Change*, 104(1):89–111.
- Hasselmann, K. (1993). Optimal Fingerprints for the Detection of Time-dependent Climate Change. *J. Climate*, 6(10):1957–1971.
- Heberger, M. (2011). Australia’s Millennium Drought: Impacts and Responses BT - The World’s Water: The Biennial Report on Freshwater Resources. In Gleick, P. H., editor, *The World’s Water Volume 7*, pages 97–125. Island Press/Center for Resource Economics, Washington, DC.
- Hegerl, G., Hoegh-Guldberg, O., Casassa, G., Hoerling, M., Kovats, S., Parmesan, C., Pierce, D., and Stott, P. (2010). Good Practice Guidance Paper on Detection and Attribution Related to Anthropogenic Climate Change. *Meeting Report of the Intergovernmental Panel on Climate Change Expert Meeting on Detection and Attribution of Anthropogenic Climate Change*, pages 1–9.
- Hegerl, G. C., von Storch, H., Hasselmann, K., Santer, B. D., Cubasch, U., and Jones, P. D. (1996). Detecting Greenhouse-Gas-Induced Climate Change with an Optimal Fingerprint Method. *J. Climate*, 9(10):2281–2306.
- Held, I. M. and Soden, B. J. (2006). Robust responses of the hydrologic cycle to global warming. *J. Clim.*, 19:5686–5699.
- Hidalgo, H. G., Dettinger, M. D., and Cayan, D. R. (2008). Downscaling with Constructed Analogues: Daily Precipitation and Temperature Fields Over the United States. Technical report, California Energy Commission, PIER EnergyRelated Environmental Research. CEC5002007123.
- Holgate, S. J. (2007). On the decadal rates of sea level change during the twentieth century. *Geophysical Research Letters*, 34(1):2001–2004.
- Holmes, J. D. and Moriarty, W. W. (1999). Application of the generalized Pareto distribution to extreme value analysis in wind engineering. *Journal of Wind Engineering and Industrial Aerodynamics*, 83(1):1–10.

- Huard, D., Mailhot, A., and Duchesne, S. (2009). Bayesian estimation of intensity-duration-frequency curves and of the return period associated to a given rainfall event. *Stochastic Environmental Research and Risk Assessment*, 24(3):337–347.
- Huntington, T. G. (2006). Evidence for intensification of the global water cycle: Review and synthesis. *Journal of Hydrology*, 319(1-4):83–95.
- Hurkmans, R. T. W. L., Terink, W., Uijlenhoet, R., Moors, E. J., Troch, P. A., and Verburg, P. H. (2009). Effects of land use changes on streamflow generation in the Rhine basin. *Water Resources Research*, 45(6):1–15.
- IPCC (2014a). Annex II: Glossary. In Mach, K. J., Planton, S., and von Srechow, C., editors, *Climate Change 2014: Synthesis Report. Contribution of Working Groups I, II and III to the Fifth Assessment Report of the Intergovernmental Panel on Climate Change*, pages 117–130, IPCC, Geneva, Switzerland. Core Writing Team, R.K. Pachauri and L.A. Meyer.
- IPCC (2014b). *Climate Change 2014: Impacts, Adaptation, and Vulnerability. Part A: Global and Sectoral Aspects. Contribution of Working Group II to the Fifth Assessment Report of the Intergovernmental Panel on Climate Change*. Cambridge University Press, Cambridge, United Kingdom and New York, NY, USA.
- Jasim, F. H., Vahedifard, F., Ragno, E., AghaKouchak, A., and Ellithy, G. (2017). Effects of Climate Change on Fragility Curves of Earthen Levees Subjected to Extreme Precipitations. In *Geo-Risk 2017*, number June, pages 498–507.
- Jongman, B., Hochrainer-Stigler, S., Feyen, L., Aerts, J. C. J. H., Mechler, R., Botzen, W. J. W., Bouwer, L. M., Pflug, G., Rojas, R., and Ward, P. J. (2014). Increasing stress on disaster-risk finance due to large floods. *Nature Climate Change*, 4(4):264–268.
- Katz, R. W. (2010). Statistics of extremes in climate change. *Climatic Change*, 100(1):71–76.
- Katz, R. W. (2013). Statistical Methods for Nonstationary Extremes. In AghaKouchak, A., Easterling, D., Hsu, K., Schubert, S., and Sorooshian, S., editors, *Extremes in a Changing Climate: Detection, Analysis and Uncertainty*, pages 15–37. Springer Netherlands, Dordrecht.
- Katz, R. W., Parlange, M. B., and Naveau, P. (2002). Statistics of extremes in hydrology. *Advances in Water Resources*, 25(8-12):1287–1304.
- Kendall, M. G. (1955). Rank correlation methods.
- Khaliq, M. N., St-Hilaire, A., Ouarda, T. B. M. J., and Bobée, B. (2005). Frequency analysis and temporal pattern of occurrences of southern Quebec heatwaves. *International Journal of Climatology*, 25(4):485–504.
- Klemeš, V. (1974). The Hurst Phenomenon: A puzzle? *Water Resources Research*, 10(4):675–688.

- Knutson, T. (2017). Detection and Attribution Methodologies Overview. In Wuebbles, D., Fahey, D., Hibbard, D., Dokken, D., Stewart, B., and Maycock, T., editors, *Climate Science Special Report: Fourth National Climate Assessment, Volume I*, chapter Appendix C, pages 443–451. U.S. Global Change Research Program, Washington, DC, USA.
- Knutson, T. R., McBride, J. L., Chan, J., Emanuel, K., Holland, G., Landsea, C., Held, I., Kossin, J. P., Srivastava, A. K., and Sugi, M. (2010). Tropical cyclones and climate change. *Nature Geoscience*, 3(3):157–163.
- Koenker, R. and Bassett, G. J. (1978). Regression Quantiles. *Econometrica*, 46(1):33–50.
- Koutrouvelis, I. A. and Canavos, G. C. (1999). Estimation in the Pearson type 3 distribution. *Water Resources Research*, 35(9):2693–2704.
- Koutsoyiannis, D. (2005). Nonstationarity versus scaling in hydrology. *Journal of Hydrology*, 324(1-4):239–254.
- Koutsoyiannis, D. (2011). Hurst-Kolmogorov Dynamics and Uncertainty. *Journal of the American Water Resources Association*, 47(3):481–495.
- Koutsoyiannis, D. and Montanari, A. (2007). Statistical analysis of hydroclimatic time series: Uncertainty and insights. *Water Resources Research*, 43(5):1–9.
- Koutsoyiannis, D. and Montanari, A. (2015). Negligent killing of scientific concepts: the stationary case. *Hydrological Sciences Journal*, 60(7-8):1174–1183.
- Krishnaswamy, J., Vaidyanathan, S., Rajagopalan, B., Bonell, M., Sankaran, M., Bhalla, R. S., and Badiger, S. (2015). Non-stationary and non-linear influence of ENSO and Indian Ocean Dipole on the variability of Indian monsoon rainfall and extreme rain events. *Climate Dynamics*, 45(1):175–184.
- Kwon, H. H. and Lall, U. (2016). A copula-based nonstationary frequency analysis for the 2012/2015 drought in California. *Water Resources Research*, 52(7):5662–5675.
- Kysely, J., Picek, J., and Beranová, R. (2010). Estimating extremes in climate change simulations using the peaks-over-threshold method with a non-stationary threshold. *Global and Planetary Change*, 72(1-2):55–68.
- Lau, N. C. and Nath, M. J. (2012). A model study of heat waves over North America: Meteorological aspects and projections for the twenty-first century. *Journal of Climate*, 25(14):4761–4764.
- Lima, C. H., AghaKouchak, A., and Randerson, J. T. (2018). Unraveling the Role of Temperature and Rainfall on Active Fires in the Brazilian Amazon Using a Nonlinear Poisson Model. *Journal of Geophysical Research: Biogeosciences*, 123(1):117–128.
- Lima, C. H. R., Kwon, H.-H., and Kim, J.-Y. (2016). A Bayesian beta distribution model for estimating rainfall IDF curves in a changing climate. *Journal of Hydrology*, 540(Supplement C):744–756.

- Lins, H. F. and Cohn, T. A. (2011). Stationarity: Wanted dead or alive? *Journal of the American Water Resources Association*, 47(3):475–480.
- Luke, A., Vrugt, J. A., AghaKouchak, A., Matthew, R., and Sanders, B. F. (2017). Predicting nonstationary flood frequencies: Evidence supports an updated stationarity thesis in the United States. *Water Resources Research*, 53(7):5469–5494.
- Madsen, H., Lawrence, D., Lang, M., Martinkova, M., and Kjeldsen, T. (2013). A review of applied methods in europe for flood-frequency analysis in a changing environment.
- Mailhot, A. and Duchesne, S. (2010). Design Criteria of Urban Drainage Infrastructures under Climate Change. *Journal of Water Resources Planning and Management*, 136(2):201–208.
- Mailhot, A., Duchesne, S., Caya, D., and Talbot, G. (2007). Assessment of future change in intensity-duration-frequency (IDF) curves for Southern Quebec using the Canadian Regional Climate Model (CRCM). *Journal of Hydrology*, 347(1-2):197–210.
- Mallakpour, I. and Villarini, G. (2017). Analysis of changes in the magnitude, frequency, and seasonality of heavy precipitation over the contiguous USA. *Theoretical and Applied Climatology*, 130(1-2):345–363.
- Manabe, S. and Wetherald, R. T. (1975). The Effects of Doubling CO₂ Concentration on the Climate of a General Circulation Model. *Journal of Atmospheric Sciences*, 32(1):3–15.
- Mann, H. B. (1945). Nonparametric Tests Against Trend. *Econometrica*, 13(3):245–259.
- Marengo, J. A. and Espinoza, J. C. (2016). Extreme seasonal droughts and floods in Amazonia: Causes, trends and impacts. *International Journal of Climatology*, 36(3):1033–1050.
- Marvel, K. and Bonfils, C. (2013). Identifying external influences on global precipitation. *Proceedings of the National Academy of Sciences*, 110(48):19301–19306.
- Massey, F. J. J. (1951). Kolmogorov-Smirnov Test for Goodness of Fit. *Journal of the American Statistical Association*, 46(253):68–78.
- Mastrandrea, M. D., Field, C. B., Stocker, T. F., Edenhofer, O., Ebi, K. L., Frame, D. J., Held, H., Kriegler, E., Mach, K. J., Matschoss, P. R., Plattner, G.-K., Yohe, G. W., and Zwiers, F. W. (2010). Guidance Note for Lead Authors of the IPCC Fifth Assessment Report on Consistent Treatment of Uncertainties IPCC Cross-Working Group Meeting on Consistent Treatment of Uncertainties. Technical report.
- Matalas, N. C. (1997). Stochastic hydrology in the context of climate change.
- Matalas, N. C. (2012). Comment on the Announced Death of Stationarity. *Journal of Water Resources Planning and Management*, 138(4):311–312.
- Matlab (2017). *version 2017a*. The MathWorks Inc., Natick, Massachusetts, United State.

- Mazdiyasni, O. and AghaKouchak, A. (2015). Substantial increase in concurrent droughts and heatwaves in the United States. *Proceedings of the National Academy of Sciences*, 112(37):11484–11489.
- Mazdiyasni, O., Aghakouchak, A., Davis, S. J., Madadgar, S., Mehran, A., Ragno, E., Sadegh, M., Sengupta, A., Ghosh, S., Dhanya, C. T., and Niknejad, M. (2017). Increasing probability of mortality during Indian heat waves. *Science Advances*, pages 1–6.
- Meehl, G. A. and Tebaldi, C. (2004). More intense, more frequent, and longer lasting heat waves in the 21st century. *Science*, 305(5686):994–997.
- Mehran, A., AghaKouchak, A., and Phillips, T. J. (2014). Evaluation of CMIP5 continental precipitation simulations relative to satellite-based gauge-adjusted observations. *Journal of Geophysical Research: Atmospheres*, 119(4):1695–1707.
- Melillo, J. M., Richmond, T. T., and Yohe, G. W. (2014). *Climate Change Impacts in the United States*.
- Mentaschi, L., Vousdoukas, M., Voukouvalas, E., Sartini, L., Feyen, L., Besio, G., and Alfieri, L. (2016). The transformed-stationary approach: a generic and simplified methodology for non-stationary extreme value analysis. *Hydrology and Earth System Sciences*, 20(9):3527–3547.
- MetOffice (2013). 1953 east coast flood - 60 years on.
- Milly, P. C. D., Betancourt, J., Falkenmark, M., Hirsch, R. M., Kundzewicz, Z. W., Lettenmaier, D. P., and Stouffer, R. J. (2008). Stationarity is dead: whither water management? *Science (New York, N.Y.)*, 319(5863):573–574.
- Min, S.-K., Zhang, X., Zwiers, F. W., and Hegerl, G. C. (2011). Human contribution to more-intense precipitation extremes. *Nature*, 470(7334):378–381.
- Ming, L., M., F. D., and Sunyong, K. (2009). Bridge System Performance Assessment from Structural Health Monitoring: A Case Study. *Journal of Structural Engineering*, 135(6):733–742.
- Mirhosseini, G., Srivastava, P., and Fang, X. (2014). Developing Rainfall Intensity-Duration-Frequency (IDF) Curves for Alabama under Future Climate Scenarios using Artificial Neural Network (ANN). *Journal of Hydrologic Engineering*, 04014022(11):1–10.
- Mirhosseini, G., Srivastava, P., and Sharifi, A. (2015). Developing Probability-Based IDF Curves Using Kernel Density Estimator. *Journal of Hydrologic Engineering*, 20(9).
- Moftakhari, H. R., AghaKouchak, A., Sanders, B. F., and Matthew, R. A. (2017a). Cumulative hazard: The case of nuisance flooding. *Earth’s Future*, 5(2):214–223.
- Moftakhari, H. R., Salvadori, G., AghaKouchak, A., Sanders, B. F., and Matthew, R. A. (2017b). Compounding effects of sea level rise and fluvial flooding. *Proceedings of the National Academy of Sciences*, 114(37):9785–9790.

- Mondal, A. and Mujumdar, P. (2015). Modeling non-stationarity in intensity, duration and frequency of extreme rainfall over India. *Journal of Hydrology*, 521:217–231.
- Montanari, A. and Koutsoyiannis, D. (2014). Modeling and mitigating natural hazards: Stationary is immortal! *Water resources research*, 50(12):9748–9756.
- Montanari, A., Young, G., Savenije, H. H., Hughes, D., Wagener, T., Ren, L. L., Koutsoyiannis, D., Cudennec, C., Toth, E., Grimaldi, S., Blöschl, G., Sivapalan, M., Beven, K., Gupta, H., Hipsey, M., Schaeffli, B., Arheimer, B., Boegh, E., Schymanski, S. J., Di Baldassarre, G., Yu, B., Hubert, P., Huang, Y., Schumann, A., Post, D. A., Srinivasan, V., Harman, C., Thompson, S., Rogger, M., Viglione, A., McMillan, H., Characklis, G., Pang, Z., and Belyaev, V. (2013). "Panta Rhei-Everything Flows": Change in hydrology and society-The IAHS Scientific Decade 2013-2022. *Hydrological Sciences Journal*, 58(6):1256–1275.
- Morales-Nápoles, O., Paprotny, D., Worm, D., Abspoel-Bukman, L., and Courage, W. (2017). Characterization of Precipitation through Copulas and Expert Judgement for Risk Assessment of Infrastructure. *Journal of Risk and Uncertainty in Engineering Systems, Part A: Civil Engineering*, 3(4):1–13.
- Nasrollahi, N., AghaKouchak, A., Cheng, L., Damberg, L., Phillips, T. J., Miao, C., Hsu, K., and Sorooshian, S. (2015). How well do CMIP5 climate simulations replicate historical trends and patterns of meteorological droughts? *Water Resources Research*, 51(4):2847–2864.
- Nelsen, R. B. (2006). *An Introduction to Copulas*. Springer Science+Business Media, Inc, New York, NY, second edition.
- NWS (2018). Hurricane Harvey and Its Impacts on Southeast Texas from August 25th to 29th, 2017.
- Obeyssekera, J. and Salas, J. D. (2013). Quantifying the Uncertainty of Design Floods Under Non-Stationary Conditions. *Journal of Hydrologic Engineering*, 19(7):1438–1446.
- Olsen, J. R., Lambert, J. H., and Haines, Y. Y. (1998). Risk of extreme events under nonstationary conditions. *Risk Analysis*, 18(4):497–510.
- Papalexiou, S. M. and Koutsoyiannis, D. (2013). Battle of extreme value distributions : A global survey on extreme daily rainfall. *Water Resources Research*, 49(1):187–201.
- Peng, R. D., Bobb, J. F., Tebaldi, C., McDaniel, L., Bell, M. L., and Dominici, F. (2011). Toward a quantitative estimate of future heat wave mortality under global climate change. *Environmental Health Perspectives*, 119(5):701–706.
- Pielke, R. A. and Landsea, C. W. (1998). Normalized Hurricane Damages in the United States: 1925–95. *Weather and Forecasting*, 13(3):621–631.

- Pisarenko, V. F. and Sornette, D. (2003). Characterization of the Frequency of Extreme Earthquake Events by the Generalized Pareto Distribution. *pure and applied geophysics*, 160(12):2343–2364.
- Ragno, E., AghaKouchak, A., Love, C. A., Cheng, L., Vahedifard, F., and Lima, C. H. R. (2018). Quantifying Changes in Future Intensity-Duration-Frequency Curves Using Multi-Model Ensemble Simulations. *Water Resources Research*, pages 1–38.
- Read, L. K. and Vogel, R. M. (2015). Reliability, return periods, and risk under nonstationarity. *Water Resources Research*, 51(1):6381–6398.
- Renard, B., Sun, X., and Lang, M. (2013). Bayesian Methods for Non-stationary Extreme Value Analysis. In AghaKouchak, A., Easterling, D., Hsu, K., Schubert, S., and Sorooshian, S., editors, *Extremes in a Changing Climate: Detection, Analysis and Uncertainty*, pages 39–95. Springer Netherlands, Dordrecht.
- Rignot, E., Velicogna, I., Van Den Broeke, M. R., Monaghan, A., and Lenaerts, J. (2011). Acceleration of the contribution of the Greenland and Antarctic ice sheets to sea level rise. *Geophysical Research Letters*, 38(5):1–5.
- Rizzo, M. L. and Székely, G. J. (2010). DISCO analysis: A nonparametric extension of analysis of variance. *Annals of Applied Statistics*, 4(2):1034–1055.
- Roberts, G. O. and Rosenthal, J. S. (2009). Examples of Adaptive MCMC. *Journal of Computational and Graphical Statistics*, 18(2):349–367.
- Roberts, G. O. and Sahu, S. K. (1997). Updating Schemes, Correlation Structure, Blocking and Parameterization for the Gibbs Sampler. *Journal of the Royal Statistical Society: Series B (Statistical Methodology)*, 59(2):291–317.
- Robinson, J. D., Vahedifard, F., and Aghakouchak, A. (2017). Rainfall-triggered Slope Instabilities under a Changing Climate: Comparative Study using Historical and Projected Precipitation Extremes. 11(September):1–11.
- Rosner, A., Vogel, R. M., and Kirshen, P. H. (2014). A risk-based approach to flood management decisions in a nonstationary world. *Water Resources Research*, 50(3):1928 – 1942.
- Sadegh, M., Ragno, E., and Aghakouchak, A. (2017). Multivariate Copula Analysis Toolbox (MvCAT): Describing dependence and underlying uncertainty using a Bayesian framework. *Water Resources Research*, pages 1–18.
- Sadegh, M., Vrugt, J. A., Xu, C., and Volpi, E. (2015). The stationarity paradigm revisited: Hypothesis testing using diagnostics, summary metrics, and DREAM(ABC). *Water Resources Research*, 51(11):9207–9231.
- Salas, J., Obeysekera, J., and Vogel, R. (2018). Techniques for assessing water infrastructure for nonstationary extreme events: a review. *Hydrological Sciences Journal*, 00(00):02626667.2018.1426858.

- Salas, J. D. and Obeysekera, J. (2014). Revisiting the Concepts of Return Period and Risk for Nonstationary Hydrologic Extreme Events. *Journal of Hydrologic Engineering*, (March):554–568.
- Salas, J. D. and Pielke Sr, R. A. (2002). Stochastic characteristics and modeling of hydroclimatic processes. *Handbook of Weather, Climate, and Water*, pages 585–603.
- Salvadori, G. and De Michele, C. (2004). Frequency analysis via copulas: Theoretical aspects and applications to hydrological events. *Water Resources Research*, 40(12):1–17.
- Samenow, J. (2017). Harvey is a 1,000-year flood event unprecedented in scale.
- Sankarasubramanian, A. and Lall, U. (2003). Flood quantiles in a changing climate: Seasonal forecasts and causal relations. *Water Resources Research*, 39(5).
- Santer, B. D., Painter, J. F., Mears, C. A., Doutriaux, C., Caldwell, P., Arblaster, J. M., Cameron-Smith, P. J., Gillett, N. P., Gleckler, P. J., Lanzante, J., Perlwitz, J., Solomon, S., Stott, P. A., Taylor, K. E., Terray, L., Thorne, P. W., Wehner, M. F., Wentz, F. J., Wigley, T. M. L., Wilcox, L. J., and Zou, C.-Z. (2013). Identifying human influences on atmospheric temperature. *Proceedings of the National Academy of Sciences*, 110(1):26–33.
- Sarhadi, A., Burn, D. H., Concepción Ausín, M., and Wiper, M. P. (2016). Time-varying nonstationary multivariate risk analysis using a dynamic Bayesian copula. *Water Resources Research*, 52(3):2327–2349.
- Sarhadi, A. and Soulis, E. D. (2017). Time-varying extreme rainfall intensity-duration-frequency curves in a changing climate. *Geophysical Research Letters*, pages 1–10.
- Schär, C., Vidale, P. L., Lüthi, D., Frei, C., Häberli, C., Liniger, M. A., and Appenzeller, C. (2004). The role of increasing temperature variability in European summer. *Nature*, 427(January):332–336.
- Schwarz, G. (1978). Estimating the Dimension of a Model. *Ann. Statist.*, 6(2):461–464.
- Seneviratne, S., Nicholls, N., Easterling, D., Goodess, C., Kanae, S., Kossin, J., Luo, Y., Marengo, J., McInnes, K., Rahimi, M., Reichstein, M., Sorteberg, A., Vera, C., and Zhang, X. (2012). Changes in climate extremes and their impacts on the natural physical environment. In Rusticucci, M. and Semenov, V., editors, *Managing the Risk of Extreme Events and Disasters to Advance Climate Change Adaptation.*, chapter 3, pages 109–230. Cambridge University Press, Cambridge, United Kingdom and New York, NY, USA.
- Serago, J. M. and Vogel, R. M. (2018). Parsimonious nonstationary flood frequency analysis. *Advances in Water Resources*, 112(November 2017):1–16.
- Serinaldi, F. and Kilsby, C. G. (2015). Stationarity is undead: Uncertainty dominates the distribution of extremes. *Advances in Water Resources*, 77:17–36.
- Sheffield, J. and Wood, E. F. (2008). Projected changes in drought occurrence under future global warming from multi-model, multi-scenario, IPCC AR4 simulations. *Climate Dynamics*, 31(1):79–105.

- Sheffield, J., Wood, E. F., and Roderick, M. L. (2012). Little change in global drought over the past 60 years. *Nature*, 491(7424):435–438.
- Shumway, R. H. and Stoffer, D. S. (2011). *Time Series Analysis and Its Applications With R Examples*. Springer Science+Business Media, Inc, New York, third edition.
- Singh, V. P. and Zhang, L. (2007). IDF Curves Using the Frank Archimedean Copula. *Journal of Hydrologic Engineering*, 12(6):651–662.
- Sklar, M. (1959). Fonctions de repartition an dimensions et leurs marges. *Publ. Inst. Statist. Univ. Paris*, 8:229–231.
- Stahl, K., Hisdal, H., Hannaford, J., Tallaksen, L. M., Van Lanen, H. A., Sauquet, E., Demuth, S., Fendekova, M., and Jodar, J. (2010). Streamflow trends in Europe: Evidence from a dataset of near-natural catchments. *Hydrology and Earth System Sciences*, 14(12):2367–2382.
- Stedinger, J. R. and Griffis, V. W. (2011). Getting From Here to Where? Flood Frequency Analysis and Climate. *JAWRA Journal of the American Water Resources Association*, 47(3):506–513.
- Stern, D. I. and Kaufmann, R. K. (2014). Anthropogenic and natural causes of climate change. *Climatic Change*, 122(1-2):257–269.
- Storn, R. and Price, K. (1997). Differential Evolution – A Simple and Efficient Heuristic for global Optimization over Continuous Spaces. *Journal of Global Optimization*, 11(4):341–359.
- Stott, P. A., Gillett, N. P., Hegerl, G. C., Karoly, D. J., Stone, D. A., Zhang, X., and Zwiers, F. (2010). Detection and attribution of climate change: a regional perspective. *Wiley Interdisciplinary Reviews: Climate Change*, 1(2):192–211.
- Stott, P. A., Stone, D. A., and Allen, M. R. (2002). Human contribution to the European heatwave of 2003. *Nature*, 107(B11):EPM 3–1–EPM 3–22.
- Swain, D. L. (2015). A tale of two california droughts: Lessons amidst record warmth and dryness in a region of complex physical and human geography. *Geophysical Research Letters*, 42(22):9999.
- Swain, D. L., Langenbrunner, B., Neelin, J. D., and Hall, A. (2018). Increasing precipitation volatility in twenty-first-century california. *Nature Climate Change*, page 1.
- Székely, G. J. and Rizzo, M. L. (2013). Energy statistics: A class of statistics based on distances. *Journal of Statistical Planning and Inference*, 143(8):1249–1272.
- Tank, K. A. M., Können, G. P., and Selten, F. M. (2005). Signals of anthropogenic influence on European warming as seen the trend patterns of daily temperature variance. *International Journal of Climatology*, 25(1):1–16.

- Tarroja, B., AghaKouchak, A., and Samuelsen, S. (2016). Quantifying climate change impacts on hydropower generation and implications on electric grid greenhouse gas emissions and operation. *Energy*, 111:295–305.
- Taylor, K. E., Stouffer, R. J., and Meehl, G. A. (2009). A Summary of the CMIP5 Experiment Design. https://cmip.llnl.gov/cmip5/docs/Taylor_CMIP5_design.pdf.
- Taylor, K. E., Stouffer, R. J., and Meehl, G. A. (2012). An overview of CMIP5 and the experiment design. *Bulletin of the American Meteorological Society*, 93(4):485–498.
- Taylor, R. G., Scanlon, B., Döll, P., Rodell, M., Van Beek, R., Wada, Y., Longuevergne, L., Leblanc, M., Famiglietti, J. S., Edmunds, M., Konikow, L., Green, T. R., Chen, J., Taniguchi, M., Bierkens, M. F., Macdonald, A., Fan, Y., Maxwell, R. M., Yechieli, Y., Gurdak, J. J., Allen, D. M., Shamsudduha, M., Hiscock, K., Yeh, P. J., Holman, I., and Treidel, H. (2013). Ground water and climate change. *Nature Climate Change*, 3(4):322–329.
- Team, R. C. (2013). R: A Language and Environment for Statistical Computing.
- Tebaldi, C. and Knutti, R. (2007). The use of the multi-model ensemble in probabilistic climate projections. *Philosophical Transactions of the Royal Society A: Mathematical, Physical and Engineering Sciences*, 365(1857):2053–2075.
- Ter Braak, C. J. F. and Vrugt, J. A. (2008). Differential Evolution Markov Chain with snooker updater and fewer chains. *Statistics and Computing*, 18(4):435–446.
- Thiemann, M., Trosset, M., Gupta, H., and Sorooshian, S. (2001). Bayesian recursive parameter estimation for hydrologic models Water Resources Research Volume 37, Issue 10. *Water Resources Research*, 37(10):2521–2535.
- Thorne, C. (2014). Geographies of UK flooding in 2013/4. *Geographical Journal*, 180(4):297–309.
- Trenberth, K. E. (2011). Changes in precipitation with climate change. *Climate Research*, 47(1/2):123–138.
- Trenberth, K. E., Dai, A., Van Der Schrier, G., Jones, P. D., Barichivich, J., Briffa, K. R., and Sheffield, J. (2014). Global warming and changes in drought. *Nature Climate Change*, 4(1):17–22.
- UN (2015). Transforming our world: The 2030 agenda for sustainable development. Technical Report 1, United Nations General Assembly.
- UNFCCC (2017). National Inventory Submissions. United Nations Framework Convention on Climate Change.
- U.S. Water Resources Council (1982). Guidelines for Determining Flood Flow Frequency. *Bulletin 17B: Reston, Virginia, Hydrology Subcommittee, Office of Water Data Coordination, U.S. Geological Survey*, page 182.

- Vahedifard, F., AghaKouchak, A., Ragno, E., Shahrokhbabadi, S., and Mallakpour, I. (2017a). Lessons from the Oroville dam. *Science*, 355(6330):1139–1140.
- Vahedifard, F., Robinson, J. D., and AghaKouchak, A. (2016). Can Protracted Drought Undermine the Structural Integrity of California’s Earthen Levees? *Journal of Geotechnical and Geoenvironmental Engineering*, 142(6):02516001.
- Vahedifard, F., Tehrani, F. S., Galavi, V., Ragno, E., and AghaKouchak, A. (2017b). Resilience of MSE Walls with Marginal Backfill under a Changing Climate: Quantitative Assessment for Extreme Precipitation Events. *Journal of Geotechnical and Geoenvironmental Engineering*, 143(9):04017056.
- Van Dijk, A. I., Beck, H. E., Crosbie, R. S., De Jeu, R. A., Liu, Y. Y., Podger, G. M., Timbal, B., and Viney, N. R. (2013). The Millennium Drought in southeast Australia (2001-2009): Natural and human causes and implications for water resources, ecosystems, economy, and society. *Water Resources Research*, 49(2):1040–1057.
- Vandenberg-Rodes, A., Moftakhari, H. R., AghaKouchak, A., Shahbaba, B., Sanders, B. F., and Matthew, R. A. (2016). Projecting nuisance flooding in a warming climate using generalized linear models and Gaussian processes. *Journal of Geophysical Research: Oceans*, 121(11):8008–8020.
- Vermeer, M. and Rahmstorf, S. (2009). Global sea level linked to global temperature. *Proceedings of the National Academy of Sciences of the United States of America*, 106(51):21527–21532.
- Viglione, A., Di Baldassarre, G., Brandimarte, L., Kuil, L., Carr, G., Salinas, J. L., Scolobig, A., and Blöschl, G. (2014). Insights from socio-hydrology modelling on dealing with flood risk - Roles of collective memory, risk-taking attitude and trust. *Journal of Hydrology*, 518(PA):71–82.
- Villarini, G., Serinaldi, F., Smith, J. A., and Krajewski, W. F. (2009a). On the stationarity of annual flood peaks in the continental United States during the 20th century. *Water Resources Research*, 45(8):1–17.
- Villarini, G., Smith, J. A., and Napolitano, F. (2010). Nonstationary modeling of a long record of rainfall and temperature over Rome. *Advances in Water Resources*, 33(10):1256–1267.
- Villarini, G., Smith, J. A., Serinaldi, F., Bales, J., Bates, P. D., and Krajewski, W. F. (2009b). Flood frequency analysis for nonstationary annual peak records in an urban drainage basin. *Advances in Water Resources*, 32(8):1255–1266.
- Vogel, R. M., Yaindl, C., and Walter, M. (2011). Nonstationarity: Flood Magnification and Recurrence Reduction Factors in the United States. *JAWRA Journal of the American Water Resources Association*, 47(3):464–474.

- Volpi, E., Fiori, A., Grimaldi, S., Lombardo, F., and Koutsoyiannis, D. (2015). One hundred years of return period: Strengths and limitations. *Water Resources Research*, 51(10):8570–8585.
- Vrugt, J., Ter Braak, C., Diks, C., Robinson, B., Hyman, J., and Hingdon, D. (2009). Accelerating Markov Chain Monte Carlo Simulation by Differential Evolution with Self-Adaptive Randomized Subspace Sampling.
- Wagener, T., Sivapalan, M., Troch, P. A., McGlynn, B. L., Harman, C. J., Gupta, H. V., Kumar, P., Rao, P. S. C., Basu, N. B., and Wilson, J. S. (2010). The future of hydrology: An evolving science for a changing world. *Water Resources Research*, 46(5):1–10.
- Wahl, T., Jain, S., Bender, J., Meyers, S. D., and Luther, M. E. (2015). Increasing risk of compound flooding from storm surge and rainfall for major US cities. *Nature Clim. Change*, 5(12):1093–1097.
- Wahl, T., Jensen, J., Frank, T., and Haigh, I. D. (2011). Improved estimates of mean sea level changes in the German Bight over the last 166 years. *Ocean Dynamics*, 61(5):701–715.
- Wang, Y. and Zhou, L. (2005). Observed trends in extreme precipitation events in China during 1961-2001 and the associated changes in large-scale circulation. *Geophysical Research Letters*, 32(9):1–4.
- Wasko, C., Sharma, A., and Westra, S. (2016). Reduced spatial extent of extreme storms at higher temperatures. *Geophysical Research Letters*, 43(8):4026–4032.
- WCRP (2018). World Climate Research Programme.
- Webster, P. J., Holland, G. J., Curry, J. A., and Chang, H.-R. (2005). Changes in Tropical Cyclone Number, Duration, and Intensity in a Warming Environment. *Science*, 309(5742):1844–1846.
- Westra, S., Alexander, L. V., and Zwiers, F. W. (2013). Global Increasing Trends in Annual Maximum Daily Precipitation. *Journal of Climate*, 26(11):3904–3918.
- White, H. (1980). A Heteroskedasticity-Consistent Covariance Matrix Estimator and a Direct Test for Heteroskedasticity. *Econometrica*, 48(4):817–838.
- Wigley, T. M. (2009). The effect of changing climate on the frequency of absolute extreme events. *Climatic Change*, 97(1):67–76.
- Willems, P., Arnbjerg-Nielsen, K., Olsson, J., and Nguyen, V. T. V. (2012). Climate change impact assessment on urban rainfall extremes and urban drainage: Methods and shortcomings. *Atmospheric Research*, 103:106–118.
- WMO (2012). A Note on Stationarity and Nonstationarity.
- Wooldridge, J. M. (2002). *Introductory Econometrics*.

- Wu, P., Christidis, N., and Stott, P. (2013). Anthropogenic impact on Earth’s hydrological cycle. *Nature Climate Change*, 3(9):807–810.
- Xiao, M., Koppa, A., Mekonnen, Z., Pagán, B. R., Zhan, S., Cao, Q., Aierken, A., Lee, H., and Lettenmaier, D. P. (2017). How much groundwater did california’s central valley lose during the 2012–2016 drought? *Geophysical Research Letters*, 44(10):4872–4879.
- Yan, H., Sun, N., Wigmosta, M., Skaggs, R., Hou, Z., and Leung, R. (2018). Next-Generation Intensity-Duration-Frequency Curves for Hydrologic Design in Snow-Dominated Environments. *Water Resources Research*, pages 1–16.
- Yilmaz, A. G. and Perera, B. J. C. (2014). Extreme Rainfall Nonstationarity Investigation and Intensity Frequency Duration Relationship. *Journal of Hydrologic Engineering*, 19(6):1160–1172.
- Zhang, X., Zwiers, F. W., Hegerl, G. C., Lambert, F. H., Gillett, N. P., Solomon, S., Stott, P. A., and Nozawa, T. (2007). Detection of human influence on twentieth-century precipitation trends. *Nature*, 448(7152):461–465.
- Zhang, X., Zwiers, F. W., and Stott, P. A. (2006). Multimodel Multisignal Climate Change Detection at Regional Scale. *Journal of Climate*, 19(17):4294–4307.
- Zheng, F., Westra, S., and Leonard, M. (2015). Opposing local precipitation extremes. *Nature Clim. Change*, 5(5):389–390.
- Zhu, J., Stone, M. C., and Forsee, W. (2012). Analysis of potential impacts of climate change on Intensity - Duration - Frequency (IDF) relationships for six regions in the United States. *Journal of Water and Climate Change*, 3(3):185–196.
- Zwiers, F. W., Zhang, X., and Feng, Y. (2011). Anthropogenic Influence on Long Return Period Daily Temperature Extremes at Regional Scales. *Journal of Climate*, 24(3):881–892.